

POLITECNICO DI TORINO

**Corso di Laurea Magistrale
in Ingegneria Civile**

Tesi di Laurea Magistrale

**Estimating sediment transport in the Mogtedo
watershed, Burkina Faso**



Relatore

prof. Paolo Vezza

Corelatori

prof. Carlo Vincenzo Camporeale

prof. Velio Coviello (Libera Università di Bolzano)

Candidato

Luca Toso

A.A. 2017/2018

Abstract

Estimating sediment transport in the Mogtedo watershed, Burkina Faso

Luca Toso

Politecnico di Torino, Department of Environment, Land and Infrastructure Engineering-DIATI
Corso Duca degli Abruzzi 24, Torino, Italy

In the Sahelian region the annual rainfall is only concentrated in a short period of the year, named wet season, where many heavy rains occur and cause floods. The intensity of rains doesn't permit the infiltration of water, which rapidly flows away, so that paradoxically rainfall is one of the main causes of soil impoverishment and erosion.

Many small dams were built in Burkina Faso to store water from the wet season to be used in the rest of the year, especially for irrigation. However, storage capacity of these dams is decreasing as a consequence of sediment transport from the rivers which provide water to the dams, with a phenomenon called siltation. As a consequence of the climate change, the amount of annual rainfall has decreased and dry periods has become longer, worsening the living conditions of the inhabitants. In the present study some sediment transport data collected by the PADI project in Mogtedo catchment, where there is small dam, were analyzed. Some sediment transport formulas were tested on field data, six of them for total load, three for suspended load and three for bedload. Results of the different formulas were compared and used to find out the formula which better fitted field data.

The research for a new suspended sediment transport formula and for a new total sediment transport formula was also performed; the new formulas were found out through the analysis of the previously tested existing formulas and the measured data.

Acknowledgements

I would like to thank first my family: Marco, Giacinta and Anna. They always supported me in the difficult moments, they raised me making who I am today. With all my love: thank you. Thanks to my grandparents, who were so important in my life, even if now they are looking down on me from the sky.

Thanks to Elena, the little flower that life brought to me.

I want to greet my best friends for all the adventures we lived together: Cristian, Emanuele, Filippo, Giacomo and Stefano.

Thanks to the people who helped me throughout the period I wrote this thesis: professors Paolo Vezza and Carlo Camporeale from Politecnico of Turin, professor Velio Coviello from University of Bolzano, Francis Guyon and Eric Hallot of the PADI project who concretely collected data in Burkina Faso.

A special thanks to the AGESCI (Association of Italian Catholic Scouts) and in particular to all guys and leaders of the scout group Savona 7, I hope that the moments we spent together really made the world a better place.

Finally, to all people who know me, even if we shared only a little stretch in the road of life, thank you.

Contents

List of Figures	iv
List of Tables	v
List of Symbols	vi
1 Context of the study	1
1.1 Burkina Faso	1
1.1.1 Geomorphology	3
1.1.2 Hydrography	4
1.1.3 Geology	4
1.1.4 Pedology	6
1.1.5 Climate	6
1.1.6 Temperatures	8
1.1.7 Vegetation	9
1.1.8 Wildlife	10
1.1.9 Naam groups	10
1.2 Mogtedo	12
1.2.1 Soil and elevation	12
1.2.2 Climate and vegetation	13
1.2.3 Hydrography	13
1.2.4 The dam and the basin	15
1.2.5 Main activities in proximity of the dam	17
2 Description of the sites and data collection	20
2.1 Localisation of the sites	20
2.2 Data collection	22
2.3 Cross sections	26
2.4 Sample of sediment	28
2.5 Analyzed dataset	30
3 Sediment transport calculation	34
3.1 Basic informations of sediment transport	34
3.1.1 Mobilization mechanisms	34
3.1.2 Hydrodynamic mechanism	36
3.1.3 Shields theory	37
3.2 Transport capacity and sediment load	43
3.3 Total sediment load	44
3.3.1 Engelund and Hansen	44
3.3.2 Ackers and White	44
3.3.3 Yang	46

3.3.4	Di Silvio	48
3.3.5	Graf and Acaroglu	48
3.4	Suspended load	50
3.4.1	Van Rijn	54
3.4.2	Smith and McLean	55
3.4.3	Garcia and Parker	55
3.5	Bedload	56
3.5.1	Meyer-Peter and Muller	56
3.5.2	Fernandez-Luque and Van Beek	57
3.5.3	Wilson	57
4	Results	58
5	Discussion	61
5.1	Comparison between tested formulas	63
5.1.1	Total sediment load	63
5.1.2	Suspended load	63
5.1.3	Bedload	64
6	Proposing a new formula	65
6.1	Partitioning of total sediment load into suspended load and bedload	77
6.2	Calculation of Root Mean Square Errors	79
6.3	Student's test	80
7	Conclusions	83
8	Bibliography	85

List of Figures

1.1	Map of West Africa [8].	1
1.2	Map of Burkina Faso [8].	2
1.3	Morphological map of Burkina Faso [8].	4
1.4	Geological map of West Africa [39].	5
1.5	Climatic zones of West Africa [8].	8
1.6	Different zones of vegetation in West Africa, from the <i>Perry-Castaneda Library Map Collection</i>	9
1.7	Location of Mogtedo Department in Burkina Faso [6].	12
1.8	Map of Burkina Faso with the position of Mogtedo and isohyets [28].	13
1.9	Hydrographic network of Bomborè catchment near Mogtedo [21].	14
1.10	Some photos of the spillway and the basin of Mogtedo dam [6].	15
1.11	Evolution of storage capacity of Mogtedo dam during time (courtesy of Francis Guyon).	16
1.12	Evolution of water volume in the basin during the year [18].	16
1.13	Cultivated fields near Mogtedo dam (courtesy of Paolo Vezza).	18
1.14	Hydraulic devices for the irrigation of fields near the dam (courtesy of Paolo Vezza).	19
2.1	Sub-catchments present in the area of the study [17].	20
2.2	Measuring points for MOG2 (violet) and MOG3 (orange).	21
2.3	Example of pressure probes used in the study [17].	22
2.4	Cans used for the collection of water samples [17].	23
2.5	Rating curve for measure station in MOG2.	23
2.6	Rating curve for measure station in MOG3.	24
2.7	Hydrogram of a flood occurred in 2013 in MOG2 sub-catchment.	24
2.8	Relation between mean flow rate and maximum flow rate for every flood.	25
2.9	Cross section of the measure station in MOG2.	26
2.10	Cross section of the measure station in MOG3.	26
2.11	Interpolation of MOG2 cross section.	27
2.12	Interpolation of MOG3 cross section.	27
2.13	Grading curve used in the present work (courtesy of Paolo Vezza).	28
2.14	Tools adoperated for the determination of the grading curve, with the sieves and the precision scale (courtesy of Paolo Vezza).	29
2.15	Dataset for Mog2 in 2013.	30
2.16	Dataset for Mog2 in 2014.	31
2.17	Dataset for Mog3 in 2013.	32
2.18	Dataset for Mog3 in 2014.	33
3.1	Forces balance in a submerged granular mass [4].	34
3.2	Scheme of active and passive stresses in a granular submerged mass [4].	35
3.3	Possible combinations of destabilizing and stabilizing stresses [35].	35
3.4	Scheme of bedload and suspended load [15].	37

3.5	Shields curve.	39
3.6	Slope correction factor calculated with an inner friction angle of 45°	41
3.7	Relative submergence correction factor.	42
3.8	Graphics for determination of n,m,A and c through experimental data.	46
3.9	Determination of fall velocity function of diameter, shape factor and temperature.	47
3.10	Rouse's profile of sediment concentration.	51
3.11	Profiles of flow velocity, suspended sediment concentration and suspended sediment load [37].	52
3.12	Graphic of the integral I1.	53
3.13	Graphic of the integral I2.	54
4.1	Results for MOG2 in 2013.	58
4.2	Results for MOG2 in 2014.	59
4.3	Results for MOG3 in 2013.	59
4.4	Results for MOG3 in 2014.	60
6.1	Graphic for the determination of suspended load formula.	67
6.2	Graphic for the determination of total load formula.	68
6.3	Results for MOG2 in 2013 with proposed formulas.	68
6.4	Results for MOG2 in 2014 with proposed formulas.	69
6.5	Results for MOG3 in 2013 with proposed formulas.	69
6.6	Results for MOG3 in 2014 with proposed formulas.	70
6.7	Field data versus predicted curves for suspended load in MOG2.	71
6.8	Field data versus predicted curves for suspended load in MOG3.	72
6.9	Field data versus predicted curves for total load in MOG2.	73
6.10	Field data versus predicted curves for total load in MOG3.	74
6.11	Comparison graphic for suspended load with literature formulas and proposed formula (6.5), obtained joining graphics 6.7 and 6.8. Coordinates of the measured data represent the mean specific discharge and the mean sediment discharge of every flood. Calculated curves are obtained evaluating sediment load as a function of specific discharge. Every formula is distinguished by a different colour, and there are two lines for every color: the solid line represents the implementation of that formula in MOG2, whereas the dashed one is referred to MOG3.	75
6.12	Comparison graphic for total load with literature formulas and proposed formula (6.11), obtained joining graphics 6.9 and 6.10. Measured data and tested formulas have to be intended as in the previous graphic. Again, every formula is distinguished by a different colour, solid lines are referred to MOG2 and dashed lines to MOG3.	76
6.13	Bedload transport rate plotted as a function of suspended load transport rate.	77

List of Tables

2	General data of Burkina Faso.	3
3	Products cultivated near Mogtedo dam.	17
4	Values of coefficient n,m,A and c.	45
5	Values of recalibrated coefficient n,m,A and c.	46
6	Parameters for Di Silvio formula.	48
7	Calculated and measured values for the four cases considered, expressed in tons per year.	60
8	Percentage differences of each formula in the four considered combinations	61
9	Sediment load values for Mogtedo basin, expressed in $\frac{tons}{km^2}$. Suspended values are the measured ones; bedload values are obtained through a mean of the tested formulas, as in the previous chapter.	78
10	Calculated RMSE for suspended load formulas.	79
11	Calculated RMSE for total load formulas.	79
12	Calculated values of F compared to critical values.	81
13	Results of the t-test for suspended load formulas.	82
14	Results of the t-test for total load formulas.	82

List of Symbols

γ	Specific weight of water	$[N/m^3]$
δ	Submerged specific gravity of sediment	[-]
ϵ	Absolute roughness	$[m]$
μ	Dynamic viscosity	$[Ns/m^2]$
ν	Kinematic viscosity	$[m^2/s]$
τ_0	Mean bed shear stress	$[N/m^2]$
τ^*	Dimensionless shear stress	[-]
τ_{cr}^*	Critical value of dimensionless shear stress	[-]
ρ	Density of water	$[kg/m^3]$
ρ_s	Density of sediment	$[kg/m^3]$
b	Channel width	$[m]$
C	Chezy coefficient	[-]
C'	Chezy coefficient related to grains	[-]
d	Grain diameter	$[mm]$
d_x	Grain diameter for which x% by weight is finer	$[mm]$
D_*	Dimensionless diameter	[-]
g	Gravitational acceleration	$[m/s^2]$
h	Water surface elevation	$[m]$
i_f	Channel bed slope	[-]
j	Energy line slope	[-]
k	Von Karman constant	[-]
n	Manning coefficient	$[s/m^{1/3}]$
q	Discharge per unit width	$[m^2/s]$
Q	Discharge	$[m^3/s]$
Re	Reynolds number	[-]
Re_p	Particle Reynolds number	[-]
R	Hydraulic Radius	$[m]$
s	Specific gravity of sediment	[-]
U	Mean velocity in the river	$[m/s]$
u_*	Shear velocity	$[m/s]$
u'_*	Skin shear velocity	$[m/s]$
u_{cr}	Critical velocity	$[m/s]$
W_s	Falling velocity	$[m/s]$
Y	Water depth	$[m]$

1 Context of the study

1.1 Burkina Faso

Burkina Faso is a landlocked country in West Africa. It covers an area of around 274,200 square kilometres and is surrounded by six countries: Mali to the north; Niger to the east; Benin to the southeast; Togo and Ghana to the south, and Ivory Coast to the southwest. Its capital is Ouagadougou. In 2014 its population was estimated at just over 17.3 million. Burkina Faso is a francophone country, with French as an official language of government and business. Formerly called the Republic of Upper Volta (1958–1984), the country was renamed "Burkina Faso" on 4 August 1984 by then-President Thomas Sankara. The words "Burkina" and "Faso" both stem from different languages spoken in the country: "Burkina" comes from Mossi and means "honest" or "honest people", while "Faso" comes from the Dyula language and means "fatherland" (lit. "father's house"). The citizens of Burkina Faso are known as Burkinabé.



Figure 1.1: Map of West Africa [8].

Burkina Faso was a French colony until 5 August 1960, when it obtained full independence; the following political history of the country is characterized by several coups. The most long-lasting govern was Blaise Campaorè's who organized a coup in 1987 in which the former president Thomas Sankara, who implemented a series of revolutionary programs which included mass-vaccinations and the expansion of women's rights, was killed along with twelve other officials. Campaorè lost power in 2014, 27 year later. The last election where held on 29 November 2015 and won by the current president Roch Marc Christian Kaboré.

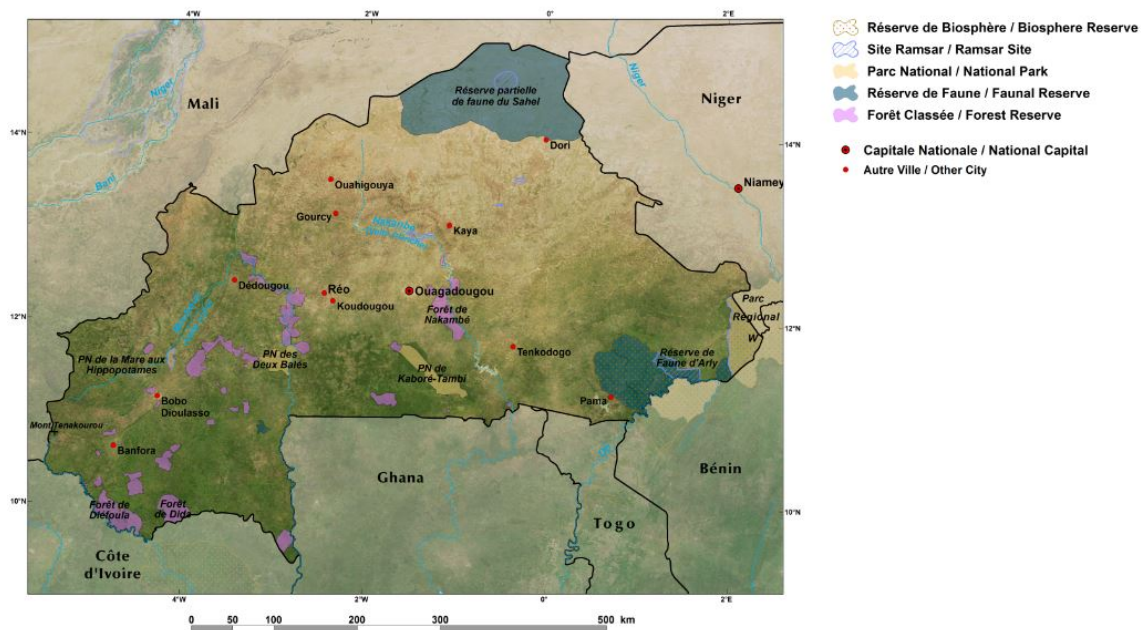


Figure 1.2: Map of Burkina Faso [8].

Population of Burkina Faso was estimated in 2017 as 20,107,509 with a density of about $73/km^2$. The main city is the capital Ouagadougou (1,915,000 inhabitant), which is the political and administrative center and a relevant agricultural market thanks to its central position. The only other city that can compete with the capital as an economic role is Bobo-Dioulasso, situated in the western part of the country, which developed thanks to the construction of the railway; Bobo-Dioulasso is well connected with neighbouring countries and the delta of Niger river, and there is also an international airport. Other smaller cities are Koudougou, Ouahigouya, Kaya and Banfora. The predominant ethnic groups are Mossi (about half of the population), Fula, Lobi, Bobo and Mandè. Conversely from many other African countries in Burkina Faso the different ethnic groups have always lived in peace and there have not been serious conflict or civil war. The main religions are Islam (60.5%), Christianity (23.2%) and Indigenous Beliefs (15.3%).

Burkina Faso is a multilingual country. An estimated 69 languages are spoken there, of which about 60 languages are indigenous. The Mossi language is spoken by about 40% of the population, mainly in the central region around the capital, Ouagadougou, along with other, closely related Gurunsi languages scattered throughout Burkina. In the west, Mande languages are widely spoken, the most predominant being Dyula (also known as Jula or Dioula), others including Bobo, Samo, and Marka. The Fula language is widespread, particularly in the north. The Gourmanché language is spoken in the east, while the Bissa language is spoken in the south.

The country is divided into 13 administrative regions. These regions encompass 45 provinces and 301 departments. Each region is administered by a Governor.

Burkina Faso is the 6th least developed country in the world (UN, 2016) and is economically depending on an archaic agriculture and a nomad pastoralism. Millet has always been the most

Area	274,200	km^2
Population	20,107,509	inh.
Density	73	inh/ km^2
Capital	Ouagadougou	-
Government	Unitary semi-presidential republic	-
Gross Domestic Production (total)	13.092 billion	\$
Gross Domestic Production (per capita)	691	\$
Currency	West African CFA franc	-
Human Development Index (HDI)	0.402	-
Life expectancy (men)	57	years
Life expectancy (women)	60	years
Literacy rate	25.3	%

Table 2: General data of Burkina Faso.

cultivated crop by Burkinabè farmers, and it's still very widespread, together with sorghum, sesame, peanut and sugarcane. Rice, vegetables and fruit are predominant in those places where it's easier to get water instead. Cotton has been cultivated since ancient times in the savanna region, and weaving has been practised since the foundation of the earliest Mossi reigns, and is still one of the most common handmade activities in villages; other typical villages' activities are small livestock of hen, pig and goat. Metalworkers and potters are also common. Mining is quite important and the prevalent materials are gold, manganese, limestone, marble and antimony.

Burkina Faso has many problems concerning to dryness of the climate, the advanceness of the desert and the presence of malaria in wet zones. Its Human Development Index (depending on life expectancy, education and GDP per capita) is 0.402, which is a very low value. Moreover the poverty of the subsoil and the difficulty in communication worsen the economical situation, as it's shown by the fact that import is increasing more than export. As in many other African countries the central government has launched programmes to improve the condition of rural areas, but often these forced actions are not shared by local communities and are likely to fail. In this context actions promoted by the population are very important, in order to revamp rural areas, face desertification and restore fertiles soils, increase agricultural production.

1.1.1 Geomorphology

Burkina Faso lies mostly between latitudes 9° and 15°N, and longitudes 6°W and 3°E. It is made up of two major types of countryside. The larger part of the country is covered by a peneplain, which forms a gently undulating landscape with, in some areas, a few isolated hills. The southwest of the country, on the other hand, forms a sandstone massif, where the highest peak, Ténakourou, is found at an elevation of 749 meters. The massif is bordered by sheer cliffs up to 150 m high. The lowest point is in the south part of the country, on the Black Volta (200 m). The average altitude of Burkina Faso is 400 m and the difference between the highest and lowest terrain is no greater than 600 m. Burkina Faso is therefore a relatively flat country.



Figure 1.3: Morphological map of Burkina Faso [8].

1.1.2 Idrography

There are three river valleys in the country: Niger's one, in the North (but Niger river does not pass through Burkina) extended $72,000 \text{ km}^2$, Comoè's and Volta's ones in the centre; Volta river, with a catchment of $120,000 \text{ km}^2$, is the most important one. It is formed by three rivers: Black Volta, White Volta and Pendjari which then reunite in Ghana generating a single river. Comoè's catchment has an extension of $18,000 \text{ km}^2$ and is situated in the south-west, near to the Ivory Coast border.

1.1.3 Geology

The most important formations of west Africa are (Figure 1.4):

- sedimentary rocks of tertiary and quaternary age in the basin of Senegal and Mauritania (in the area of Dakar and Nouakchott) and in Lullemeden basin in east;
- primary formation in the North-West of Occidental Africa;
- sandstone of the Precambrian age all over the south part of the sedimentary basin of Taoudènit sited in the South and in the North-West part of Mali and in a large part of Ghana;

- metamorphic formation of the middle Precambrian age covering most part of Burkina Faso and Ivory Coast.

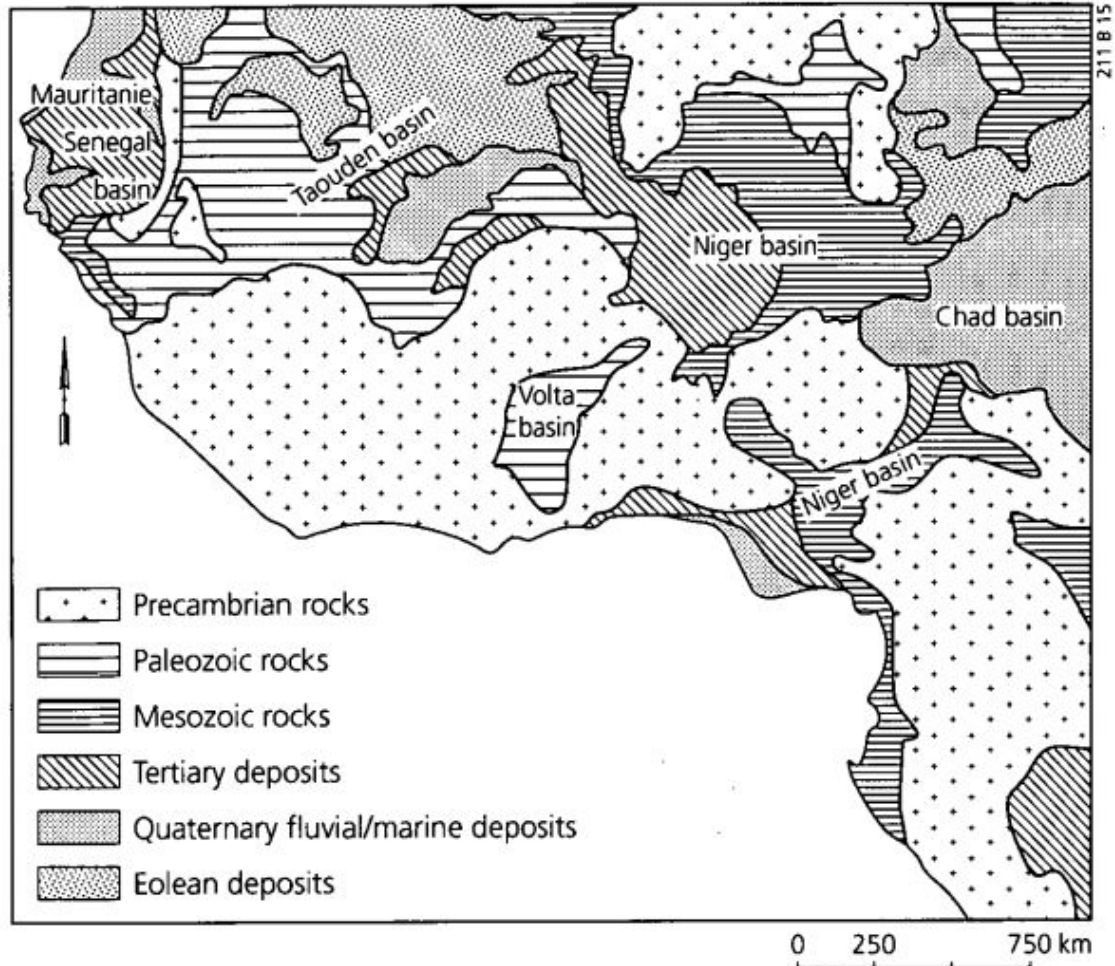


Figure 1.4: Geological map of West Africa [39].

Burkina Faso is situated over two geological system: a Precambrian base and the sedimentary cover. The first one is composed by metamorphized sediments, meta-igneous rocks and many plutonic granites, occupies three quarters of the country and has an age of about a billion years. Sedimentary cover, usually 20 to 100 cm deep, includes primary and tertiary infracambrian formations and also recent; the latest ones are the dune in sedimentary formations sited in the northern part of the country (Gondo plain) and the widespread laterithic shell. The western border of the area is occupied by the edges of an ancient lakes, an old sedimentary basin from the Precambrian to the Ordovician age. Sandy rocks, shale and lime rocks are herein presents. Burkina Faso has a good reserve of golden deposits, where it is possible to find quartz or in some occasions sulphate minerals, in some areas in cristalline deposits or in alluvional gravels. They are in the North of the country, except for Poura and Dossi which are in the South-West.

1.1.4 Pedology

Studies on the soil have been performed by the Bureau National de Sols (BUNASOL), a governmental structure of Burkina Faso, and have found that the territory is covered by the following soils:

- lithosol and soils of class I (mineral raw soils), characterized by little or none chemistry and biology alteration, with some parts of organic material less than 20 cm deep and almost absent biologic activity;
- few developed soils, with little erosion and with some parts of organic material less than 20 cm deep;
- *vertisols*, mostly situated in valleys, generally characterized by high expansion power clay, which increase and decrease their volume according to the alternance of wet and dry period;
- dark antropical tropical soils, which represents the best soils of the country and are often situated in depression areas, in Gondo plain and on the uplands;
- sub-arid dark soils, present in the northern part of the country, have an highly wet organic material, highly mineral alteration, high standard of free iron and sometimes a red colour;
- ferruginous soils spread in the greater part of the country which have a generally scarce organic material;
- ferrous soils weakly or on average degraded, which developed on few wet materials and on schistose materials or stoneware; they have a complete alteration of primary minerals, abundance of synthesis products (e.g aluminium silicate), a well developed organic material;
- hydromorphic soils situated in the alluvial plains.

The area of cultivable land is about 8,900 km^2 , while forests and grazing land are about 14,000 km^2 , and their total is the 8% of the national territory.

1.1.5 Climate

Atmospheric circulation above West Africa depends both on high tropical pressures and the position of "meteorological" Equator, whose seasonal movements influence air fluxes and the consequent weather.

During boreal winter the meteorological Equator moves South until 4° N, under the influence of Azore and Sahara anticyclone. In this way there are two circulations of trade winds, of different nature, incentivized by the two anticyclons which determines the weather during the dry seasons, lasting four months in West Africa and until seven in North Africa.

Burkina Faso has a primarily tropical climate with two very distinct seasons. In the rainy season, the country is subjected to heavy rains; in the dry season, the harmattan – a hot dry wind from the

Sahara – blows. The rainy season lasts approximately four months, from May/June to September, and is shorter in the north of the country. When harmattan blows it carries sand from the Sahara and increases desert advance. During the rainy season, instead, trade wind from South-West blows from the sea and causes short heavy rains; water can't seep through the land and flows away carrying the thin fertile layer of soil. For this reason rain is one of the predominant causes of soil impoverishment. Near to the Ivory coast border, in the South-West, total annual volume of rainfall is about 1300 mm, whereas in the North-East is less than 200 mm.

The different climatic zones of West Africa are shown in figure 1.5

- Saharan region: The Sahara, or Saharan Region, stretches across the whole northern extent of West Africa, formed by the Sahara Desert. It consists of a variety of arid landscapes varying from sandy sheets and dune fields to gravel plains, low plateaus, and rugged mountains. Vegetation cover is sparse to absent, except in depressions, wadis, and oases, where water is present at or just below the surface. Average annual rainfall ranges from 0 to 150 mm per year;
- Sahelian region: The Sahel, or Sahelian Region, is a broad semiarid belt, extending from the Atlantic Ocean to Sudan, averaging about 350 km wide. Climatically, it is characterized by average annual rainfall between 150 and 600 mm, with great variability in amount and timing in a given year. It has an ecologically dry season of 8 to 9 months. Vegetation in the Sahel is generally characterized by open herbaceous types (steppe and short grass savanna) often mixed with woody plants. It is known for its thorny trees, particularly from the genus *Acacia*, and mostly annual grasses from the genera *Aristida* and *Cenchrus*. The number of woody plant species is relatively low. The present physiognomy of Sahelian vegetation results from long-term human and animal presence. Annual grass fires often sweep across its landscapes where there is ample grass cover.;
- Sudanian region: The Sudan, or Sudanian Region, consists of a very large belt immediately south of the Sahel, with average annual rainfall between 600 and 1,200 mm and an ecologically dry season of 5 to 7 months. It is the domain of the savanna — ranging from open tree savannas to wooded savannas to open woodlands. As in the Sahel, rainfall is spread over the months when the sun is high (typically May to October). The short, annual grasses of the Sahel are replaced in the Sudan Region by tall, perennial grasses, mainly of the genus *Andropogon*;
- Guinean region: The Guinean Region lies immediately south of the Sudanian Region, generally defined by average annual rainfall between 1,200 and 2,200 mm. This is the domain of the seasonally wet-and-dry deciduous or semi- deciduous forest. Despite the relatively high rainfall, this region has a distinct dry season of 7 to 8 months, which distinguishes it from the Guineo-Congolian Region. The forest canopy is generally dense and closed, forming over a heterogeneous woody understory. Tree height is high, averaging 18 to 20 m;
- Guineo-Congolian region: The Guineo-Congolian Region is the wettest in West Africa, with average annual rainfall between 2,200 and 5,000 mm. The rainfall can be distributed across

most of the year, or in two rainy seasons with short drier periods between the rains. The forests are dense, with trees reaching over 60 m. The upper tier usually has a discontinuous canopy, towering over a lower, dense canopy. In the undergrowth, woody climbers and epiphytes are characteristic. Herbaceous ground cover may be found but can also be absent.

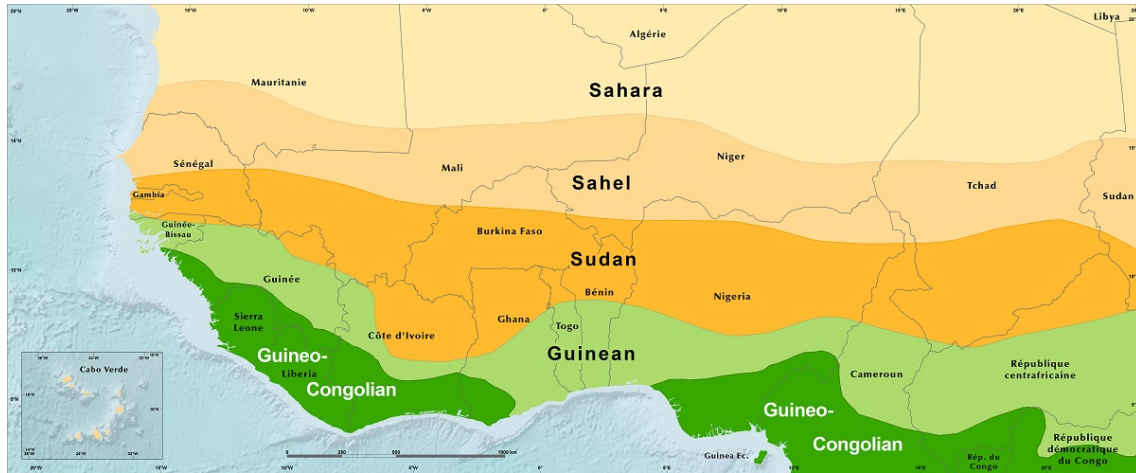


Figure 1.5: Climatic zones of West Africa [8].

Pluviometric data are provided by ASECNA (aerial navigation safety agency) and DSN (meteorological service). Rainfalls start in April in the South, irregular in the beginning and then more constant, and spread to the North in June; their maximum is in August and they stop quite rapidly in September.

An important aspect is rain variability, both in space and in time, which is one of the main causes of the high drought risk present in many parts of the country. For example, are shown some mean annual data collected in the station of Dori:

- 503.2 mm in 38 days between 1922 and 1948;
- 612.1 mm in 53 days (wet episode) between 1949 and 1967;
- 432.7 mm in 44 days between 1968 and 1988.

An increase in temperatures is associated to the decrease in rainfall volume, worsening the difficult situation of the country.

1.1.6 Temperatures

During the year it is possible to find four different periods, two very hot and two quite fresh:

- the first hot period is in March/April, and the mean maximum temperatures are about 37°C in the South and 41°C in the North of the country, the mean minimum temperatures are about 25°C;

- the second hot period is after wet season and it's colder than the first one: the mean maximum temperatures are between 34°C and 38°C, while the mean minimum temperatures are about 21°C;
- the fresh period from December to February has the mean maximum temperatures between 33°C and 35°C, while the mean minimum temperatures are 14°C to 19°C;
- the second fresh period is the wet season, when humidity raises the maximum values because of the trade wind from the sea, which causes heavy rains especially in the South of the country. Minimum and maximum temperatures have important variations due to irregularity of rains, and this variability in time and space, both with shortness of wet season, is a limiting factor for vegetal production and the most damaging for vegetal cover.

Dew formation is important in the South where formation between 0.8 mm and 1 mm have been observed.

1.1.7 Vegetation

The different vegetation zones of West Africa are shown in figure 1.6 and three of them are predominant in the area of the present study:

- steppe zone;
- brush-grass savannah zone;
- deciduous forest-woodland savannah zone.

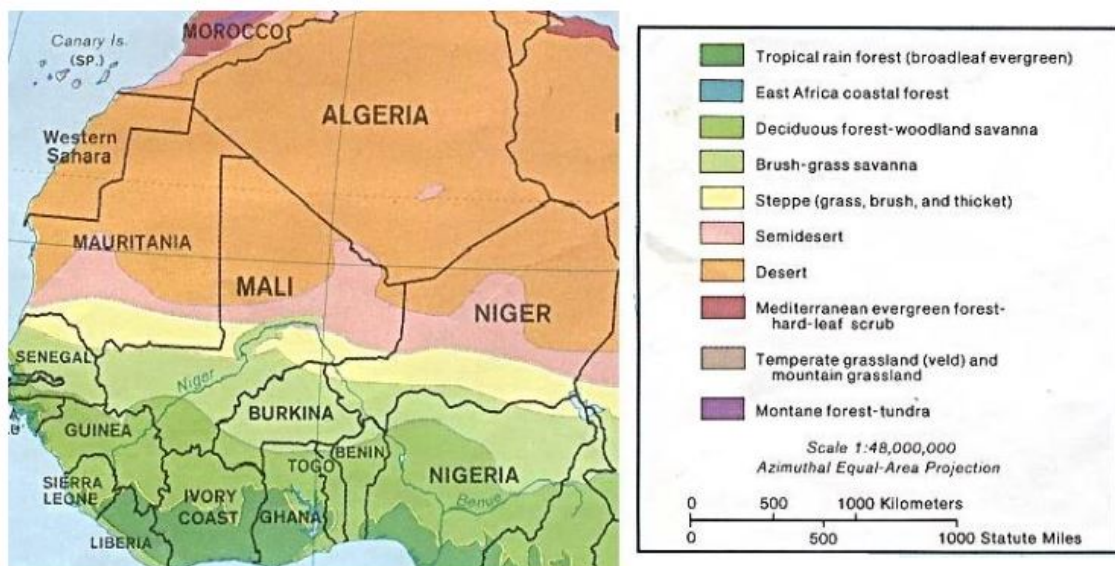


Figure 1.6: Different zones of vegetation in West Africa, from the *Perry-Castaneda Library Map Collection*.

Steppe zone is characterized by the presence of acacia group, which is widespread on sandy soil. It includes *Acacia senegal*, *Balanites aegyptiaca*, *Boscia senegalensis*, *Ziziphus mauritiana*, *Capparis decidua*, *Aristida mutabilis*, etc. The worsening of vegetal cover is showed by the diffusion of *Balanites aegyptiaca* and *Cenchrus biflorus* (Cram Cram), while for grass the *Schoenefeldia gracilis* covers for *Chloris prieuri*.

Brush-grass savannah is divided into three sectors (Jaeger, 1968):

- Sudan-Subsaharian sector (500 to 700 mm of annual rainfall);
- Sudan sector (700 to 1000 mm of annual rainfall);
- Sudan Guinean sector (1000 to 1600 mm of annual rainfall);

Sudan-Subsaharian sector is characterized by the vegetal group of *Acacia seyal*, on clay soil, and *Combretum latinosum* on lighter soil. *Acacia seyal* group include high trees, like *Adansonia digitata* (Baobab), *Sterculia tomentosa*, *Guiera senegalensis*, *Maytenus senegalensis*, *Combretum glatinosum*, *Anogeissus leiocarpus* and spiny species like *Balanites aegyptiaca* and *Ziziphus mauritiana*.

1.1.8 Wildlife

In Burkina Faso there are many species of wild animals. Elephant is quite common and there are more than in many other country in West Africa. It is possible to find also lions, buffalos and leopards; the red buffalo or dwarf is also present, a smaller reddish-brown animal which looks like a fierce kind of short-legged cow. Other large predator are the cheetah, the caracal or african lynx, the african wild dog (one of the most endangered species) and the spotted hyena.

There are four national parks in Burkina Faso:

- W national park in the East (in common with Benin and Niger)
- Arly national park in the East;
- Léraba-Comoé Classified Forest and Partial Reserve of Wildlife in the West;
- Mare aux Hippopotames in the West.

1.1.9 Naam groups

During the last decades throughout the Sahelian region many local organisations have developed in order to face the difficult economical, social and environmental situation. An important example of this groups is the Naam movement, arised in Burkina Faso in 1967 and formed by many different spontaneous farmers' groups which operate to improve life conditions in villages according to traditional cultures and techniques. During the years the Naam movement has become an important rural movement, non-party and non-religious, with a complex inner organisation and

recognised also by the international community.

Their way of action is based on the restoration of an ancient traditional kind of association: the *Kombi-Naam*. It was, in the tradition, a young seasonal association, for males from 20 to 35 years old and females from 15 to 20 years old, organized so that everyone had a specific role in a sort of "social game", and in this way young people were introduced to adults' society. The main activities of the groups were the cultivation of community fields, cultural activities, socialization, common interest works in villages and extraordinary work in fields of those who requested it.

In the present form, Naam groups are based on the idea that in a difficult situation it is up to the inhabitants of the region to become aware of the importance of the changes happening and to find a future direction. The basic principle of Naam groups is that every development must begin from "what the farmer really is, what he knows and is familiar to him and what he is able to do". Nowadays Naam groups are present in almost all the villages as associations made of volunteers, organized in a unique federation (in 1991 were found 4,263 Naam groups in Burkina Faso, jointed in 56 regional unions).

Naam groups participate in development programs as representant of the farmers to improve life conditions of rural areas of Burkina Faso; they also collaborate with international projects to increase their knowledge and possibility of intervention.

1.2 Mogtedo

Mogtedo is a town situated about 80 km East from the capital Ouagadougou in the Plateau-Central region; it is in the province of Ganzourgou and is the capital of Mogtedo Department which includes also other eight villages. Its population was estimated 15,076 in 2005 for the entire department and 4,445 for the town of Mogtedo with a growth rate of 1.15% (INSD, 2008). More than 70% of the population has a birth certificate (source: Monographie de la region du Plateau Central, November 2009) and the potable water access rate is 77.6% (INO, 2015).

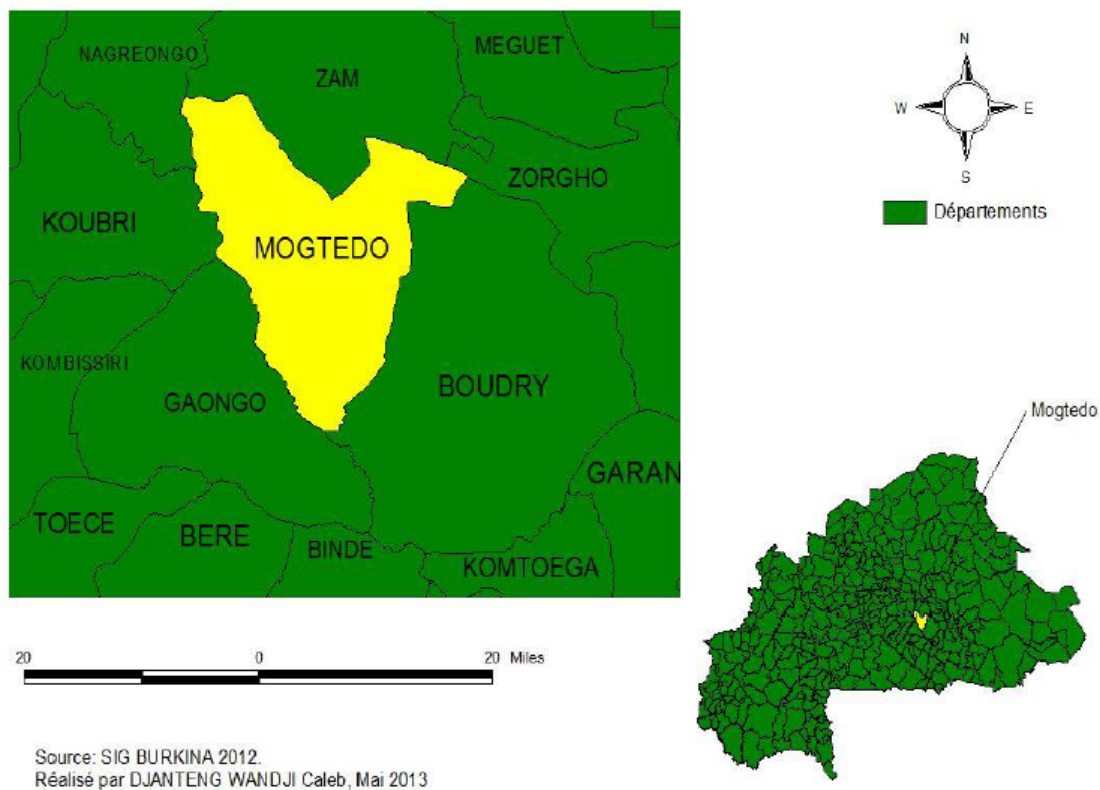


Figure 1.7: Location of Mogtedo Department in Burkina Faso [6].

1.2.1 Soil and elevation

Mogtedo area is quite flat, as the entire Plateau-Central, and there are only some sparse hills. The average elevation is about 280 m.

As a geologic point of view, it is possible to find some volcanic-sedimentary outcrops, with sectors of metavolcanic rocks over a migmatites layer.

The different kinds of soil that are possible to find are the following ones:

- alomorphic soil over sandy clay material and few evolved hydromorphic soil over gravel material (class of Vertisoils and paravertisoils); it occupies an area of 231.1 km^2 , which is the 48.7% of the total;

- lithosol over ferrous shell (class of few evolved soils); it occupies an area of 36.5 km^2 , the 7.7% of the total;
- few evolved hydromorphic soil over gravel material and pseudogley soil over different origin clay materials (class of Sesquioxides soils); it occupies an area of 207.2 km^2 , the 43.6% of the total.

1.2.2 Climate and vegetation

Climate in Mogtredo is the one of Sudan-Sahel zone (figure 1.5), with a wet season of four to five months.

Vegetation is damaged because of human activities (with frequent brush fires) and clearance of woodlands. Trees density is quite low; the greater part of brush savanne is found to be in the South-East and in the Centre-East of the catchment. The most important human centres and cultivable fields are situated near the main rivers.

The mean annual rainfall in Mogtredo is between 600 and 900 mm.

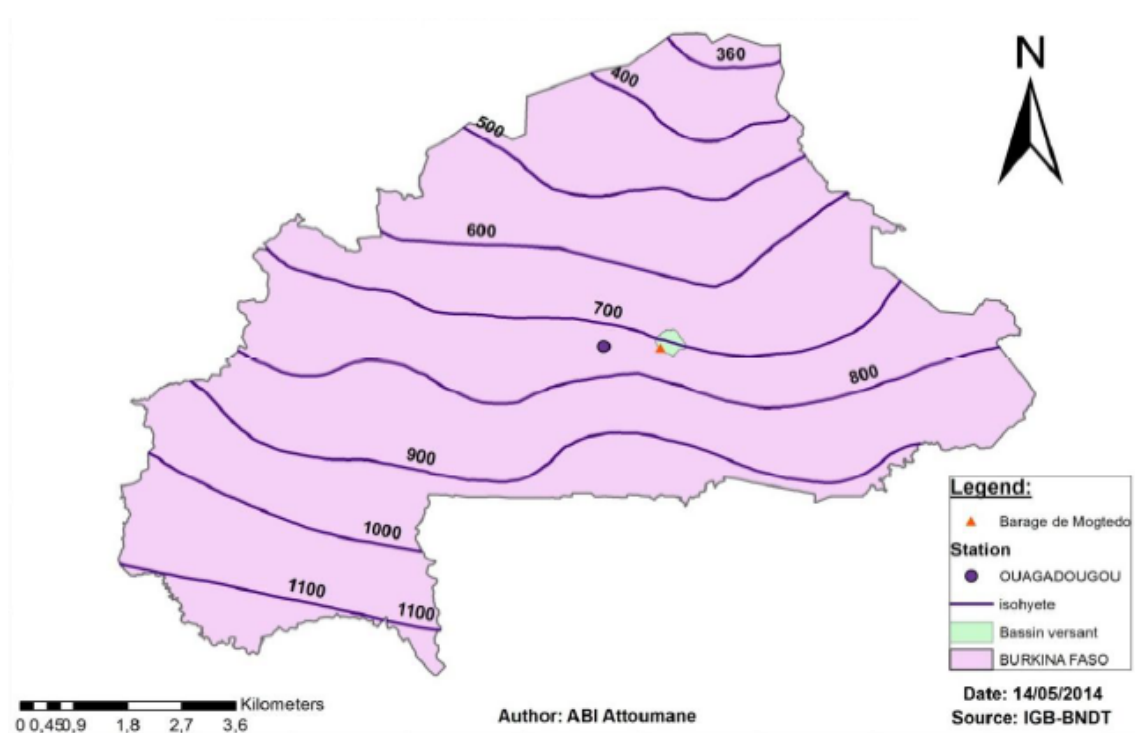


Figure 1.8: Map of Burkina Faso with the position of Mogtredo and isohyets [28].

1.2.3 Hydrography

The hydrographic network is made up by two temporary rivers: the main river is called Bomborè (which named the catchment) and flows from North to South, the other one is in right bank. They flow mainly by a rocky substratum and the river beds are locally occupied by some recent

sand deposits of 3 to 4 m. The more the confluence with Volta river becomes closer the more Bomborè bed contracts because of regressive erosion.

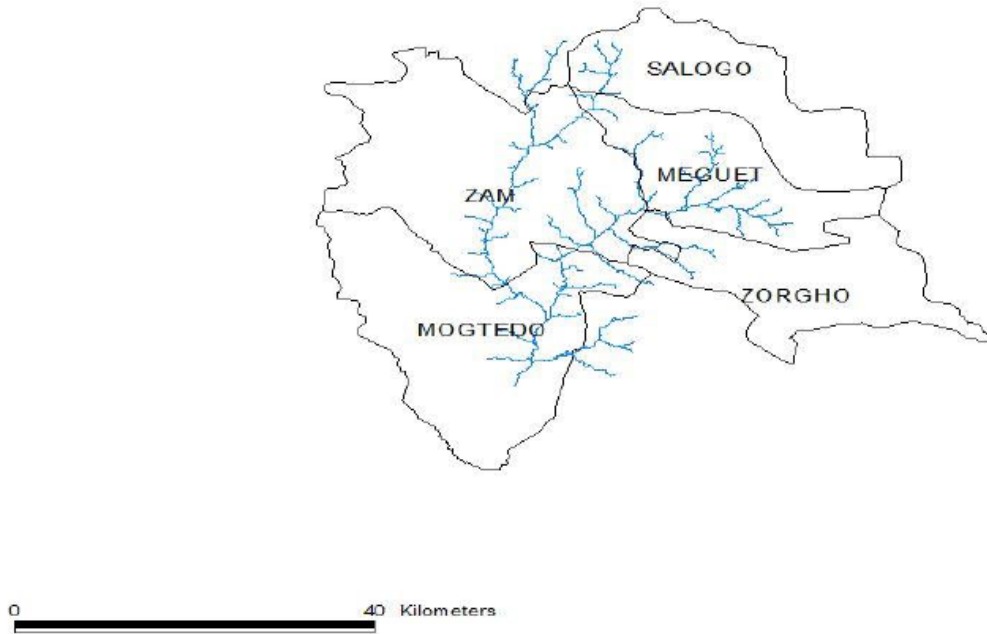


Figure 1.9: Hydrographic network of Bomborè catchment near Mogtedo [21].

Some general data of the catchment are herein provided:

- the surface of the catchment is $S = 477km^2$;
- the length of the perimeter of the catchment is $P = 93km$;
- density index (also called shape coefficient), is calculated as the ration between the perimeter P and the circumference of a circle with the same surface; it is found by the formula $Id = 0.282PS^{-1/2}$, where P is expressed in km and S in km^2 . In this case $Id=1.2$;
- length of equivalent rectangle: it is the rectangle which has the same surface, the same density index and the same hypsometric distribution of the catchment; it is calculated by the equation $L = S^{0.5} \frac{Id}{1.128} (1 + (1 - (\frac{1.128}{Id})^2)^{0.5})$, where S is expressed in km^2 . In this case $L=32.23$ km;
- drainage density: it is defined as the ratio between the total length of the rivers and the surface of the catchment, $Dd = \frac{\sum Li}{S}$, where Li are expressed in km and S in km^2 . In this case $Dd=1.014$ km/km^2 .

1.2.4 The dam and the basin

It is present an earth-dam built in 1964 of 2600 m length with a maximum height of 5 m. The dam has a lateral spillway of 650 m. The coordinates of the dam are: 00°50' West, 12°11' North; it is situated at 272 m above sea level.



Figure 1.10: Some photos of the spillway and the basin of Mogtedo dam [6].

The initial storage capacity was $10\,561\,100\ m^3$, but this value has considerably decreased during the years because of erosion and consequently sediment transport. Some topographic and bathymetric studies carried out in 2012 by PADI/BF103 (Programme for Development of Irrigation) found a storage capacity of $7\,194\,000\ m^3$.

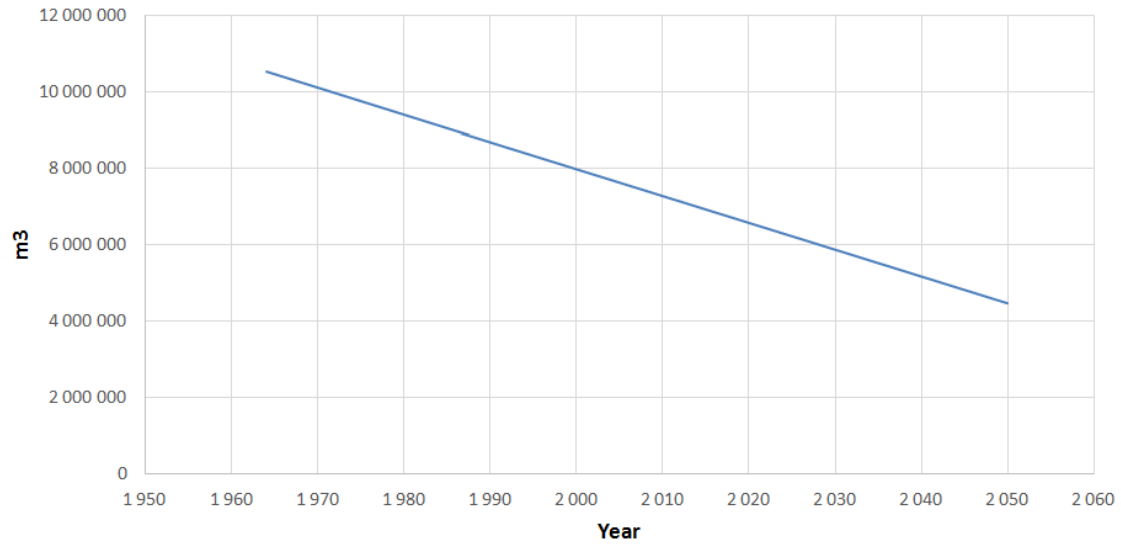


Figure 1.11: Evolution of storage capacity of Mogtedo dam during time (courtesy of Francis Guyon).

As shown in figure 1.11, if conditions remain the same as the past, in 2050 the storage capacity will be a little more than $4\,000\,000\text{ m}^3$. This decrease is a paramount danger for the area of Mogtedo, for which the dam carries out the function of collecting water during the wet season, which is then provided for different uses during the rest of the year. This fact is well shown in figure 1.12, where it is possible to find out that the basin is almost empty at the end of dry season and is rapidly filled by heavy rains of wet season.

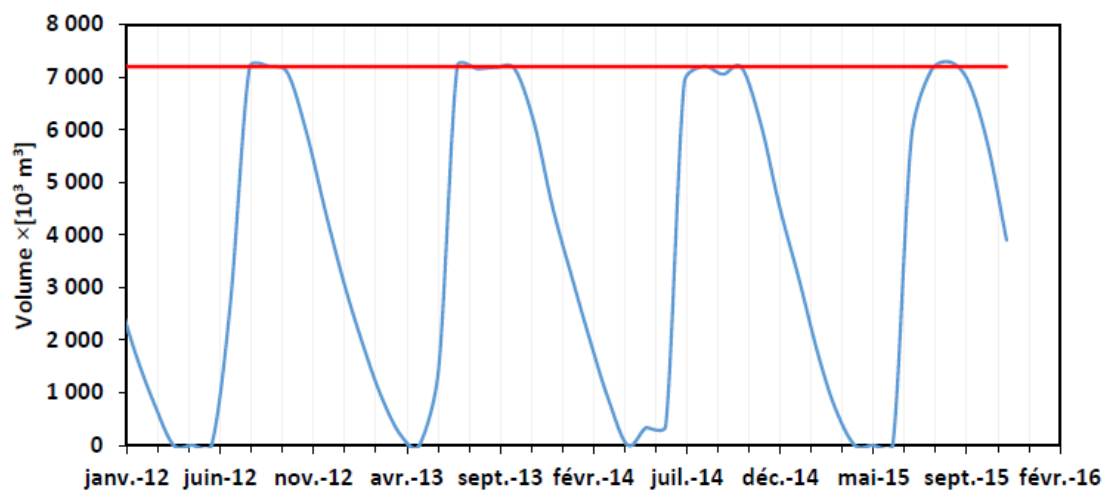


Figure 1.12: Evolution of water volume in the basin during the year [18].

1.2.5 Main activities in proximity of the dam

Irrigation The main activity regarding the dam is irrigation, which is essential for horticulture and rice growing. The most cultivated vegetables are onions, hot peppers, aubergine, cabbage, gumbos, tomatoes, courgettes, cucumber and carrots.

Irrigation is also the use which needs more water. There are two periods of production, one during the wet season and one during the dry season; in every periods are cultivated different products, as shown in table 3. Downline of the dam an area of more than 100 ha is irrigated by gravity; this

DRY SEASON	WET SEASON
cabbage	rice
onion	corn
tomato	white sorghum
aubergine	red sorghum
gombo	millet
pepper	
fresh corn	

Table 3: Products cultivated near Mogtedo dam.

area is divided into different plots of 0.20 ha, 0.25 ha or 0.50 ha of 378 farmers (Francine Ki et al., 2010). Out of this area, about 500 farmer uses pumps and PVC hoses to get water.



Figure 1.13: Cultivated fields near Mogtedo dam (courtesy of Paolo Vezza).

Livestock farming About 500 farmers water their livestock in the basin, with a total of about 35 000 animals. With the diffusion of irrigation access to the reservoir has become more difficult for farmers because of the lack of access points. Farmers which actually water their livestock practice this activity only for three months, from December to February.

During the dry season most farmers dig some pits to water livestock, while during the wet season they lead animals to the borders of backwaters and puddles. They don't move fore more than 3 or 4 km to water livestock (Francine Ki et al., 2010).



Figure 1.14: Hydraulic devices for the irrigation of fields near the dam (courtesy of Paolo Vezza).

Mining activity It has been certified that some mining activity is present near the basin (Djanteng Wandji Caleb, 2013); there are some gold panners facilities and sometimes even women searching for gold.

2 Description of the sites and data collection

2.1 Localisation of the sites

Bomborè catchment near Mogtèdo is divided into four sub-catchment, which are herein named MOG1,MOG2,MOG3 and MOG4.

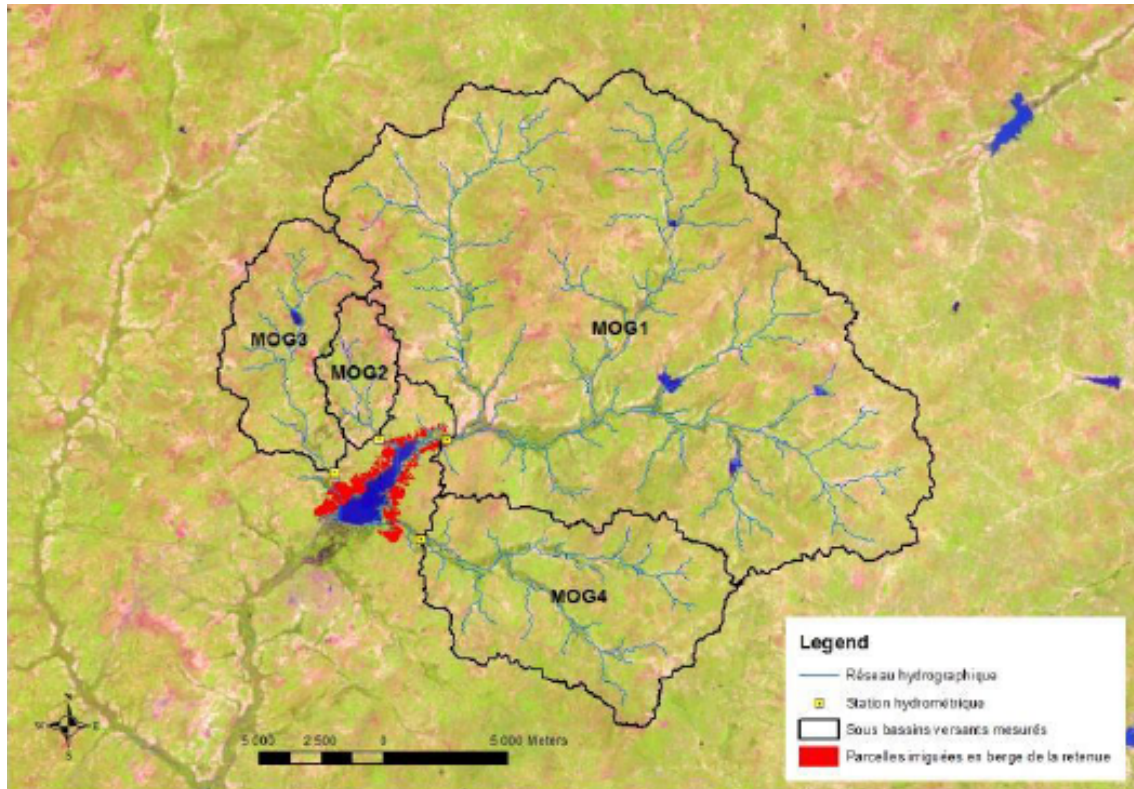


Figure 2.1: Sub-catchments present in the area of the study [17].

The areas of each sub-catchment are the following [17]:

- MOG1: 31 212 ha;
- MOG2: 1 373 ha;
- MOG3: 3 833 ha;
- MOG4: 7 568 ha.

This study was focused on the sub-catchments MOG2 and MOG3, that are the ones where more data were collected that were more investigated.

In these sub-catchment some topographic data were collected; this permitted to get the slope of the rivers using the programme QGIS. In figure 2.2 the measuring points of MOG2 and MOG3 are highlighted.

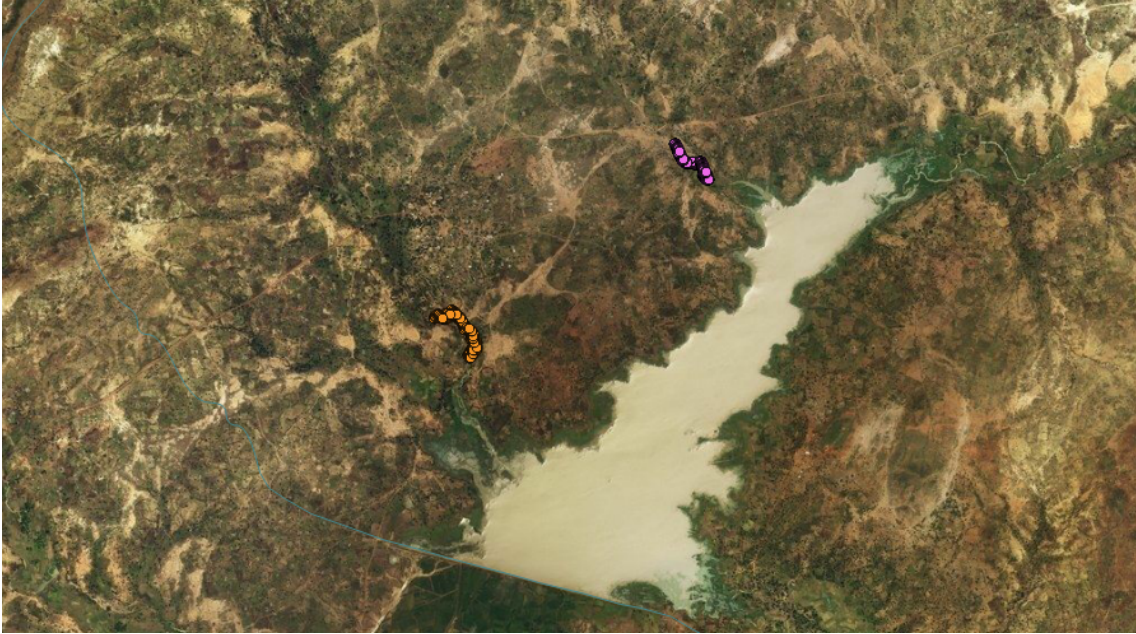


Figure 2.2: Measuring points for MOG2 (violet) and MOG3 (orange).

The values of riverbed slope (i_f) calculated through the topographic data are the following:

- MOG2: $i_f = 0.0033$;
- MOG3: $i_f = 0.0015$.

2.2 Data collection

Field data were collected in 2013 and 2014 during a study managed by Francis Guyon and Eric Hallot [19]. The main object of the study was to evaluate the amount of sediment that is yearly carried in the basin and decrease the available volume. For this reason the attention was focused on the finer part of the grading curve, which represents the suspension load, because fine grains are those who are carried more distant; however some trenches were built to evaluate bedload, even if this part of the study was less developed.

Water height was measured through some pressure probes like those in figure 2.3.



Figure 2.3: Example of pressure probes used in the study [17].

Water was collected using some cans positioned at different heights on a rod, with two lips for each can to make water enter into it: this was necessary because suspended particle concentration is different according to water height, and in this way it is possible to obtain a representative value for each event by the mean of the values collected at different heights.



Figure 2.4: Cans used for the collection of water samples [17].

Water height data were converted into discharge data through the rating curves of the two sections, showed in the next figures.

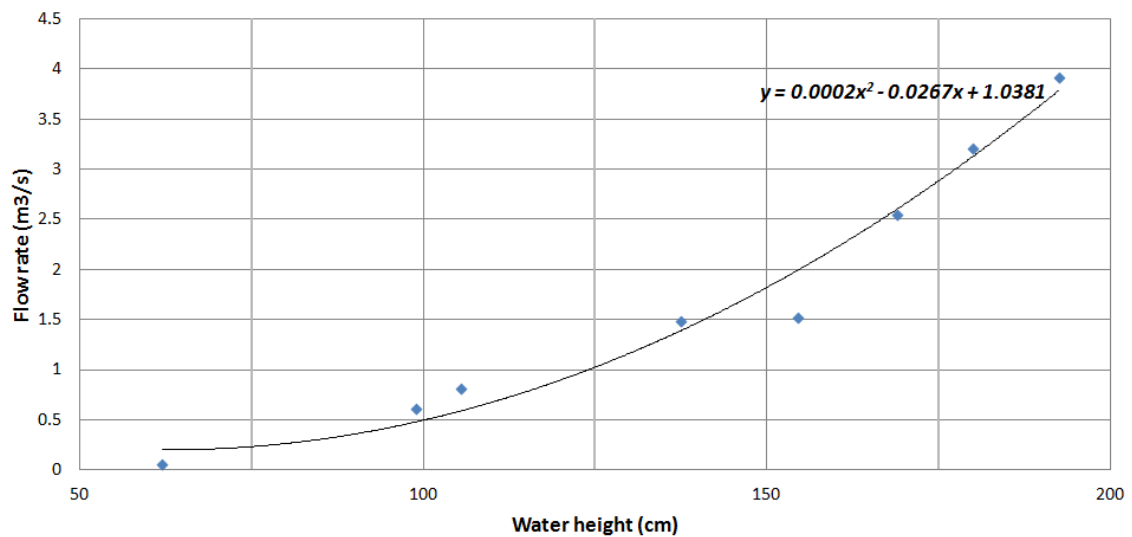


Figure 2.5: Rating curve for measure station in MOG2.

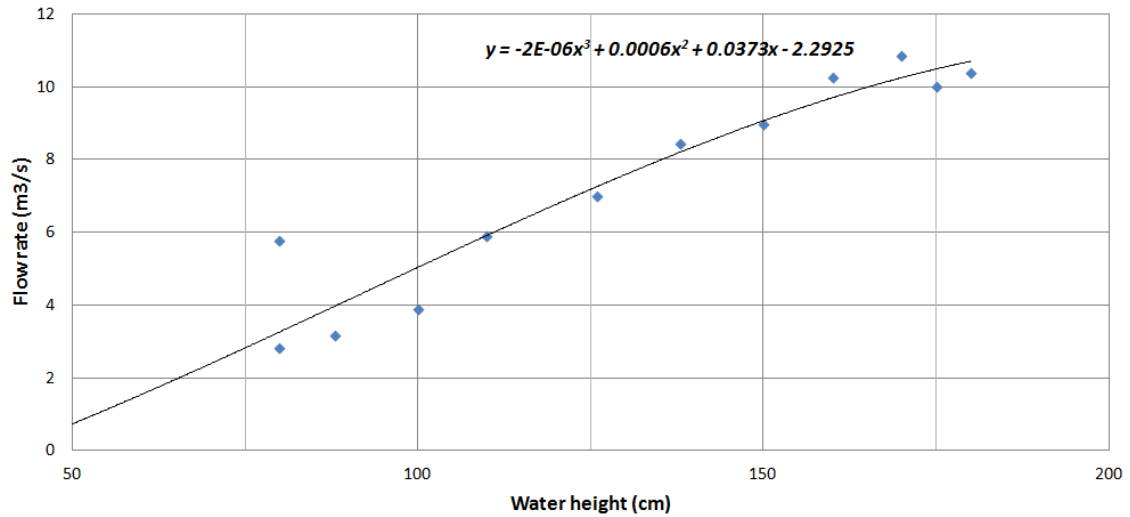


Figure 2.6: Rating curve for measure station in MOG3.

Water height data and flow rate data were available as complete hydrograms; the form of hydrograms in sub-sahelian rivers is usually characterized by a first part where discharge rapidly increases, followed by a decreasing part where discharge declines at first quite rapidly and then more slowly. In the following figure is shown a typical hydrogram as those considered in this thesis.

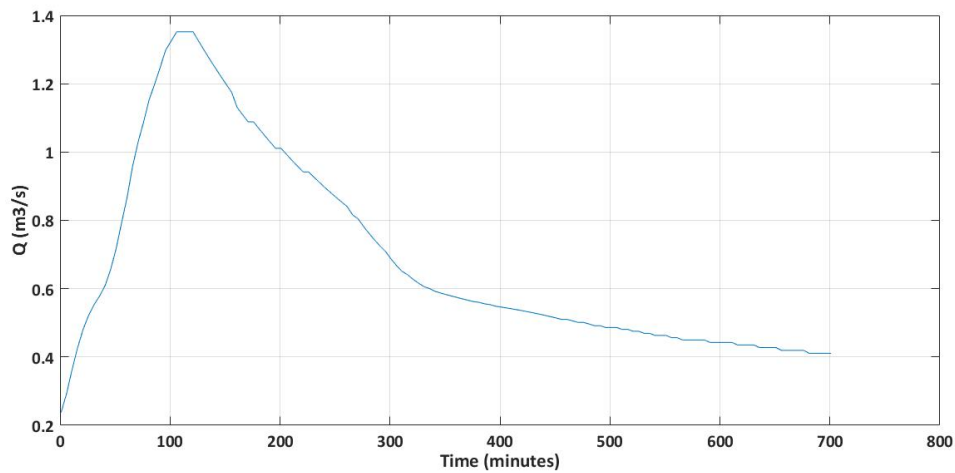


Figure 2.7: Hydrogram of a flood occurred in 2013 in MOG2 sub-catchment.

An interesting fact is the relation between mean and maximum flow rate of each flood; if we plot on a graphic the points representing each flood it is possible to find out if there is a good correspondence. This is true for MOG2 sub-catchment, which has less flow rate values, but for MOG3 there is less correspondence (see figure 2.8). Probably results for MOG3 are therefore less

accurate since they have been calculated through the mean flow rate of the floods.

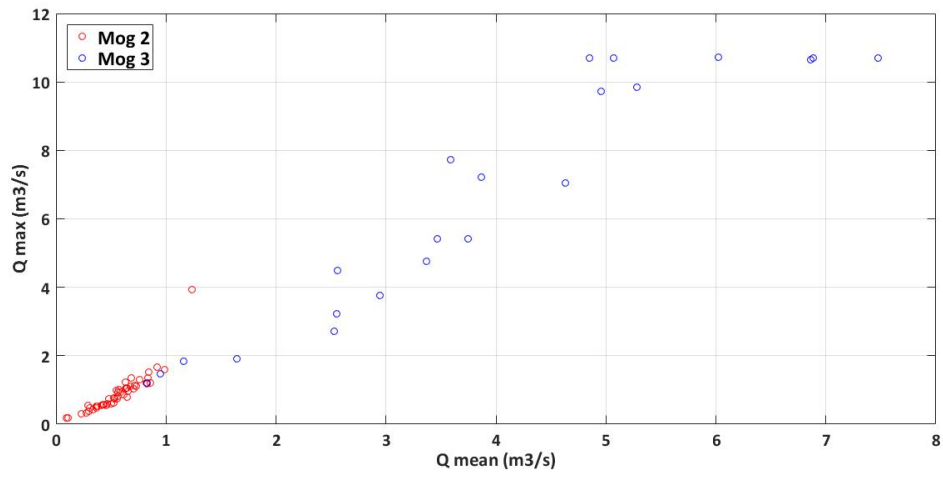


Figure 2.8: Relation between mean flow rate and maximum flow rate for every flood.

2.3 Cross sections

The knowledge of the cross sections at the measure points is of paramount importance to find out some informations that are necessary to compute sediment transport, such as the hydraulic radius and the wetted area. In this study cross sections are known through a sequence of points which define the perimeter. The cross sections for MOG2 and MOG3 are shown in the following figures. Horizontal distance starts at the beginning of the section (the first point), while elevation does not represent the value over sea level but is defined in a custom scale, whose purpose is only to explain the vertical development of the section and not its absolute height.

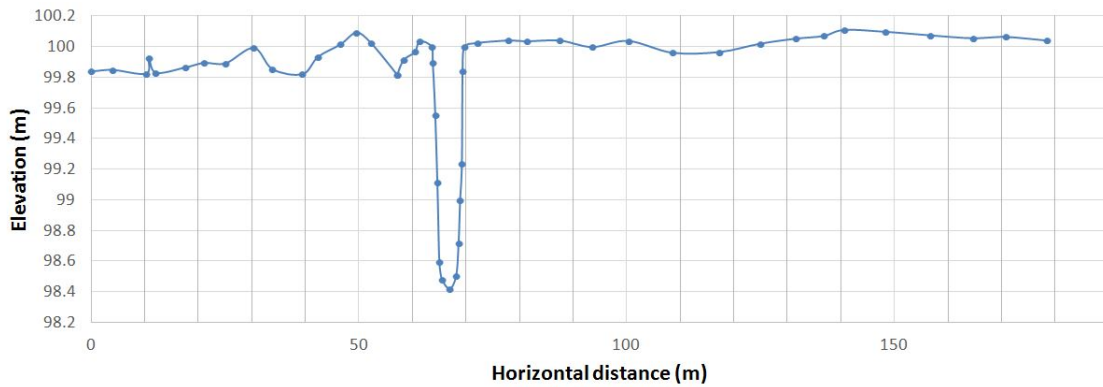


Figure 2.9: Cross section of the measure station in MOG2.

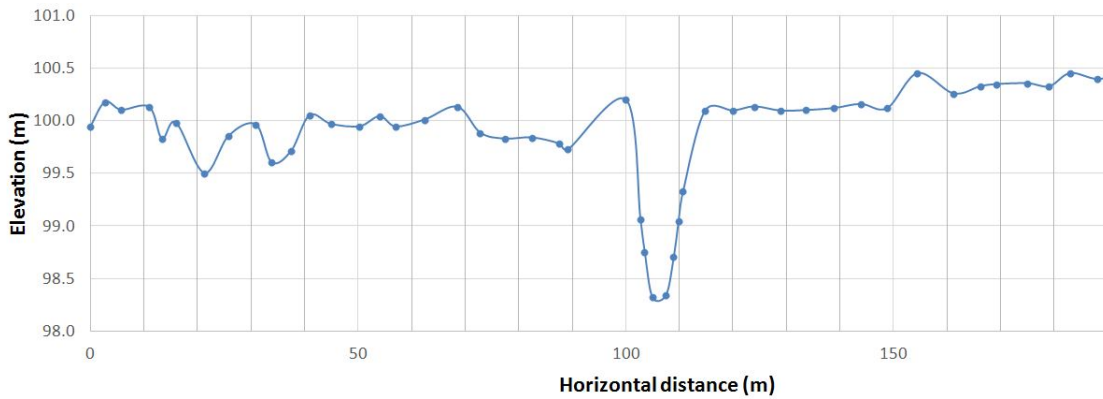


Figure 2.10: Cross section of the measure station in MOG3.

To define the parameters which are needed for this study the knowledge of the previous information is not enough; in fact the points that define the cross sections are too sparse to be used in the MATLAB code which has been written for the calculations. For this reason the river bed has been interpolated with a polynomial function (using the minimum square criteria) to obtain a continuous curve. The degree of the interpolating polynome has been changed to find a better

approximation, and a good result has been achieved with a six degree polynome. The results are shown in figures 2.11 and 2.12.

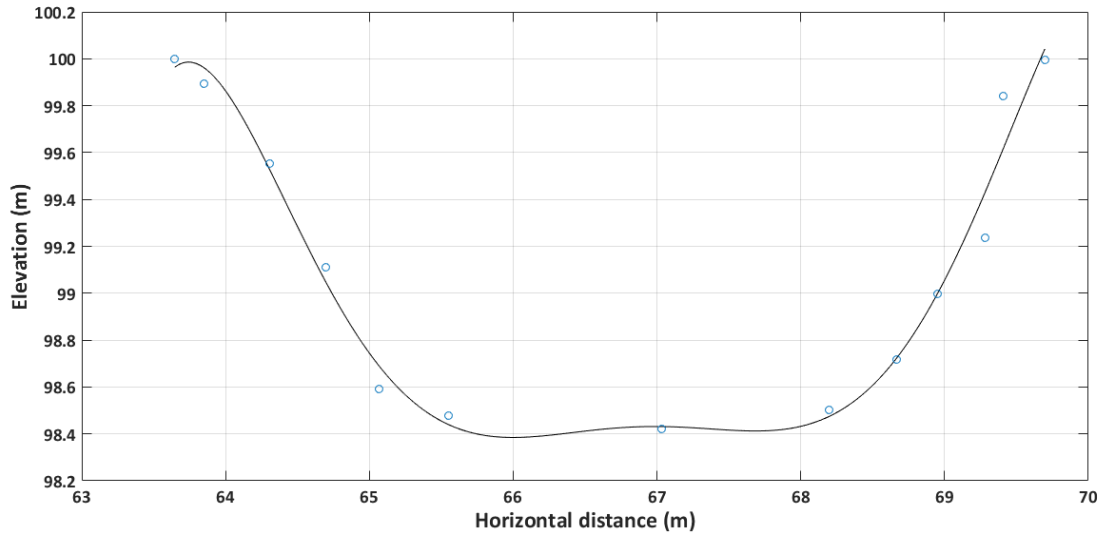


Figure 2.11: Interpolation of MOG2 cross section.

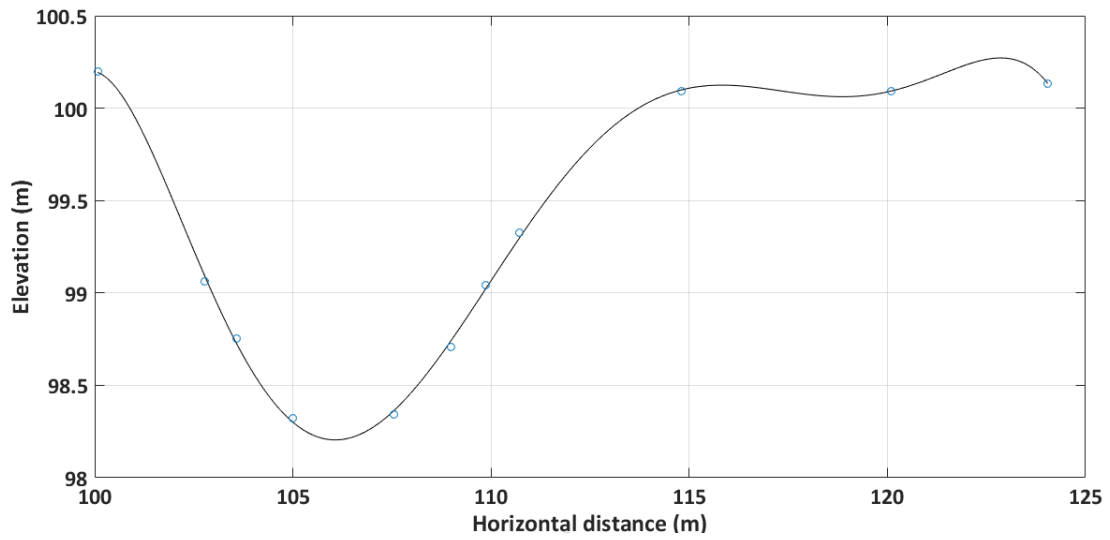


Figure 2.12: Interpolation of MOG3 cross section.

2.4 Sample of sediment

The research for some samples of sediment from Mogtedo basin was unfortunately fruitless, also because of the situation in Burkina Faso which worsened in the last months when there was an attack in the capital Ouagadougou.

However some data from Laaba basin, situated in the North of Burkina Faso, were available from a previous research that professor Paolo Vezza carried out in that place [16]. As explained, Burkina Faso is a quite flat country, and the orography of Laaba region is similar to Mogtedo's one; the hydrological regime of the two sites is also similar. The assumption that Mogtedo sediment is similar to Laaba's should not be wrong, and Laaba's sediment should represent the best approximation available. More precise calculation could be done in future with Mogtedo data to improve the analysis.

In the following figures are shown the granulometric curve of the sediment and the tools used for its determination.

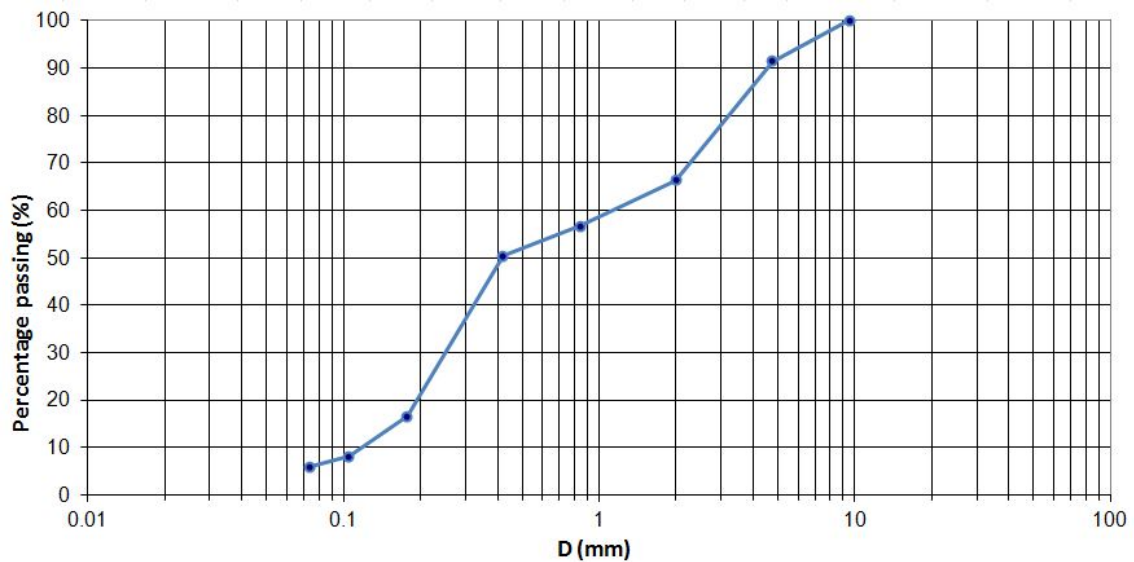


Figure 2.13: Grading curve used in the present work (courtesy of Paolo Vezza).



Figure 2.14: Tools adoperated for the determination of the grading curve, with the sieves and the precision scale (courtesy of Paolo Vezza).

As regards sediment density, some laboratory experiments carried out at Politecnico of Turin on Laaba's samples permitted to find a value of $\rho_s = 2950 \frac{kg}{m^3}$.

2.5 Analyzed dataset

As explained, rainfall in the Sahelian region is only concentrated in the wet season, where many heavy rains occur. Dataset provided to us were about the hydrograms which define the flood events caused from the rains and the calculated transported sediment. In the following figures are shown the characteristics of the flood events, for the four combinations of sub-catchments and years considered,. The first column represents the progressive number of the events during the wet season; the second and the third columns show the day in which the events started and ended (the hour is not reported for a readability reason); the next column shows the total volume of water passed through the measure sections during the event; the last two columns represent the mean value of the suspended sediment concentration and the value of transported sediment, respectively. The transported sediment is obtained by multiplying the passed volume and the mean concentration.

Event code	Start date	End date	Water volume (m3)	Mean concentration (g/l)	Transported sediment (tons)
1	27/05/2013	27/05/2013	16 543	4.26	70.46
2	30/05/2013	30/05/2013	9 178	4.26	39.09
3	15/06/2013	15/06/2013	9 987	11.81	117.91
4	17/06/2013	18/06/2013	11 732	3.68	43.21
5	23/06/2013	24/06/2013	7 888	13.66	107.75
6	27/06/2013	27/06/2013	38 110	18.07	688.84
7	02/07/2013	02/07/2013	16 484	11.20	184.70
8	07/07/2013	08/07/2013	4 877	13.08	63.79
9	24/07/2013	24/07/2013	13 576	14.95	202.98
10	02/08/2013	02/08/2013	21 410	15.29	327.35
11	06/08/2013	06/08/2013	18 871	12.67	239.07
12	07/08/2013	07/08/2013	27 979	8.97	250.94
13	12/08/2013	12/08/2013	29 072	8.66	251.72
14	15/08/2013	15/08/2013	7 564	28.94	218.89
15	21/08/2013	21/08/2013	14 930	13.96	208.39
16	22/08/2013	23/08/2013	26 267	13.96	366.64
17	03/09/2013	03/09/2013	15 140	10.39	157.32
18	11/09/2013	11/09/2013	2 444	14.63	35.75
19	12/09/2013	13/09/2013	17 538	12.46	218.51
20	17/09/2013	18/09/2013	1 776	10.39	18.45
21	21/09/2013	21/09/2013	4 176	10.39	43.39
22	30/09/2013	30/09/2013	6 216	4.09	25.41
23	02/10/2013	03/10/2013	20 434	23.68	483.84

Figure 2.15: Dataset for Mog2 in 2013.

Event code	Start date	End date	Water volume (m3)	Mean concentration (g/l)	Transported sediment (tons)
1	25/05/2014	25/05/2014	8143.478	3.189	25.97
2	11/06/2014	11/06/2014	5119.444	5.370	27.49
3	13/06/2014	13/06/2014	6316.842	1.820	11.50
4	17/06/2014	17/06/2014	11975.371	11.853	141.95
5	22/06/2014	22/06/2014	9831.202	10.810	106.27
6	03/07/2014	03/07/2014	10499.869	19.639	206.20
7	07/07/2014	07/07/2014	13897.818	16.786	233.29
8	14/07/2014	14/07/2014	7581.874	8.647	65.56
9	17/07/2014	17/07/2014	11734.571	9.338	109.58
10	22/07/2014	23/07/2014	11178.256	9.851	110.11
11	24/07/2014	24/07/2014	9898.668	12.803	126.74
12	26/07/2014	26/07/2014	6724.402	7.315	49.19
13	02/08/2014	02/08/2014	6375.867	8.582	54.72
14	10/08/2014	10/08/2014	11092.278	8.454	93.77
15	12/08/2014	12/08/2014	3284.255	9.772	32.09
16	15/08/2014	15/08/2014	8311.746	19.541	162.42
17	15/08/2014	15/08/2014	10586.557	19.376	205.12
18	16/08/2014	16/08/2014	14223.704	18.678	265.67
19	16/08/2014	17/08/2014	16563.916	42.971	711.76
20	19/08/2014	20/08/2014	13932.376	32.813	457.16
21	22/08/2014	23/08/2014	7077.929	27.142	192.11
22	01/09/2014	01/09/2014	6636.431	22.274	147.82
23	01/09/2014	02/09/2014	8590.505	34.413	295.63
24	04/09/2014	05/09/2014	14960.340	11.652	174.31
25	05/09/2014	05/09/2014	13993.268	19.410	271.61
26	14/09/2014	14/09/2014	13862.286	11.609	160.93
27	16/09/2014	16/09/2014	11630.000	13.076	152.08
28	23/09/2014	23/09/2014	7442.149	4.257	31.68
29	29/09/2014	30/09/2014	7046.997	18.105	127.59

Figure 2.16: Dataset for Mog2 in 2014.

Event code	Start date	End date	Water volume (m3)	Mean concentration (g/l)	Transported sediment (tons)
1	20/05/2013	20/05/2013	41 295.115	9.113	376.32
2	27/05/2013	27/05/2013	4 753.465	9.113	43.32
3	30/05/2013	30/05/2013	4 921.204	9.113	44.85
4	17/06/2013	18/06/2013	6 747.872	13.469	90.89
5	23/06/2013	24/06/2013	23 176.734	19.299	447.28
6	27/06/2013	28/06/2013	213 682.069	8.683	1 855.45
7	02/07/2013	02/07/2013	108 363.017	11.019	1 194.07
8	24/07/2013	24/07/2013	281 731.682	19.299	5 437.08
9	28/07/2013	29/07/2013	285 909.114	6.202	1 773.23
10	02/08/2013	02/08/2013	153 220.812	3.500	536.24
11	06/08/2013	06/08/2013	142 559.440	4.916	700.77
12	07/08/2013	07/08/2013	394 549.658	3.938	1 553.88
13	12/08/2013	13/08/2013	314 054.712	7.412	2 327.83
14	15/08/2013	15/08/2013	45 941.300	10.886	500.12
15	21/08/2013	21/08/2013	52 285.554	2.880	150.59
16	22/08/2013	23/08/2013	342 929.428	2.355	807.46
17	27/08/2013	27/08/2013	31 349.760	3.903	122.37
18	03/09/2013	03/09/2013	91 024.158	8.734	794.97
19	11/09/2013	11/09/2013	8 875.050	13.642	121.07
20	12/09/2013	13/09/2013	117 184.198	18.550	2 173.80
21	30/09/2013	01/10/2013	122 720.490	13.642	1 674.15
22	02/10/2013	03/10/2013	385 106.470	8.728	3 361.23

Figure 2.17: Dataset for Mog3 in 2013.

Event code	Start date	End date	Water volume (m3)	Mean concentration (g/l)	Transported sediment (tons)
1	15/06/2014	18/06/2014	180930.435	12.510	2 263.40
2	22/06/2014	24/06/2014	180930.435	10.693	1 934.70
3	03/07/2014	05/07/2014	54556.351	14.459	788.82
4	07/07/2014	09/07/2014	54556.351	15.697	856.39
5	22/07/2014	24/07/2014	54556.351	24.522	1 337.83
6	31/07/2014	03/08/2014	45201.369	28.449	1 285.94
7	12/08/2014	13/08/2014	45201.369	16.225	733.40
8	15/08/2014	17/08/2014	35846.386	51.409	1 842.84
9	19/08/2014	20/08/2014	32565.538	38.207	1 244.23
10	22/08/2014	24/08/2014	32439.091	53.511	1 735.83
11	01/09/2014	02/09/2014	26452.555	57.275	1 515.08
12	04/09/2014	07/09/2014	26452.555	78.049	2 064.58
13	14/09/2014	16/09/2014	24213.646	41.848	1 013.28
14	18/09/2014	18/09/2014	24213.646	12.259	296.83
15	20/09/2014	20/09/2014	24213.646	13.876	336.00
16	23/09/2014	24/09/2014	24213.646	30.490	738.27
17	26/09/2014	26/09/2014	24213.646	12.181	294.95
18	29/09/2014	03/10/2014	21974.737	57.719	1 268.36

Figure 2.18: Dataset for Mog3 in 2014.

We must notice that in the last figure, meaning dataset for Mog3 in 2014, the shown values were reconstructed and we don't know the entire hydrograms of the floods but only daily values.

3 Sediment transport calculation

3.1 Basic informations of sediment transport

3.1.1 Mobilization mechanisms

Different mobilization mechanisms and the existence of each one are explained considering a saturated granular mass with uniform grain size d , with a thickness D , an angle of internal friction ϕ , ρ_s the density, delimited at the top by a plain interface sloping by an angle θ ; above the interface flows a stream with depth h_0 which produces a stress τ_0 on the mass, considered steady. C is the volume concentration of the particles in the mass, therefore $p=(1-C)$ represents the porosity.

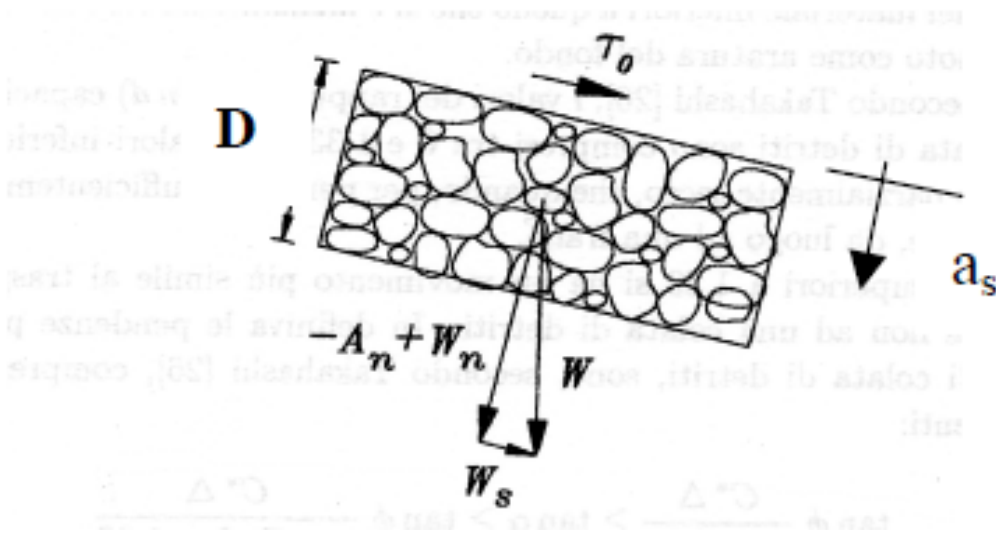


Figure 3.1: Forces balance in a submerged granular mass [4].

The destabilizing forces acting on a parallelepiped of unitary thickness a_s are:

- hydrodynamic force at the bottom: $\tau_0 = g\rho h_0 \sin \theta$;
- weight of submerged material: $W_s = C a_s g \rho_s \sin \theta$;
- weight of interstitial water in the mass: $W_a = (1 - C) a_s \rho \sin \theta$.

Analogously the stabilizing forces are:

- weight of submerged material: $W_n = C a_s g \rho_s \cos \theta$;
- Archimede's push on submerged particles: $A_n = -C a_s g \rho \cos \theta$.

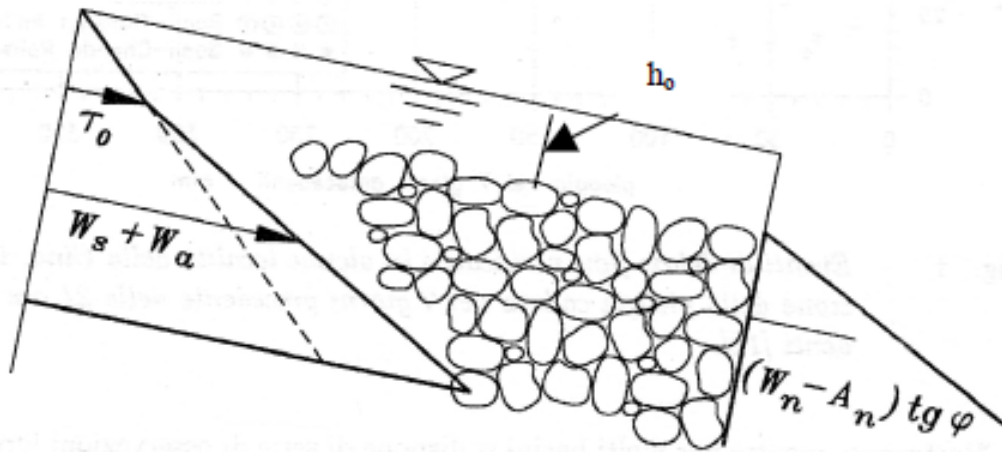


Figure 3.2: Scheme of active and passive stresses in a granular submerged mass [4].

The destabilizing stresses τ_s and the stabilizing stresses τ_l are respectively (see figure 3.2):

$$\tau_s = g \sin \theta C(\rho_s - \rho)a_s + g \sin \theta \rho(a_s + h_0) \quad (3.1)$$

$$\tau_l = g \cos \theta C(\rho_s - \rho)a_s \tan \phi \quad (3.2)$$

The possible combinations of destabilizing stresses τ_s and the stabilizing stresses τ_l are shown in figure 3.3:

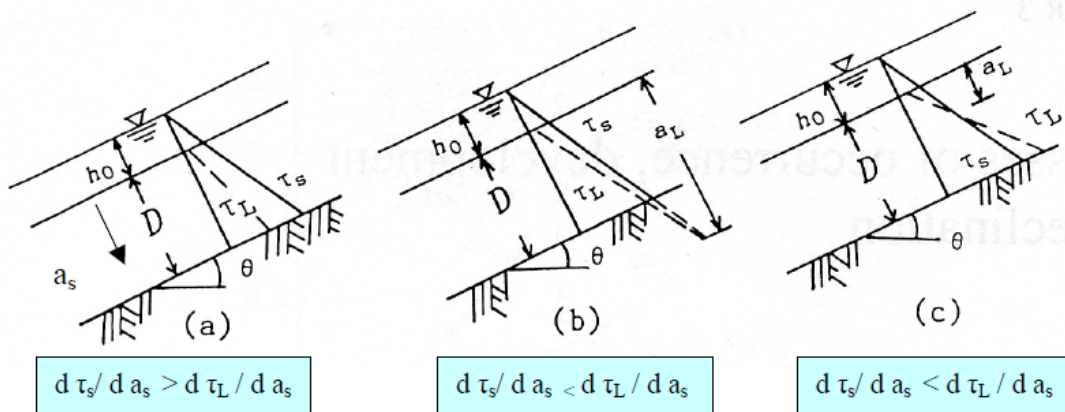


Figure 3.3: Possible combinations of destabilizing and stabilizing stresses [35].

From the previous figure is possible to find out that for the case (a) $\frac{d\tau_s}{da_s} > \frac{d\tau_l}{da_s}$, which means that all layer of granular material is mobilized; in case (b), instead, is $\frac{d\tau_s}{da_s} < \frac{d\tau_l}{da_s}$ but $a_l > D$, so is mobilized the whole layer of granular material again; finally for case (c) $\frac{d\tau_s}{da_s} < \frac{d\tau_l}{da_s}$ as for case

(b), but now $a_l < D$, and only a part of the material is mobilized.

From the equivalence of 3.1 and 3.2 it is possible to find out the thickness a_l of mobilized layer:

$$a_l = \frac{\tau^* d}{C \tan \phi \cos \theta \left(1 - \frac{\tan \theta}{\tan \theta_s}\right)} \quad (3.3)$$

where τ_* is Shields stress defined as:

$$\tau^* = \frac{\tau_0}{(\gamma_s - \gamma)d} \quad (3.4)$$

and

$$\tan \theta_s = \frac{C \tan \phi}{C + \frac{1}{(s-1)}} \quad (3.5)$$

represents the upper limit of the slope which ensures the stability of a saturated mass without superficial flow.

From equation 3.3 the following deductions can be made about the thickness of mobilized material:

1. it is negligible for low values of slope and not very big values of Shields parameter;
2. it grows, until values of about ten to twenty times $\tau^* d$, for values of θ of about 10° to 15° ;
3. it affects the whole mass for values of θ close to the limit value θ_s (equation 3.5), which for dry mass corresponds to the angle of internal friction.

These three conditions represent different mechanisms of sediment mobilization:

- the first one is typical of bedload and suspended load and is called *hydrodynamic mechanism*;
- the second one is the *dispersive-viscoplastic mechanism* typical of the hyperconcentrated flows (immature and mature debris flows);
- the last one is the *quasistatic mechanism* typical of landslides.

3.1.2 Hydrodynamic mechanism

In ordinary sediment transport hydrodynamic actions govern sediment mobilization; this is typical of the valley part of rivers, where slope is lower. Sediment movement depends on hydrodynamic actions of water associated with the presence, irregular in time and space, of turbulent events.

It has been found out that bedload is mostly associated to the presence of *sweeps*, some coherent turbulence structures of the type of return sprays which impact in a slanting way to the side [7].

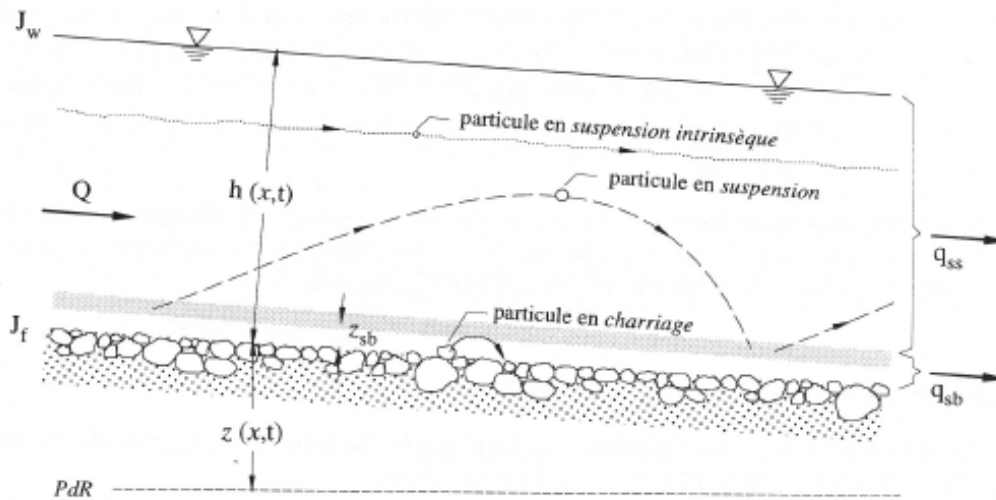


Figure 3.4: Scheme of bedload and suspended load [15].

Suspended transport instead is activated by *burst*, coherent structures that originate from ejection from side region of fluid particles with low longitudinal velocity [22]. Transport is therefore a system where side turbulent events launch *clusters* of particles that after a while return to the side waiting for being activated again.

In bedload trajectory remains close to the side, whereas in suspended load particles reach the outer region.

Mean particles movements in bedload are of the same order of their mean diameter. If they move rolling it is possible to assume that the weight of the particles is greater than lift force, whereas if they move jumping the lift force is greater than the weight. If the lift force is big enough to prevail over the weight and the trajectories of the particles are of the same order of water depth they move in suspension.

Lift force is connected to critical flow velocity and weight is connected to fall velocity in steady water; for this reason it is possible to find out the manner of transport that occurs through the ratio between the fall velocity W_s and the shear velocity $u_* = \sqrt{\frac{\tau_0}{\rho}}$.

The following scheme explains the previous idea:

- $6 > \frac{W_s}{u_*} > 2$ rolling bedload
- $2 > \frac{W_s}{u_*} > 0.8$ jumping bedload
- $0.8 > \frac{W_s}{u_*} > 0$ suspended load

3.1.3 Shields theory

It is possible to divide the forces acting on a particle as an active force F_a which makes the particle moving and a resistant force F_r which takes position against movement.

The active force F_a is proportional to the stress τ_0 existing surrounding the grain, to the square of

the diameter of the sediment and to a coefficient ϕ .

$$F_a = \phi\tau_0 d^2 \quad (3.6)$$

Through sperimental information the coefficient ϕ has been related to a number similar to Reynolds one, made up by the quantities characteristic of the movement near the grains:

- shear velocity $u_* = \sqrt{\frac{\tau_0}{\rho}}$;
- grain diameter d ;
- cinematic viscosity $\nu = \frac{\mu}{\rho}$;

the number herein created is $Re^* = \frac{u_* d}{\nu}$, and is called *boundary Reynolds number*.

Resistant force F_r is supposed to depend on the weight of submerged grains:

$$F_r = \alpha(\gamma_s - \gamma)d^3 \quad (3.7)$$

Obviously in case of incipient movement is $F_a = F_r$, from which:

$$\phi\tau_0 d^2 = \alpha(\gamma_s - \gamma)d^3 \quad (3.8)$$

reducing and introducing a dimensionless stress dividing for $(\gamma_s - \gamma)d$:

$$\tau^* = \frac{\tau_0}{(\gamma_s - \gamma)d} = f(Re^*) \quad (3.9)$$

The following figure shows the relation between τ^* and Re^* ; over the curve is found the field where particles move, whereas under the curve there is no movement.

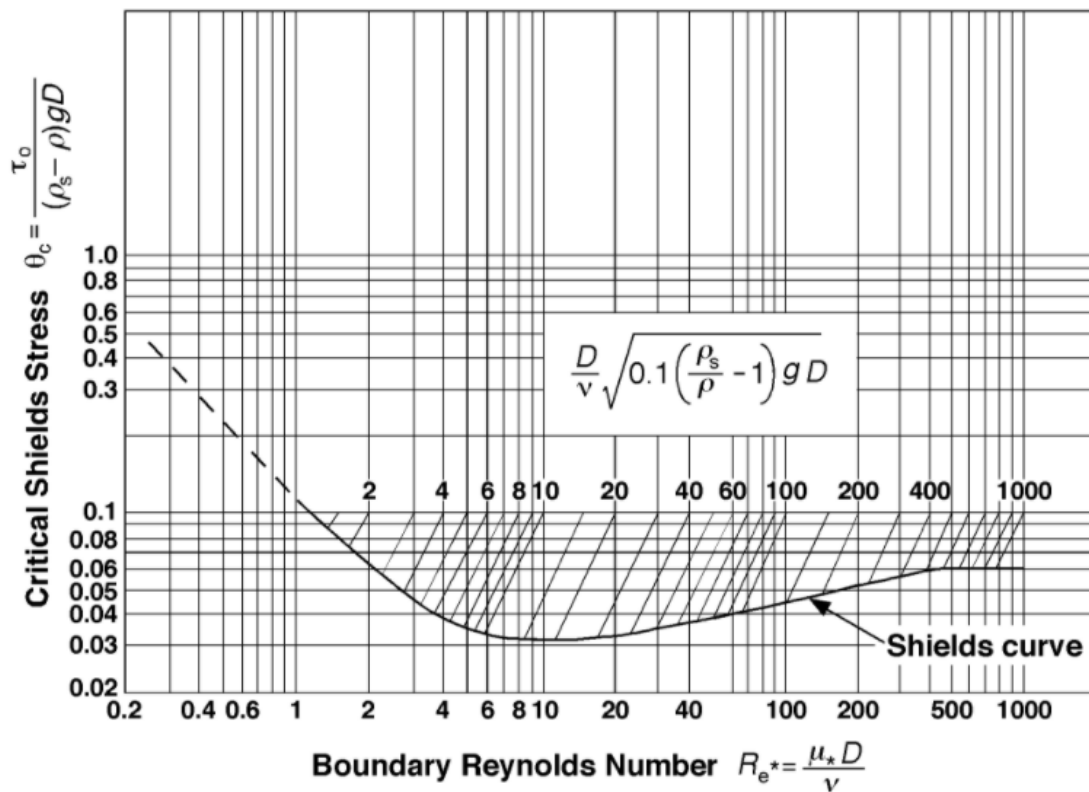


Figure 3.5: Shields curve.

Shields proposed a value of τ_{cr}^* , meaning the value of dimensionless stress from which the grains movement begins, of 0.058 [32]. This value has to be taken as a reference point, because actually sediment transport has not a clear threshold from which it begins.

Shields theory, even if largely discussed by scientific community, is practically the most diffused. Other authors, through a large number of experiments both in laboratory and in field, have suggested values of τ_{cr}^* that varies from 0.03 to 0.06 [25, 20, 31, 26]. This is due both to the difficulty to define the beginning of movement and to other secondary phenomenon related to grain assortment and the variability of hydraulic parameters.

The value of τ_{cr}^* equal to 0.06 can be associated to a sediment transport rate which is not null, but close to zero; this is a value contained in some validated sediment transport formulas, like the ones from Pica, Sckotlish or Smart and Jaggi, as underlined from Lamberti, Montefusco and Paris [23]. We can also notice that $\tau_{cr}^* = 0.045$ proposed by Zeller [42] is indicated by the manual for design of stables channels compiled by the U.S. Army Corps of Engineers as the beginning value of effective sediment transport.

Hiding correction In real rivers irregularity of grains size lead to the fact that movement conditions of a single grain are influenced by the presence of the others; smaller particles are "protected" by particles of bigger dimensions, and therefore their mobility is reduced. In order to consider this

phenomenon (named "hiding" or "sheltering") many formulas have been proposed, but the more diffused is the parameter proposed by Egiazaroff [9]; according to him the correction factor for the hiding phenomenon calculated for the i -th granular fraction is:

$$\xi_i = \left(\frac{\log_{10} 19}{\log_{10} 19 \frac{d_i}{d_m}} \right)^2 \quad (3.10)$$

where

- d_i is the diameter of the i -th fraction;
- d_m is the mean diameter of the sediment.

Accurated calculations have proved that hiding correction is very important for water depths associated to very large grains ($\gg d_{50}$) and very small grains ($\ll d_{50}$), which is reduced in the first case and increased in the second.

An other effect to be considered is the "sheltering" phenomenon: small grains are easily eroded by little flow, which are also more frequent, because their mobility is greater than critical mobility. In this way the riverbed surface is composed by only greater grains, which have a minor mobility, and not by the entire granulometric curve of the site. This is a phenomenon typical of sandy and gravelly rivers which is even now object of study.

Slope correction Slope reduces the grain stability by reducing the stabilizing contribute of gravity. In the limit case for which slope is equal to the angle of inner friction of the sediment it is obviously $\tau_{cr}^* = 0$, which means that grains move for $\tau = 0$.

The correction factor to be used is

$$A = \cos \alpha \left(1 - \frac{\tan \alpha}{\tan \phi} \right) \quad (3.11)$$

where

- α is the slope of the river;
- ϕ is the angle of inner friction of the sediment.

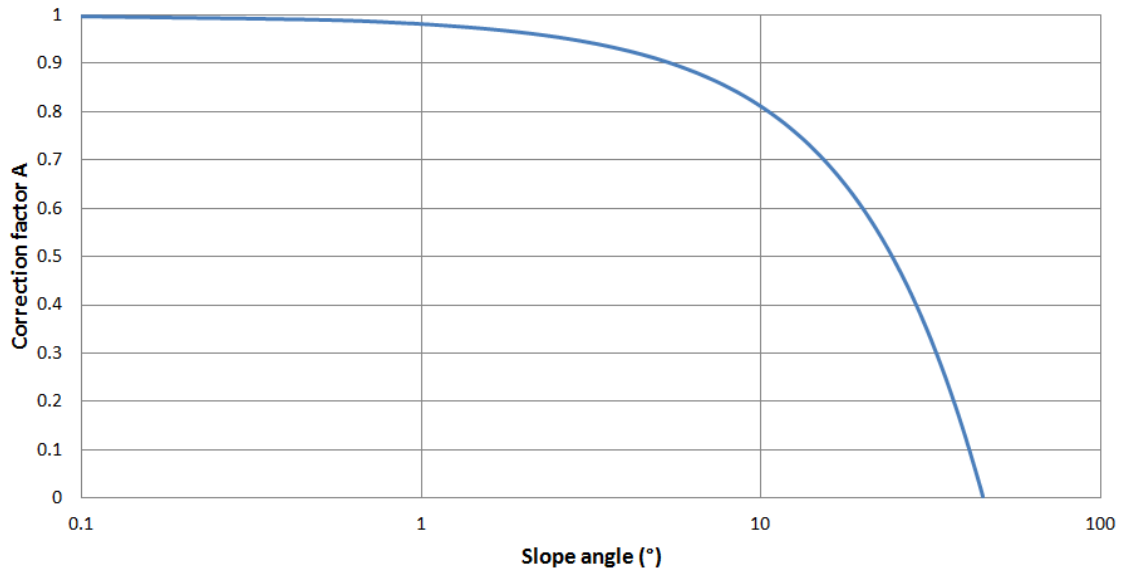


Figure 3.6: Slope correction factor calculated with an inner friction angle of 45° .

Low relative submergence factor If the grain diameter is similar to water depth relative submergence is low (this is typical for mountain rivers, where is possible to find large grains and high values of slope which reduce water depth). Shields proposed his theory for grains' dimensions lower than water depth (h), but for value of $\frac{h}{d_{50}} < 6$ the incipient movement threshold must be corrected, and it is inversely proportional to $\frac{h}{d_{50}}$. This effect is due to the deformation of velocity profiles: the relation between u_d and u_* is different from the usual cases and is consequently different the relation between stresses on the riverbed (meaning head losses) and grain mobility; this is reduced when $\frac{h}{d_{50}}$ is reduced.

The correction factor to be used in this case has been proposed by Armanini [3] and is the following:

$$B = 1 + 0.67\sqrt{\frac{d}{h}} \quad (3.12)$$

notice that for high value of $\frac{h}{d_{50}}$ the correction factor is equal to 1, and this means that for high values of relative submergence Shields' theory is correct and doesn't need corrections.

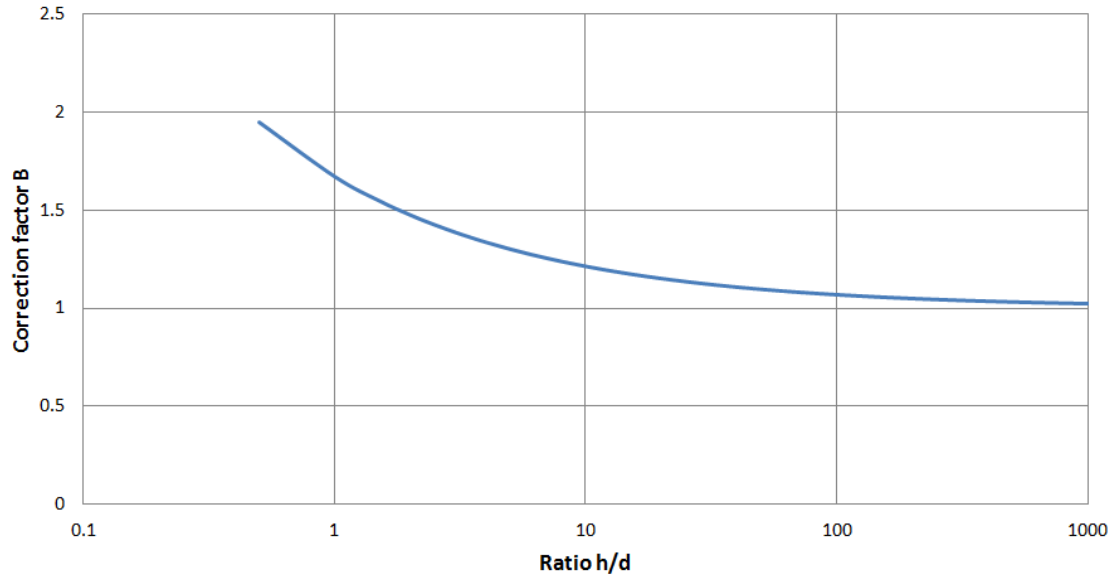


Figure 3.7: Relative submergence correction factor.

Relation between slope and submergence As shown in the previous paragraphs the effects of slope and relative submergence are conflicting; this is because when the relative submergence is low the slope is usually high (mountain rivers), and vice versa. Combining these facts it is possible to obtain the real trend of Shields stress on varying the ratio $\frac{h}{d}$, which is similar to those of figure 3.7 but where the curve bends downwards for $\frac{h}{d} < 1$.

Other criteria In scientific literature there are other criteria of incipient movement, related to different parameters, as a critical flow (q_c), a critical slope or a critical Froude number (F_c).

Some of them are herein proposed:

- $\tau_{cr}^* = 0.042 \cdot 10^{2.2 \cdot i}$, for slope $i = 0.02$ to 0.2 , proposed by Graf and Suszka;
- $\tau_{cr}^* = 0.0851 \left(\frac{h}{d_{50}}\right)^{-0.266}$, for $\frac{h}{d_{50}} = 0.5$ to 50 , proposed by Suszka;
- $F_c = 1.58 \left(\frac{h}{d_{50}}\right)^{0.1}$, proposed by Neille;
- $\frac{q_s}{\sqrt{gd^3}} = 0.15i^{-1.12}$, proposed by Bathurst et al., for $i = 0.002$ to 0.1 .

3.2 Transport capacity and sediment load

With the expression *transport capacity* is intended the maximum quantity of a certain sediment that the stream is able to carry. If there is not enough sediment in the river to reach the transport capacity, the river carries all the sediment, and in this case the effective sediment load is lower than the transport capacity.

Usually large sediments adapt rapidly to a sudden variation of the hydrodynamic characteristics of the stream, whereas fine sediments adapt more slowly. Moreover as a consequence of an increase in stream velocity fine sediments can not be present in such a quantity to satisfy transport quantity, and in this case sediment load is lower than transport capacity.

The sediment transport of the finest fraction of material is then independent from hydrodynamic conditions, and the sediment transport which verifies is named *wash load*, which is different from the *bed-material load*, that means the sediment load of the fraction of material which is present in the river. For the bed-material load it is possible to define a sediment transport formula, which is a relation between the sediment load, the hydrodynamic conditions and the grains' characteristics; wash load is instead depending on the amount of material coming from upstream.

However the granulometric distribution of the sediment carried by the stream is usually different from those of the material present in the riverbed, and usually a variation in the distribution of sediment in the riverbed causes a variation also in carried sediment and vice versa; in general the mean diameter of the carried sediment is lower than the mean diameter of the material in the riverbed.

3.3 Total sediment load

There are two methods to determine the total sediment load.

The first method (direct method) simply sums the bedload and the suspended sediment, each calculated with appropriate relations. The second one (indirect method) calculates the total sediment load in unique formula, without dividing bedload from suspended load. Here are presented the formulas of the indirect method adoperated in the present work.

3.3.1 Engelund and Hansen

The formula proposed by Engelund and Hansen in 1967 [11] for total sediment load is the following:

$$Q_{st} = 0.05C^2\tau_*^{2.5}\sqrt{\delta gd_{50}^3} \cdot b \cdot \rho_s \quad (3.13)$$

where $C = \sqrt{\frac{k_s^2 y^{1/3}}{g}}$ and k_s is the Gaukler-Strickler coefficient.

This is a formula developed for fine materials, for sand or finer.

3.3.2 Ackers and White

The formula proposed by Ackers and White in 1973 [1] is one of the more diffused to evaluate total sediment load. It is based on phisycal considerations and dimensional analysis.

Authors introduced a dimensionless grain diameter, which expresses the relation between submerged weight and viscous forces:

$$D_{gr} = d_{35} \left(\frac{g(s-1)}{\nu^2} \right)^{1/3} \quad (3.14)$$

with the diameter in meters.

A mobility parameters is then proposed:

$$F_{gr} = \frac{u_*^n}{\sqrt{(s-1)gd}} \left(\frac{U}{\sqrt{32 \log\left(\frac{10Y}{d}\right)}} \right)^{1-n} \quad (3.15)$$

as well as a transport parameter:

$$G_{gr} = c \left(\frac{F_{gr}}{A} - 1 \right)^m \quad (3.16)$$

The concentration of sediment particles is expressed as

$$X = G_{gr} \frac{s \cdot d}{Y} \left(\frac{U}{u_*} \right)^n \quad (3.17)$$

The coefficient n,m,A and c have been determined through regression using results of about 1000 laboratory experiments and 250 field measures with both uniform and assorted sediments. Their values, only depending on the dimensionless grain diameter D_{gr} , are:

Coeff.	$D_{gr} > 60$	$1 < D_{gr} < 60$
n	0	$1 - 0.56 \log D_{gr}$
m	1.5	$\frac{9.66}{D_{gr}} + 1.34$
A	0.17	$\frac{0.23}{D_{gr}^{0.5}} + 0.14$
c	0.025	$\log c = 2.86 \log D_{gr} - (\log D_{gr})^2 - 3.53$

Table 4: Values of coefficient n,m,A and c.

Structure of equation 3.15 highlights that fine sediment transport is due to total bed shear stress, whereas large sediment transport is due to grain shear stress; you can notice that for fine sediment D_{gr} tends to 1, and coefficient n tends to 1 too; this fact implies that in equation 3.15 the exponent of the second factor tends to 0 and has no more weight. If D_{gr} tends to 60 instead, which is the case of large sediments, exponent n tends to 0 and in this case the factor which has no weight in equation 3.15 is the first one, whereas the exponent of the second factor tends to 1.

In case of assorted sediment the grain diameter to be used is the d_{35} .

Feasibility limits of this method concern the determination of coefficients n,m,A and c, because authors found out the relations between the coefficients and D_{gr} only for a certain range of sediment grain dimension; in particular for D_{gr} higher than 60 the coefficients are constant, but their validity is no more verified for $D_{gr} > 100$, because of the lack of experimental analysis.

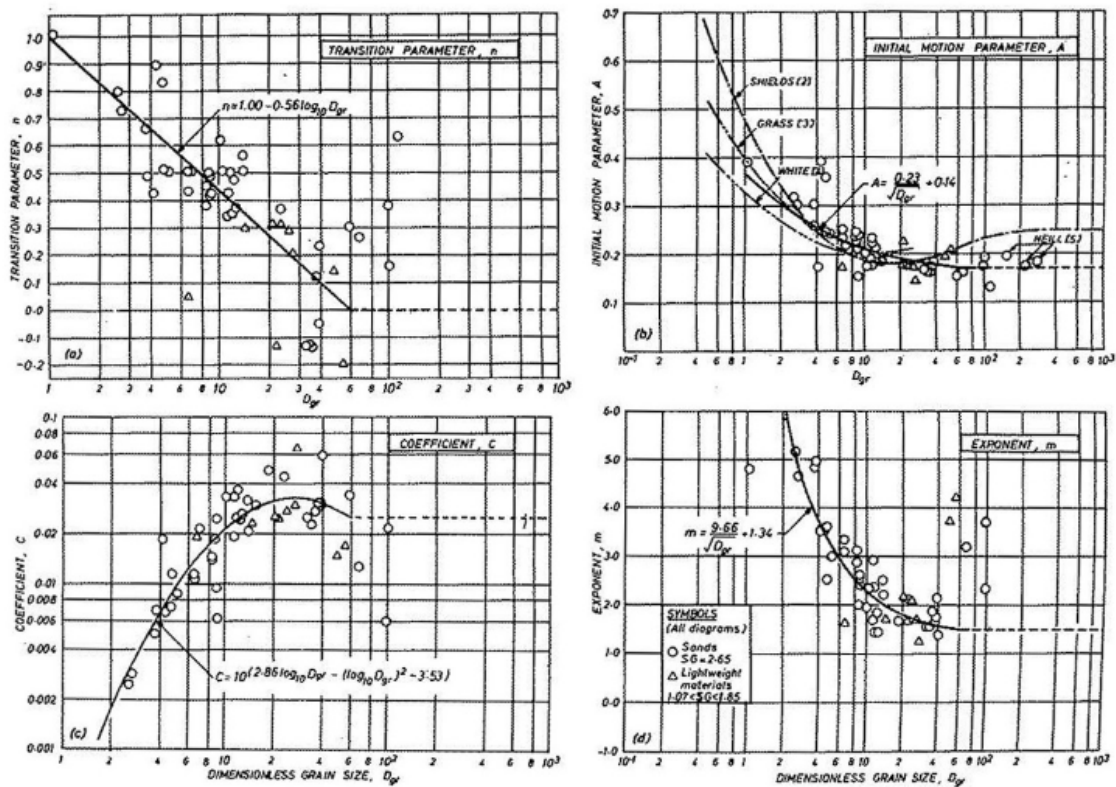


Figure 3.8: Graphics for determination of n,m,A and c through experimental data.

In 1993 Ackers and White corrected the coefficients through new experiments; the recalibration of parameters have permitted a better fit of data. In table 5 the new values are shown .

Coeff.	$D_{gr} > 60$	$1 < D_{gr} < 60$
n	0	$1 - 0.56 \log D_{gr}$
m	1.78	$\frac{6.83}{D_{gr}} + 1.67$
A	0.17	$\frac{0.23}{D_{gr}^{0.5}} + 0.14$
c	0.025	$\log c = 2.79 \log D_{gr} - 0.98 (\log D_{gr})^2 - 3.46$

Table 5: Values of recalibrated coefficient n,m,A and c.

Ackers and White suggest that their formula should be used only in those cases where the Froude number, defined as $F_r = \frac{u}{\sqrt{gy}}$, is lower than 0.8.

3.3.3 Yang

Yang developed in 1973 [40] a formula for the determination of total sediment concentration in prevalent sandy rivers. Its formula is based on a dimensional analysis and on the concept of *unit stream power*, which represents the potential energy losses per unit width, and it is calculated

through the product of velocity and slope $u \cdot i$.

The formula is the following:

$$\log C = 5.435 - 0.286 \log \left(\frac{W_s d}{\nu} \right) - 0.457 \log \left(\frac{u_*}{W_s} \right) + \left(1.799 - 0.409 \log \left(\frac{W_s d}{\nu} \right) - 0.314 \log \left(\frac{u_*}{W_s} \right) \right) \log \left(\frac{u_i}{W_s} - \frac{u_{cr} i}{W_s} \right) \quad (3.18)$$

where the fraction of critical stream velocity and fall velocity $\frac{u_{cr}}{W_s}$ is expressed as:

- $\frac{2.5}{\log\left(\frac{u_* d}{\nu}\right) - 0.06} + 0.66$ if $1.2 < \frac{u_* d}{\nu} < 70$;
- 2.05 if $70 \leq \frac{u_* d}{\nu}$;

The concentration C is expressed as ppm in weight.

Coefficients of the previous formulas were determined through regression analysis on 463 laboratory measurements; the experiments were carried out on sediments from 0.015 mm to 1.71 mm of diameter.

The fall velocity is determined through the graphic of figure 3.9.

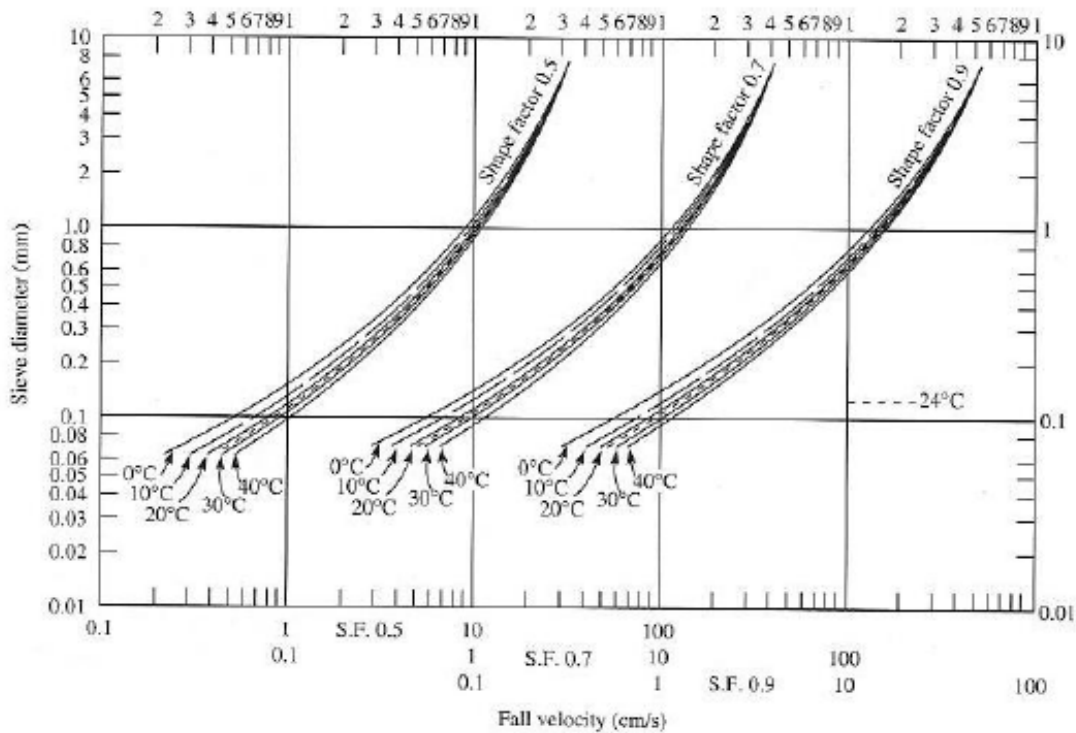


Figure 3.9: Determination of fall velocity function of diameter, shape factor and temperature.

In 1979 Yang [41] proposed another formula for total sediment load to be adopted in case of high sediment concentration in sandy rivers, when C is higher than about 100 ppm. This second

formula is due to the fact that in case of high concentration is no more necessary to include the criteria of incipient motion.

The 1979 formula is the following:

$$\log C = 5.165 - 0.153 \log \left(\frac{W_s d}{\nu} \right) - 0.297 \log \left(\frac{u_*}{W_s} \right) + \left(1.780 - 0.360 \log \left(\frac{W_s d}{\nu} \right) - 0.480 \log \left(\frac{u_*}{W_s} \right) \right) \log \left(\frac{ui}{W_s} \right) \quad (3.19)$$

However the author says both the formulas are accured in calculation of concentration of sediment higher than 100 ppm by weight.

3.3.4 Di Silvio

Di Silvio proposed in 1980 a formula suitable both for mountain rivers and plain rivers. The formula contains some parameters which vary and have to be calibrated on field data.

The structure of the formula is:

$$Q_{st} = \alpha \frac{Q_i^{m;n}}{b^p d^q} \quad (3.20)$$

The parameters m,n,p and q have a range of variation according to the type of river, as shown in table 6:

Mountain rivers	Plain rivers
m=1.5 to 1.8	m=1.67 to 2
n=1.75 to 2.1	n=1.67 to 2
p=2.5 to 0.8	p=1.5 to 1
q=0.75 to 1.2	q=1 to 1.5

Table 6: Parameters for Di Silvio formula.

The parameter α is set equal to 0.124.

Di Silvio formula is therefore:

$$Q_{st} = 0.124 \frac{Q_i^{1.8} i^{1.8}}{b^{1.75} d_{50}^{1.25}}$$

where the exponents are chosen for a plain river.

3.3.5 Graf and Acaroglu

Graf and Acaroglu proposed in 1968 [14] a formula based on about 800 laboratory experiments and 80 field measures; it can be used also for non uniform sediment adoperating the d_{50} as characteristic diameter.

$$\phi_A = 10.39 \psi_A^{-2.52} \quad (3.21)$$

where

$$\phi_A = \frac{\frac{q_s}{q} UR}{\sqrt{(s-1)gd^3}}$$

and

$$\psi_A = \frac{(s-1)d}{jR}$$

. J is the energy line slope which in case of permanent motion can be assumed equal to the river slope. Note that the parameter ψ_A is simply the reciprocal of τ^* .

The conditions under which the formula can be adoperated are

- $10^{-2} < \phi_A < 10^3$;
- $\psi_a \leq 14.6$.

3.4 Suspended load

The suspended sediment load which passes through a generic section ω in a uniform stream can be written in the form

$$Q_{ss} = \int_{\omega} cud\omega \quad (3.22)$$

where c is the mean volumetric concentration in a point of the section, meaning the mean value of the ratio between the volume of sediment contained in a volume near the detection point and the considered volume. U is the velocity in the generic point (which is the mean velocity, considering turbulent variations).

Considering a very large rectangular section Q_{ss} is well approximated by the relation

$$Q_{ss} = bq_{ss} \quad (3.23)$$

where b is section width and q_{ss} is suspended sediment load per unit width, which is defined as

$$q_{ss} = \int_a^y c(y)u(y)dy \quad (3.24)$$

with y the stream depth and a the *reference height*, meaning a level where is present a *reference concentration* C_r , which provides an evaluation of volumetric concentration near the bottom.

The computation of q_{ss} requires therefore the knowledge of velocity distribution $u(y)$ and concentration $c(y)$.

Rouse determined $c(y)$ in 1937 as the solution of the continuity equation of sediment [29]. It is made by a balance between the unitary sediment flow directed downwards related to sedimentation of grains ($-W_s c$, with W_s the fall velocity of grains and c the concentration) and the unitary sediment flow directed upwards related to sediment transport by turbulent fluctuations. The last one is expressed as $-D_t \frac{dc}{dy}$ with D_t the turbulent diffusivity, whose form has been found by Rouse as

$$D_t = ku_* y \left(1 - \frac{y}{Y}\right) \quad (3.25)$$

with k the Barnum constant equal to 0.4 and $u_* = \sqrt{\frac{\tau_0}{\rho}}$ the shear velocity.

This fact implies the Reynolds analogy between sediment diffusion and turbulent diffusion of momentum in the liquid phase.

Considering that at the reference height $y = a$ it is obviously $c = C_r$, meaning that the concentration must be equal to the reference concentration, it is possible to obtain the Rouse's profile:

$$c = C_r \left(\frac{Y - y}{y} \frac{a}{Y - a} \right)^Z \quad (3.26)$$

where Z is called Rouse's number and is defined as

$$Z = \frac{W_s}{ku_*} \quad (3.27)$$

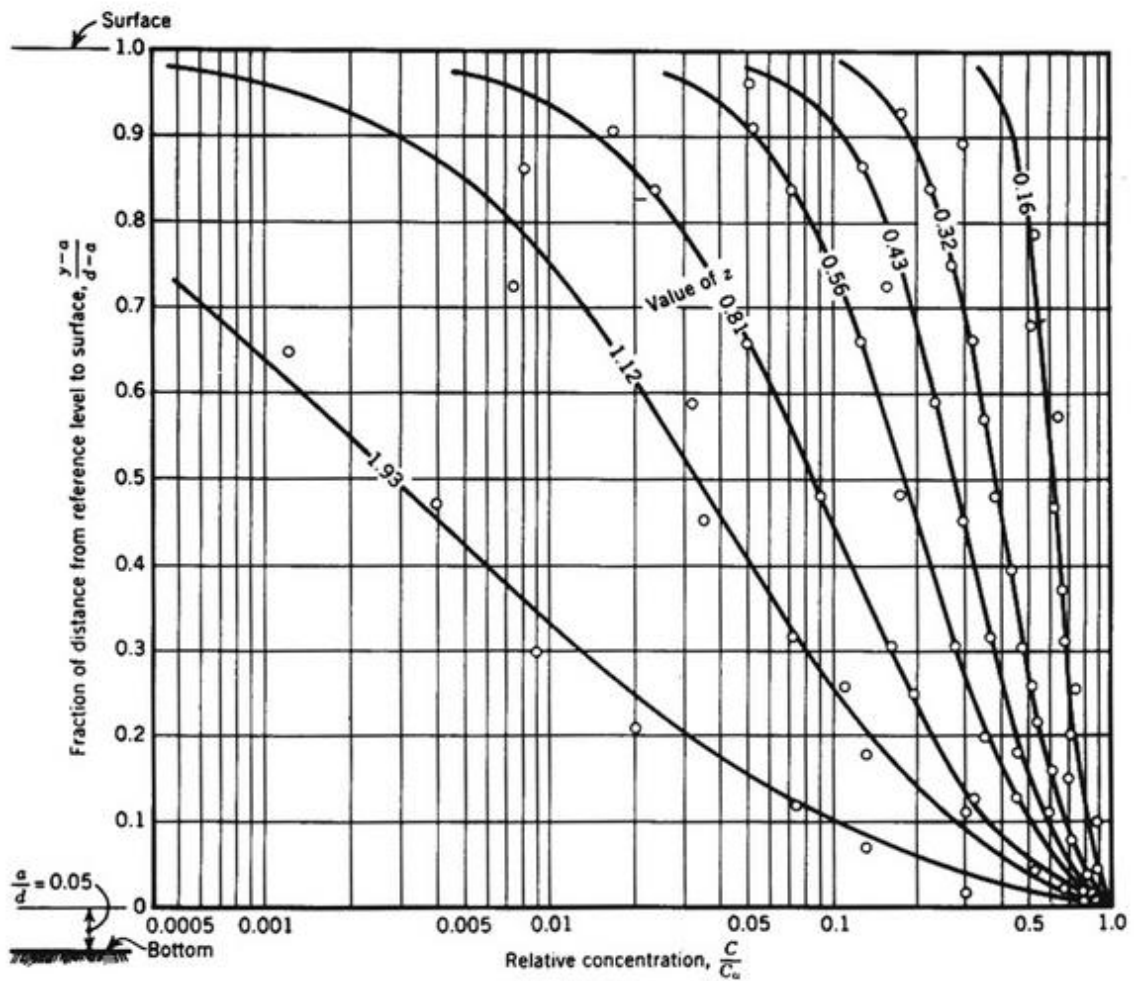


Figure 3.10: Rouse's profile of sediment concentration.

As shown in figure 3.10 the Rouse's number influences the form of the profiles and in particular if Z grows, which means that sedimentation velocity is higher, the profiles are flatter and the concentration towards the surface is lower; this is obvious, because grains tend mainly to fall to the bottom and therefore they reach the surface with more difficulty.

The velocity distribution is assumed as the one of a plane turbulent flow for a rough tube, whose form is:

$$u = \frac{u_*}{k} \ln 30 \frac{y}{\epsilon} \quad (3.28)$$

where ϵ is the absolute roughness.

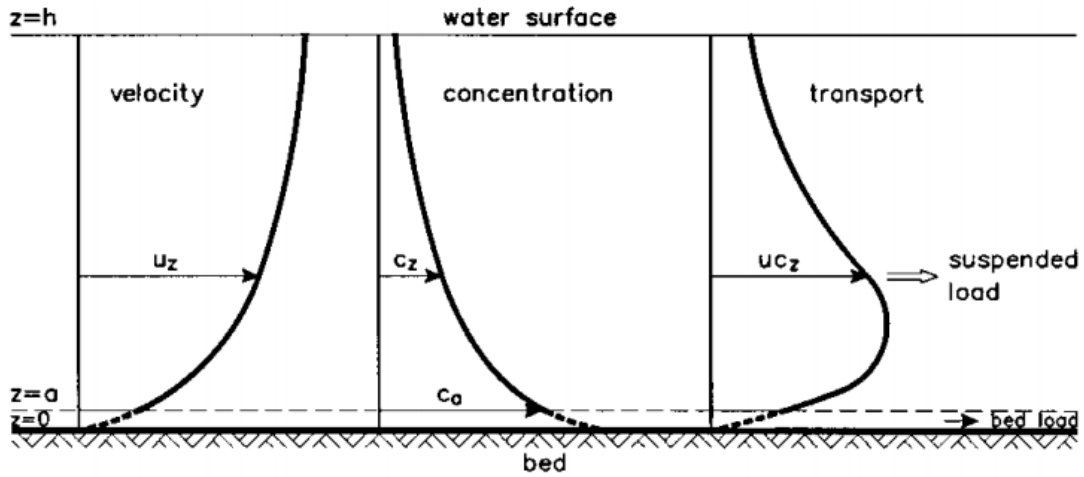


Figure 3.11: Profiles of flow velocity, suspended sediment concentration and suspended sediment load [37].

Combining the precedent equations you get to the following expression:

$$q_{ss} = \int_a^Y c(y)u(y)dy = \int_a^Y C_r \left(\frac{Y-y}{y} \frac{a}{Y-a} \right)^Z \frac{u_*}{k} \ln 30 \frac{y}{\epsilon} dy = 11.6 C_r u_* a \left(I_1 \ln 30 \frac{Y}{\epsilon} + I_2 \right) \quad (3.29)$$

The expressions I_1 and I_2 are two integrals depending on the dimensionless parameters Z and $\tilde{a} = \frac{a}{Y}$. Their form is:

$$I_1 = 0.216 \frac{\tilde{a}^{Z-1}}{(1-\tilde{a})^Z} \int_{\tilde{a}}^1 \left(\frac{1-y}{y} \right)^Z dy \quad (3.30)$$

and

$$I_2 = 0.216 \frac{\tilde{a}^{Z-1}}{(1-\tilde{a})^Z} \int_{\tilde{a}}^1 \left(\frac{1-y}{y} \right)^Z \ln y dy \quad (3.31)$$

The previous integrals are also provided through diagrams, as in the following figures (the Rouse number is here named ξ).

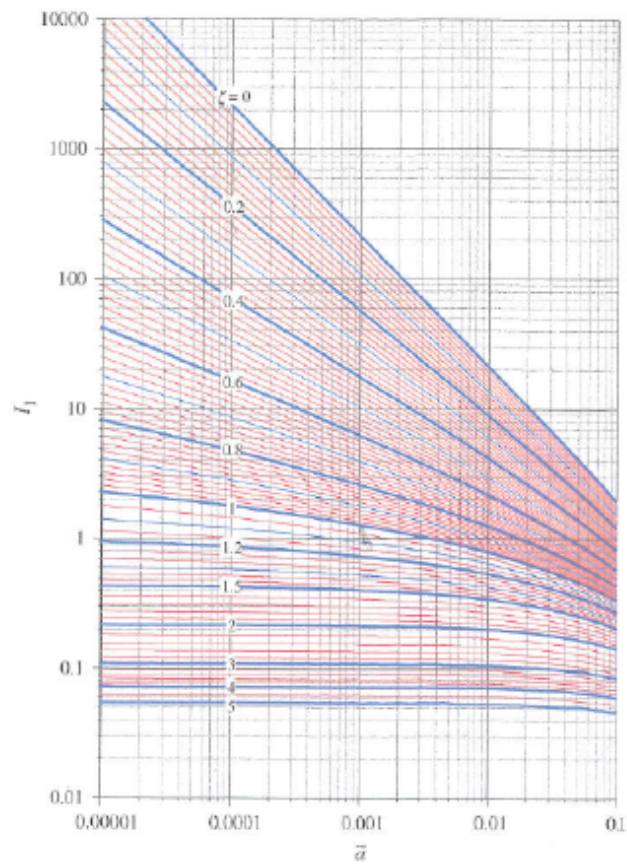


Figure 3.12: Graphic of the integral I_1 .

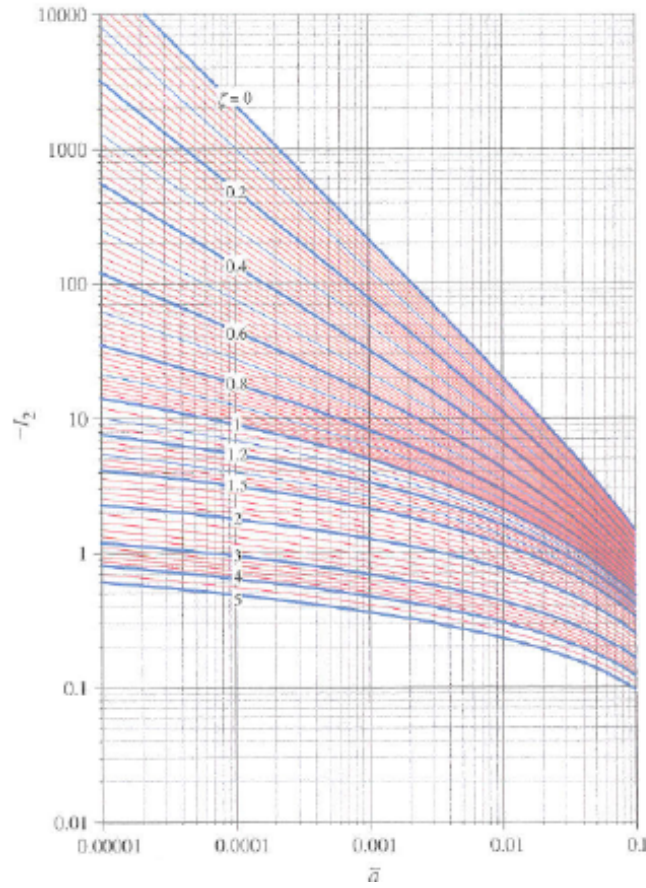


Figure 3.13: Graphic of the integral I_2 .

Notice that in figure 3.13 the y-axis is named $-I_2$, that means that the integral I_2 is negative; this is due to the presence of the logarithm which, operating on numbers lower than 1, assumes always a negative value.

The only remaining problem is to determine the reference height a and the reference concentration C_r ; many authors have proposed a solution to this issue, but the results have to be considered as an estimation of the size order of q_{ss} .

3.4.1 Van Rijn

Van Rijn in 1984 [27] proposed the reference concentration as

$$C_r = 0.015 \frac{d_{50}}{a} \frac{T^{1.5}}{D_*^{0.3}} \quad (3.32)$$

in which d_{50} is the median grain diameter; T is the bed-shear stress parameter expressed as

$$T = \frac{\tau' - \tau_{cr}^*}{\tau_{cr}^*} \quad (3.33)$$

in which $\tau' = \frac{\rho u_*'^2}{(\rho_s - \rho)gd_{50}}$ with $u_*' = \frac{\bar{u}\sqrt{g}}{C'}$ which is the bed-shear velocity related to grains, $C' = 18 \ln\left(\frac{12Y}{3d_{90}}\right)$ is the Chezy coefficient related to grains, d_{90} the 90% particle diameter of bed material, \bar{u} the depth-mean flow velocity, τ_{*cr} the critical bed-shear stress according to Shields.

D_* is the dimensionless size diameter, defined as

$$D_* = d_{50} \left(\frac{(s-1)g}{\nu^2} \right)^{0.3} \quad (3.34)$$

in which s is the specific density, g the gravity acceleration and ν the kinematic viscosity.

When the bedform height is unknown, as in this case, the reference height a is set equal to the equivalent roughness height, that as a rule of thumb is equal to d_{65} [10].

If $d_{65} < 0.01 \cdot Y$, then a is taken equal to $0.01 \cdot Y$.

3.4.2 Smith and McLean

Smith and McLean proposed in 1977 [33] a formula to evaluate C_r and a ; C_r is found through the following equation:

$$C_r = 0.65 \frac{0.0024 \left(\frac{\tau'}{\tau_{*cr}} - 1 \right)}{1 + 0.0024 \left(\frac{\tau'}{\tau_{*cr}} - 1 \right)} \quad (3.35)$$

with $\tau' = \frac{\rho u_*'^2}{(\rho_s - \rho)gd_{50}}$ as for Van Rijn.

The reference height a is:

$$a = 26.3(\tau' - \tau_{*cr})d + \epsilon \quad (3.36)$$

in which ϵ is the absolute wall roughness, that can be set equal to d_{65} as for Van Rijn.

3.4.3 Garcia and Parker

In 1991 Garcia and Parker [13] proposed the following relations to determine a and C_r . Reference concentration C_r is found as

$$C_r = \frac{AZ_u^5}{\left(1 + \frac{AZ_u^5}{0.3}\right)} \quad (3.37)$$

in which $A = 1.3 \cdot 10^{-7}$ and $Z_u = \frac{u_*' R_p^{0.6}}{W_s}$, with $R_p = \frac{\sqrt{(s-1)gd^3}}{\nu}$ named Reynolds particle number, W_s the sedimentation velocity and with $u_*' = \frac{\bar{u}\sqrt{g}}{C'}$ as previously.

The reference height is $a = 0.05Y$, with Y the stream depth.

3.5 Bedload

Data for the present study were mostly collected concerning suspended load, which is the prevalent part of sediment load during heavy rains typical of the rainy season in Burkina Faso; however some trenches were built to evaluate bedload, and even if this part of the study has not been largely developed by people who got field data, some bedload formulas have been tested in the present thesis.

Generally the sediment load which passes through a section in a certain time is expressed by some relations which combines hydraulic parameters of the stream, cross section geometry and sediment characteristics.

The relations are of these kinds:

- $q_s = f(U/U_c), f(U - U_c)$
- $q_s = f(i - i_c)$
- $q_s = f(\tau - \tau_c), f(\tau/\tau_c)$
- $q_s = f(\tau^* - \tau_c^*)$
- ...analogous

where q_s is the sediment load per unit width, U the stream velocity, i the slope, τ the stress on the riverbed and τ^* the Shield parameter; obviously the previous parameters in critical conditions are marked with the letter 'c'.

In this study have been used relations derived from the following general equation:

$$\phi = \Gamma(\tau^* - \tau_c^*)^\alpha (\sqrt{\tau^*} - \sqrt{\tau_c^*})^\beta$$

where $\phi = \frac{q_s}{d\sqrt{\delta}gd}$ is a dimensionless sediment load per unit width (with $\delta = \frac{\gamma_s}{\gamma} - 1$). This formula derives from a semi-empirical approach based on the works of Achida-Michiue, Fernadez-Van Bek and Seminara-Solari [5, 12, 34].

The parameters γ , α and β and the critical Shields stress τ_c^* have to be determined experimentally, and different authors have proposed some formulas. Here are the ones adopted in this thesis.

3.5.1 Meyer-Peter and Muller

The formula proposed by Meyer-Peter and Muller is the following [24]:

$$\phi = 8(\tau^* - \tau_c^*)^{1.5} \tag{3.38}$$

and the suggested value for critical Shields stress is $\tau_c^* = 0.047$.

3.5.2 Fernandez-Luque and Van Beek

The formula proposed by Fernandez-Luque and Van Beek is the following [12]:

$$\phi = 5.7(\tau^* - \tau_c^*)^{1.5} \quad (3.39)$$

the suggested value for critical Shields stress is $\tau_c^* = 0.05$ to 0.058 , and a mean value of 0.054 has been adopted.

3.5.3 Wilson

The formula proposed by Wilson is the following [38]:

$$\phi = 12(\tau^* - \tau_c^*)^{1.5} \quad (3.40)$$

and the value for critical Shields stress has to be read from Shields diagram, which means that in the present case it is equal to 0.033 .

4 Results

The calculation of sediment load was performed for MOG2 and MOG3 sub-catchments both for 2013 and 2014.

Sediment load was calculated for each flood event that occurred during the investigated period of time using hydrograms defined every five minutes. Later, data from each flood were summed to obtain the total load of the year; the number of floods in a year was between 18 and 29. It is worth to say that the flow values of each flood for MOG3 in 2014 were not available as complete hydrograms, but only with a single value. This is due to the fact that those who collected data had a problem with measure devices in that year, but they managed to reconstruct values they provided us.

All the twelve formulas presented in the present work were tested:

- six for total sediment load: Di Silvio, Engelund and Hansen, Graf and Acaroglu, Ackers and White, Yang (1979), Yang (1973);
- three for suspended load: Garcia and Parker, Smith and McLean, Van Rijn;
- three for bedload: Meyer-Peter and Muller, Fernandez-Luque and Van Beek, Wilson.

Comparison between the different formulas and the measured values are provided in the following figures, where total load formulas are indicated with blue bars, suspended load formulas with red bars and bedload formulas with green bars.

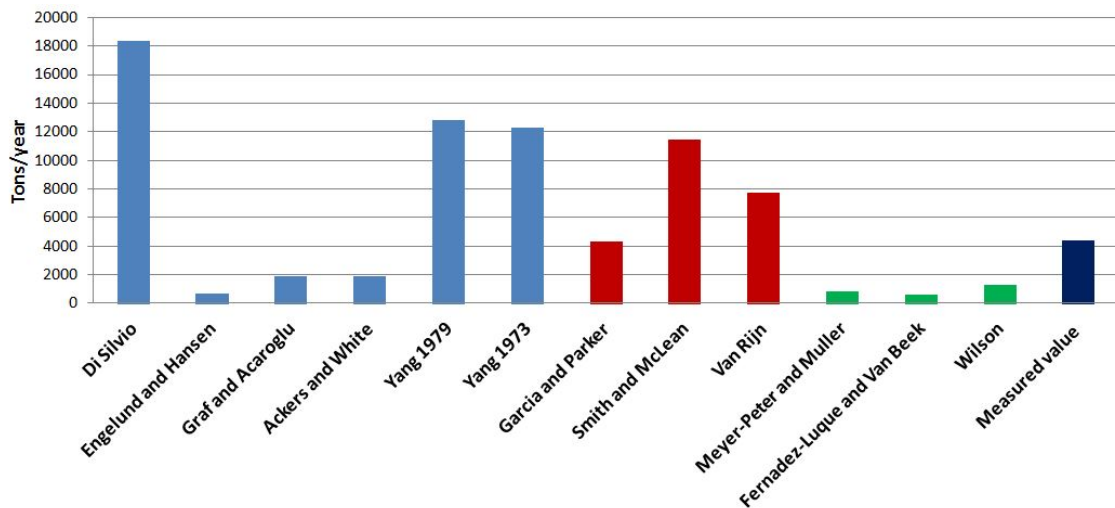


Figure 4.1: Results for MOG2 in 2013.

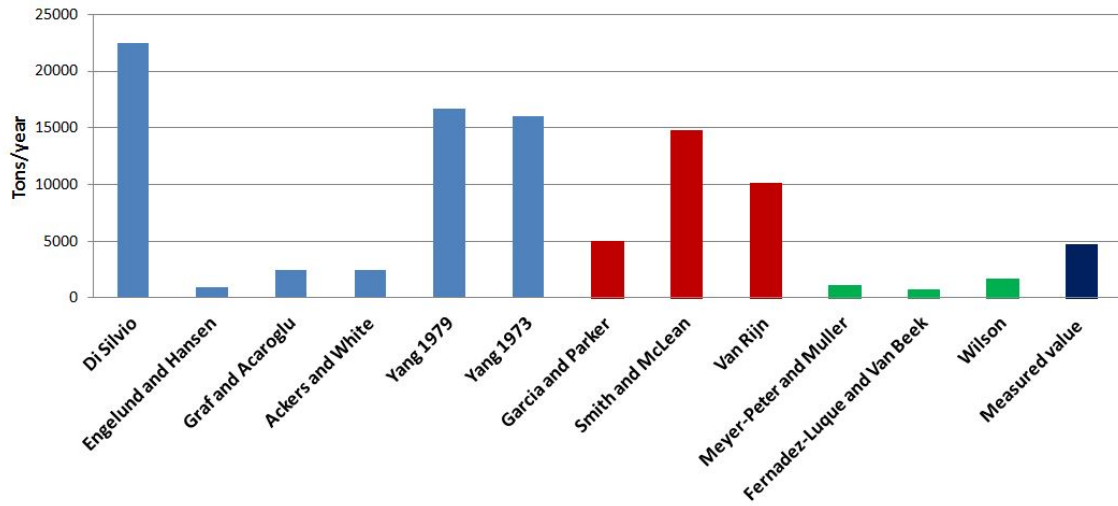


Figure 4.2: Results for MOG2 in 2014.

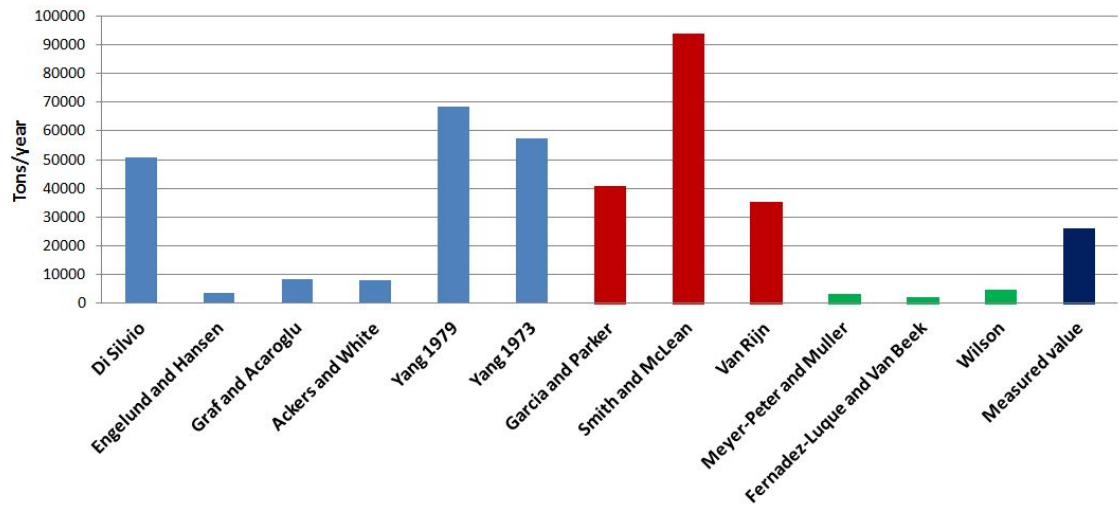


Figure 4.3: Results for MOG3 in 2013.

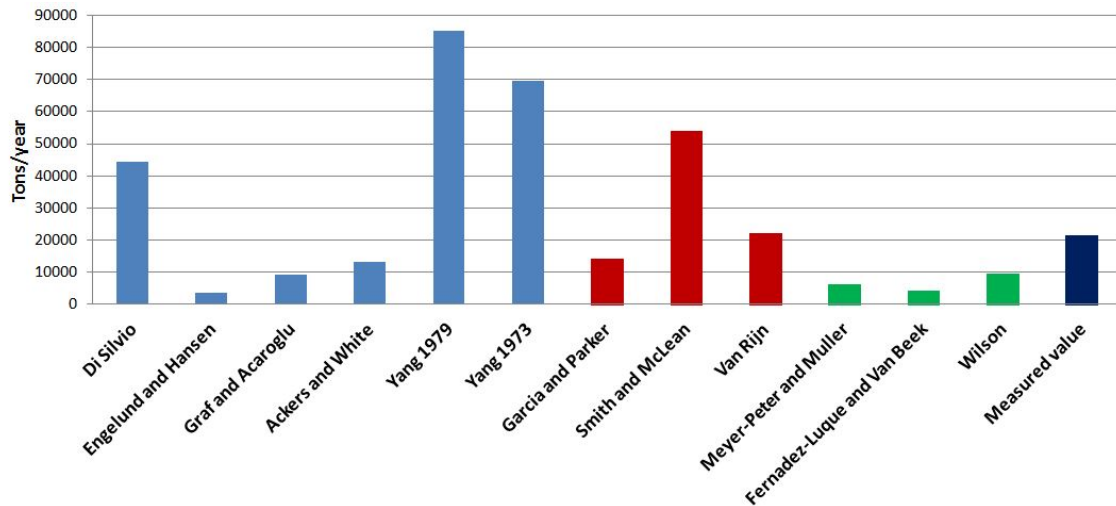


Figure 4.4: Results for MOG3 in 2014.

The results for all the formulas tested in the four conditions of sub-catchment and year considered are summarized in the following table.

	MOG2 2013	MOG2 2014	MOG3 2013	MOG3 2014
Di Silvio	18371.317	22466.324	50963.128	44289.782
Engelund and Hansen	692.867	903.381	3593.887	3574.213
Graf and Acaroglu	1895.941	2461.719	8241.573	9288.892
Ackers and White	1874.471	2461.044	8110.915	13284.656
Yang 1979	12809.505	16661.641	68303.466	85207.450
Yang 1973	12292.565	15985.056	57249.713	69509.984
Garcia and Parker	4318.919	5023.771	40890.260	14360.505
Smith and McLean	11477.970	14744.230	93767.383	54131.373
Van Rijn	7712.749	10154.145	35388.314	22099.344
Meyer-Peter and Muller	845.895	1080.126	3130.243	6174.582
Fernandez-Luque and Van Beek	596.287	761.896	2208.518	4323.194
Wilson	1319.452	1680.844	4787.899	9586.991
Measured value	4364.381	4750.329	26086.986	21550.744

Table 7: Calculated and measured values for the four cases considered, expressed in tons per year.

5 Discussion

As shown in table 7 calculated sediment transport values are scattered. This is a common situation in sediment transport evaluation, since the phenomenon that the different formulas try to describe is very complex and the number of parameters involved is high.

We have to specify that measured data are values of suspended load, since they have been found through the concentration of suspended particles in sample cans (see figure 2.4). However it was made the assumption that suspended load was the greater part of total sediment load, according to the consideration that during floods the concentration of suspended particles can be very high.

To better understand the precision of each formula the percentage differences were calculated, according to the equation $\frac{Q_{s,calculated}-Q_{s,measured}}{Q_{s,measured}} \cdot 100$. A positive percentage difference means that the calculated value is higher than the measured one and vice versa. The obtained differences are shown in the following table.

	MOG2 2013	MOG2 2014	MOG3 2013	MOG3 2014
Di Silvio	320.9	372.9	95.4	105.5
Engelund and Hansen	-84.1	-81.0	-86.2	-83.4
Graf and Acaroglu	-56.6	-48.2	-68.4	-56.9
Ackers and White	-57.1	-48.2	-68.9	-38.4
Yang 1979	193.5	250.7	161.8	295.4
Yang 1973	181.7	236.5	119.5	222.5
Garcia and Parker	-1.0	5.8	56.7	-33.4
Smith and McLean	163.0	210.4	259.4	151.2
Van Rijn	76.7	113.8	35.7	2.5
Meyer-Peter and Muller	-80.6	-77.3	-88.0	-71.3
Fernandez-Luque and Van Beek	-86.3	-84.0	-91.5	-79.9
Wilson	-69.8	-64.6	-81.6	-55.5

Table 8: Percentage differences of each formula in the four considered combinations

As previously explained, data for MOG3 in 2014 were reconstructed, but since results are similar for 2013 and 2014 the reconstruction should not have significantly influenced the calculations. The main differences between MOG2 and MOG3 sub-catchments are bed slope and the geometry of the cross section; the dimension of the sediment, in fact, is supposed to be the same.

We also have to say that those who collected data did not perform an evaluation of the precision of their measures, in order to know which percentage of the real sediment load is represented by field data of this study. Measured data were found multiplying a single value of sediment concentration in a flood per the total water volume of the flood; we can easily imagine that the reality of the phenomenon is more complicated, since sediment concentration varies in time during the

flood and in space according to the position in the cross section. For these reasons the measured values of sediment load should not be considered as absolutely precise data, but they are however the only field data it is possible to have.

5.1 Comparison between tested formulas

An analysis of the different formulas is herein performed to determine the best ones and those which should be rejected.

5.1.1 Total sediment load

Di Silvio's formula provides for MOG2 higher values than for MOG3; for MOG3, indeed, the calculated values are a little lower than measured ones, but since Di Silvio's formula also considers bedload this means that the total sediment load is underestimated. However this is a quite simple formula, and the determination of the exponents is essential to reach a good result. In this work the exponents are set to the mean values in the range suggested for plain rivers and they fit better for MOG2 than for MOG3.

Engelund and Hansen's and Graf and Acaroglu's formulas return very low values, comparable with bedload ones, but they should represent total load. A possible explanation is that these formulas consider as main parameter the dimensionless shear stress τ^* , as in the formulas used for bedload calculation; even if Engelund and Hansen's and Graf and Acaroglu's formulas present τ^* elevated to a higher exponent than for bedload formulas the obtained values are quite low because the dimensionless shear stress is often close to 1 or even lower. In case of number from 0 to 1, indeed, the elevation of the number to a higher exponent provides a lower value.

The formula proposed by Ackers and White provides low values, very close to Graf and Acaroglu's for MOG2 and just a little higher for MOG3. Probably this is due to the fact that this formula should be used for rivers with Froude number lower than 0.8, and this condition is often not respected.

The two Yang's formulas provide high results both for MOG2 and MOG3; the obtained values are higher than measured data but bedload has to be considered in this difference. The 1979 formula provides always higher values than 1973 one, especially for MOG3 where the ratio between the two formulas is about 1.3, whereas for MOG2 is 1.04. In general Yang's formulas seem to overestimate total load, but they are however considered as good formulas for sub-sahelian rivers, as previously explained by Grimaldi [16], who suggested to use Yang's 1979 formula for these rivers.

5.1.2 Suspended load

Concerning suspended load, Garcia and Parker's formula provides good results; it is worth to say that actually only suspended load's formula represents an appropriate description of measured values, which are in fact values of concentration. Garcia and Parker's formula fits very well field data for MOG2, but varies a bit for MOG3, providing higher values in 2013 and lower in 2014. This could be explained by the fact that data for MOG3 in 2014 are provided as a single value in a day, and don't describe the complete hydrograms. Probably this leads to an underestimation of suspended sediment load because the peaks are not involved in the calculation, and a flat daily hydrogram implicates a low flow speed, from which directly depend suspended load formulas.

Smith and McLean's and Van Rijn's formulas follow the same evolution of Garcia and Parker's one, providing higher values for MOG3 in 2013 than in 2014. The main difference is that in general Smith and McLean's one have the highest values, whereas Van Rijn's one is situated in the middle. However Van Rijn's is the one which better fits MOG3 data, since it has the lowest percentage differences both for 2013 and 2014, and for 2013 it provides lower values than Garcia and Parker's.

5.1.3 Bedload

As regards bedload the calculated values are always much smaller than measured suspended values; this means that suspended load is the prevalent part of total load, as supposed (since we remind that total load is the sum of bedload and suspended load). The calculation of bedload can provide some information in particular on the ratio between suspended load and bedload. Comparing data from table 7 the ratio between the mean calculated suspended load and the mean calculated bedload is about 4.74 for MOG2 in 2013, 4.05 for MOG2 in 2014, 7.72 for MOG3 in 2013 and 3.20 for MOG3 in 2014. The difference between the last ratio and the previous ones is certainly due to the different nature of data used, as explained for suspended load. If we hypothesize that data for MOG3 in 2014 are less accurate than the others we can say that in general suspended load is about 5 times bigger than calculated bedload. However the ratio between suspended load and bedload will be more investigated in the next section.

Some bedload data were actually provided to us, since some trenches were built to collect bedload. After every flood the filling percentage of the trenches was calculated and they were emptied; however trenches data are not useful for this research, since the filling percentage was always at least 90-95 %, and this means simply that trenches were completely filled by bedload (a trench filled at 90%, indeed, can be considered as a completely filled one, where water stream has dragged the surface part). In order to evaluate bedload, trenches should have been built of bigger dimensions, since a $4m^3$ trench is too small to collect the bedload of an entire flood.

6 Proposing a new formula

The purpose of this thesis is to find a new formula for sediment transport in small, data-scarce Sahelian basins where often common literature formulas have not been widely tested.

One problem we have to face is that measured values are available only one for every flood, whereas flow and water height are available as hydrograms every five minutes. To cope with this issue we have to consider the mean value for every flood of the quantity we want to compare with field data in order to set the parameters of the new formula.

As regards suspended load, the formulas tested in the present work are similar and the only differences are due to the determination of the reference concentration and the reference height. However we don't have concentration measures at the different heights, and neither information about the concentration profiles of suspended particles. For these reasons the formula we are looking for has to be of a different kind, since the tested suspended load formulas were determined through different kind of data, also in laboratory.

The parameters we have concern cross sections geometry, sediment particles dimension, bed slope, hydrograms with the relative water height and discharge and the measured suspended load value for each flood. The best way to find a new formula seems to relate the measured values with the characteristic parameters of the river. In particular, a relation between dimensionless parameters is to prefer in order to generalize the relation obtained.

Two of the most diffused formulas for dimensionless sediment discharge are

$$\phi = \frac{q_s}{d\sqrt{\delta g d}}$$

proposed by Einstein and used for the bedload formulas tested, and

$$\phi = \frac{\frac{q_s}{q} UR}{\sqrt{(s-1)gd^3}}$$

which is used in Graf and Acaroglu relation. Even if the first relation is also adoperated by Englund and Hansen for total sediment load, the dimensionless formula of Graf and Acaroglu has been preferred since more parameters are involved, and this is supposed to better describe flow conditions. The dimensionless parameter to which data are related has therefore been identified in the dimensionless shear stress $\tau^* = \frac{Ri_f}{\delta d_{50}}$, to maintain the parameters adopted in Graf and Acaroglu's formula and since τ^* should well represent the hydrodinamic stress in the river.

The form of the new formula is therefore found of the type

$$\phi = f(\tau^*) \tag{6.1}$$

The problem now consists in the determination of the function f which relates τ^* and ϕ .

As explained, the dimensionless sediment discharge according to Graf and Acaroglu is

$$\phi = \frac{Q_s u R}{\sqrt{\delta g d_{50}^3}} \quad (6.2)$$

where in the present case $Q_s = Q_{s,sus}$ is the mean suspended load obtained by dividing the mass of suspended load for every flood by the duration of the flood; since it is a constant, the instantaneous dimensionless sediment discharge in the same flood can be written as:

$$\phi = Q_{s,sus} \frac{\frac{uR}{Q}}{\sqrt{\delta g d_{50}^3}} = Q_{s,sus} \cdot \phi' \quad (6.3)$$

with $\phi' = \frac{\frac{uR}{Q}}{\sqrt{\delta g d_{50}^3}}$.

From the instantaneous values it is possible to obtain the mean value for every flood, which is equal to

$$\bar{\phi} = Q_{s,sus} \bar{\phi}' \quad (6.4)$$

where with the bar are intended the mean values of the parameters during the same flood.

It is now possible to compare the dimensionless sediment discharge and the dimensionless shear stress for every flood, and study their relation on a $\bar{\tau}^* - \bar{\phi}$ graphic.

For every flood, both for MOG2 and MOG3, the two parameters $\bar{\phi}$ and $\bar{\tau}^*$ were calculated; the obtained values for the four year and sub-catchment combinations were joined in a single vector. Results were plotted in a graphic and some different types of trend lines were tested. For every trend line the correlation factor R^2 was calculated; in order to maintain the similitude with the reality, for which if the discharge tends to zero also sediment load must tend to zero, only functions which pass through the origin of the axis were considered. The trend line which provided the higher R^2 value was identified as the function f we were looking for.

The best trend line seemed to be a power, with $R^2 = 0.37$. The expression of the function is therefore

$$\phi = 24 \cdot \tau^{* 1.493} \quad (6.5)$$

The obtained graphic with the chosen trend line is shown in the following figure.

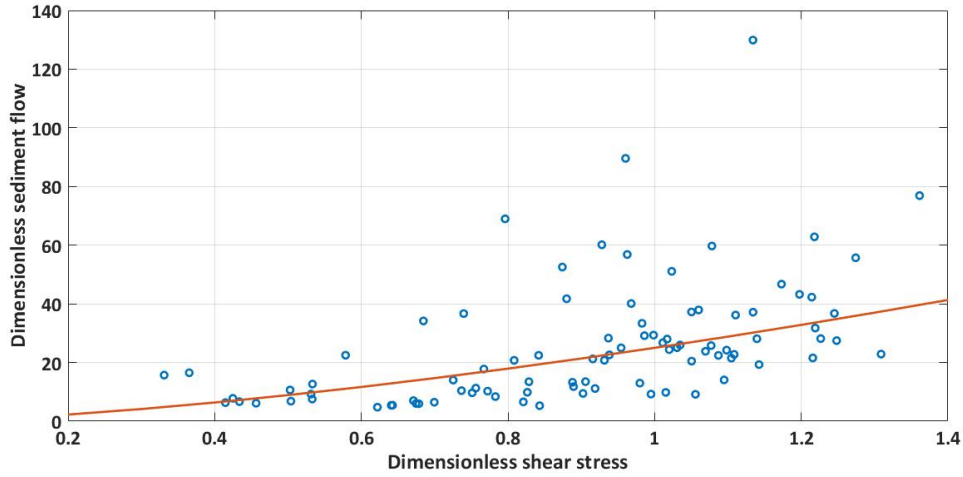


Figure 6.1: Graphic for the determination of suspended load formula.

Through the data we have it is also possible to determine a new formula for total sediment load. By considering the total sediment load as the sum of suspended load and bedload

$$Q_{s,tot} = Q_{s,sus} + Q_{s,bed} \quad (6.6)$$

and substituting in equation 6.2 we can write

$$\phi = \frac{Q_{s,sus} + Q_{s,bed} uR}{\sqrt{\delta g d_{50}^3}} \quad (6.7)$$

where the suspended load is the same as previous, whereas bedload is the mean of the values calculated with the three formulas tested in this thesis. Dividing the fraction into two parts we obtain

$$\phi = Q_{s,sus} \frac{uR}{\sqrt{\delta g d_{50}^3}} + \frac{Q_{s,bed} uR}{\sqrt{\delta g d_{50}^3}} \quad (6.8)$$

which can be written as

$$\phi = Q_{s,sus} \phi' + \phi'' \quad (6.9)$$

with $\phi' = \frac{uR}{\sqrt{\delta g d_{50}^3}}$ as previously and $\phi'' = \frac{Q_{s,bed} uR}{\sqrt{\delta g d_{50}^3}}$.

Note that since bedload is calculated, it can be evaluated every five minutes and it can be included in ϕ'' ; suspended load, instead, is a constant during a flood and multiplies ϕ' , since its variation during the event is unknown. The mean dimensionless sediment flow for every flood is now

$$\bar{\phi} = Q_{s,sus} \bar{\phi}' + \bar{\phi}'' \quad (6.10)$$

which can be plotted in a graphic as for suspended load.

The same procedure was followed and the best trend line was again a power, with $R^2 = 0.46$, whose form is

$$\phi = 30.35 \cdot \tau^{*1.489} \quad (6.11)$$

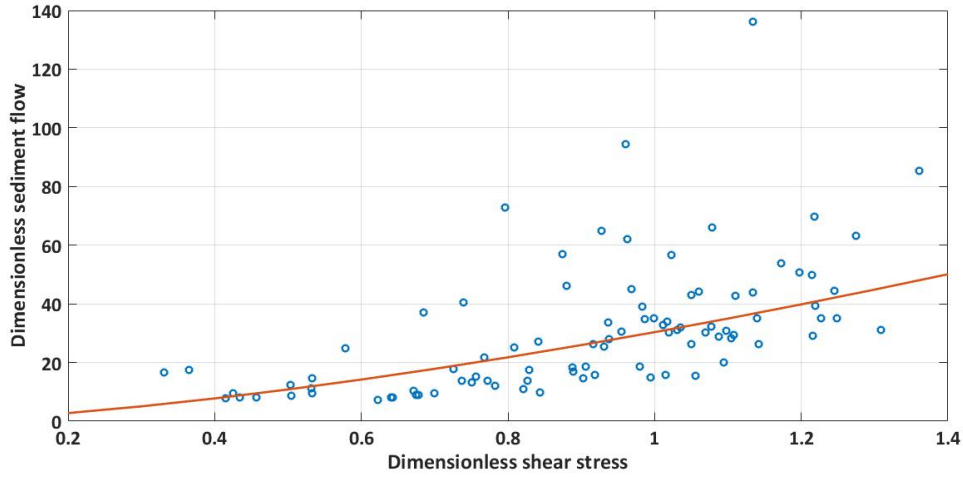


Figure 6.2: Graphic for the determination of total load formula.

The obtained formulas were then adoperated to evaluate the sediment load for the four combinations of sub-catchment and year considered in this work, to verify their accuracy. The results are herein shown (for readability reasons the bedload formulas are not shown, but their magnitude is the same as in the previous chapter). As previously, the formulas for total load are showed in blue and the formulas for suspended load in red. The proposed formulas are indicated with TL if referred to total load and with SL if referred to suspended load.

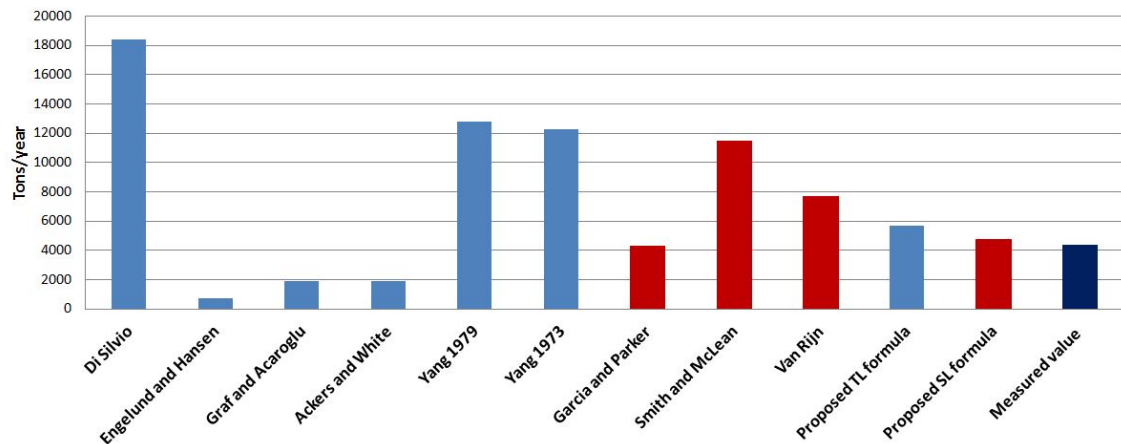


Figure 6.3: Results for MOG2 in 2013 with proposed formulas.

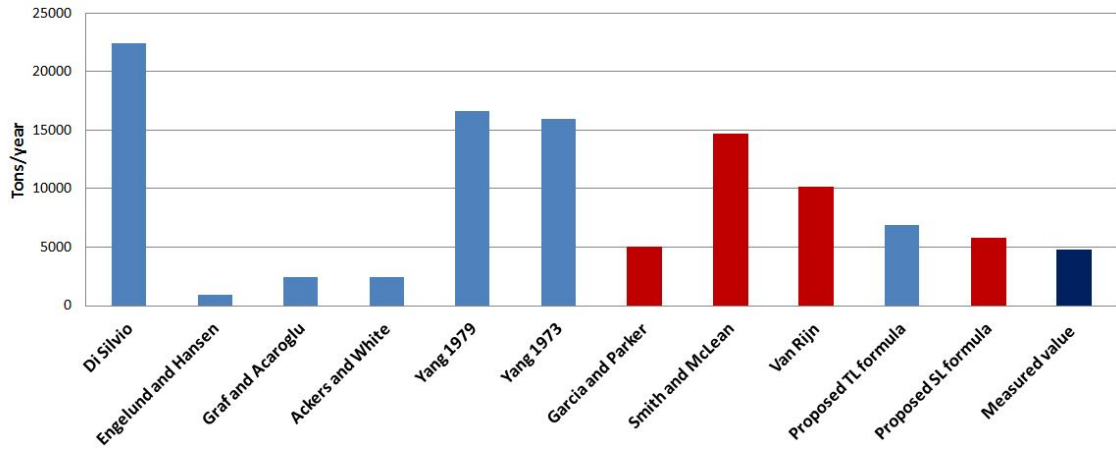


Figure 6.4: Results for MOG2 in 2014 with proposed formulas.

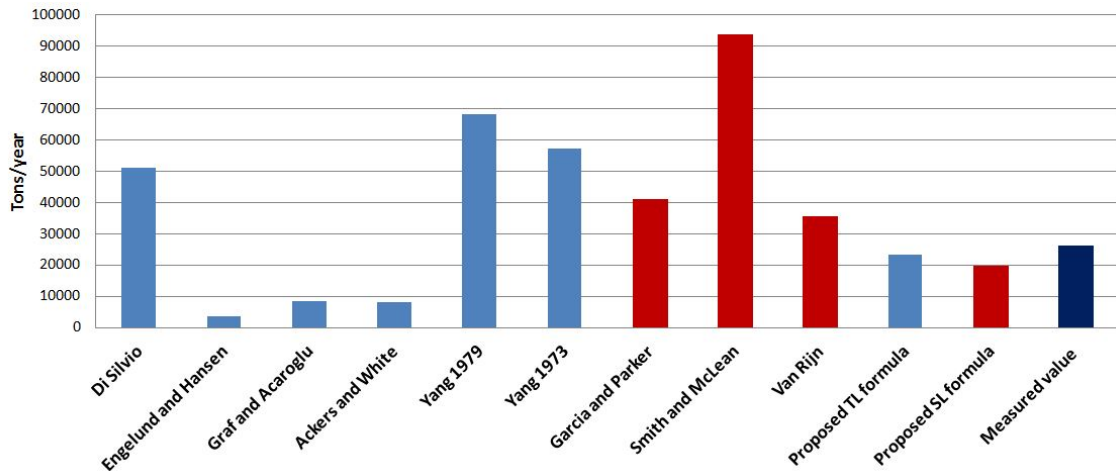


Figure 6.5: Results for MOG3 in 2013 with proposed formulas.

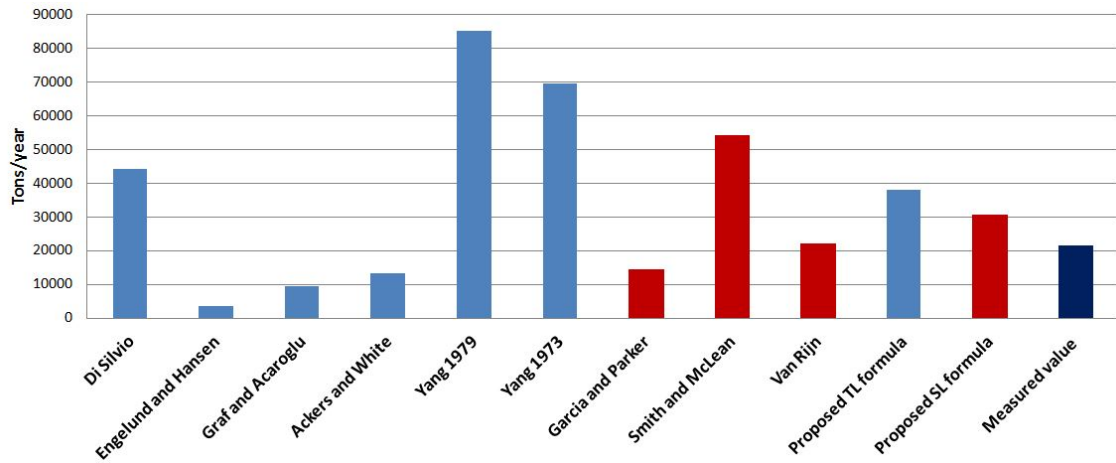


Figure 6.6: Results for MOG3 in 2014 with proposed formulas.

An interesting point of view is provided through the relationship between discharge in the river and sediment flow, and in particular by the comparison between calculated and predicted values. For every flood analyzed in this thesis the mean discharge and the mean sediment discharge were calculated and the obtained values are shown in the following figures, compared to predicted values obtained through the formulas tested in this work. For the proposed formulas is intended equation 6.5 for graphics 6.7 and 6.8 (concerning suspended load), and equation 6.11 for graphics 6.9 and 6.10 (concerning total load).

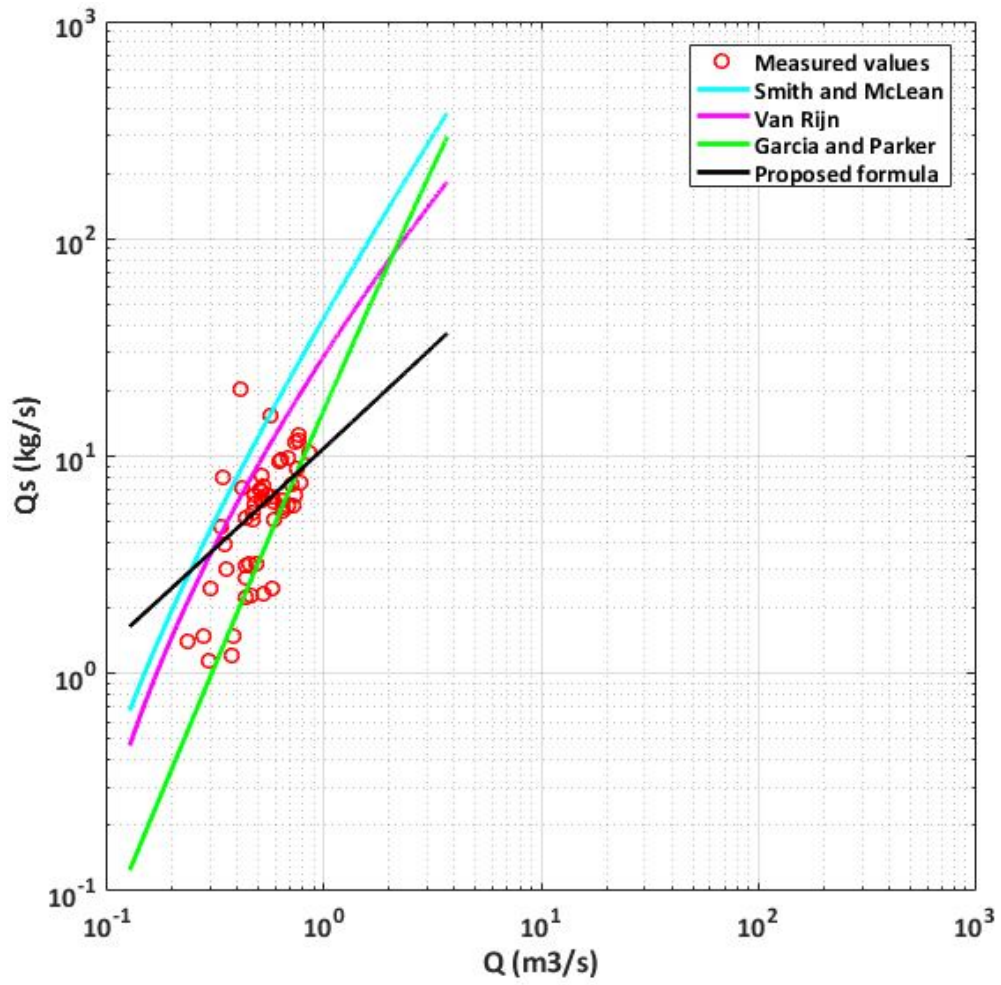


Figure 6.7: Field data versus predicted curves for suspended load in MOG2.

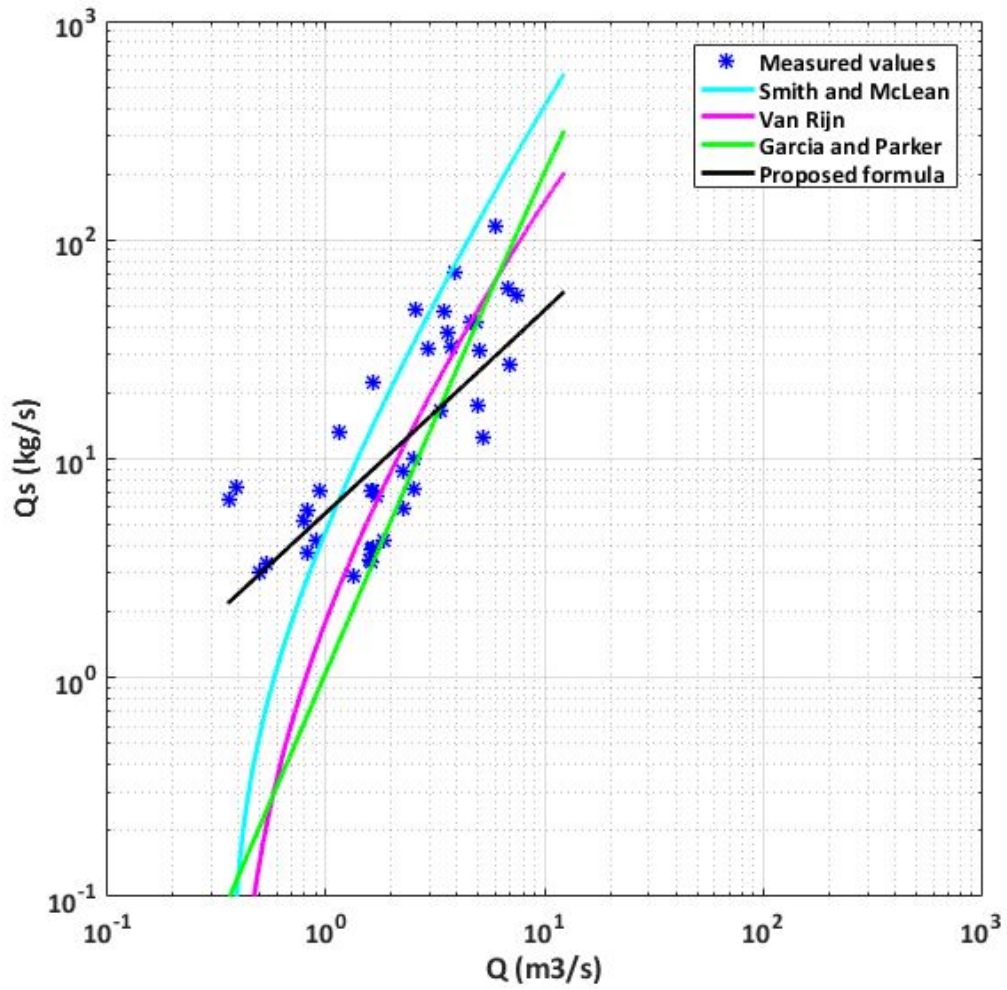


Figure 6.8: Field data versus predicted curves for suspended load in MOG3.

The same graphics have been made for total load formulas, but in this case the measured values are provided by the sum of suspended measured values and bedload values calculated through the bedload formulas tested in this thesis. This is necessary because measured suspended values couldn't be compared with total load formulas. Since there are not any usable bedload measures, bedload was estimated through different literature formulas and the mean value was summed to measured suspended data to have an evaluation of total load.

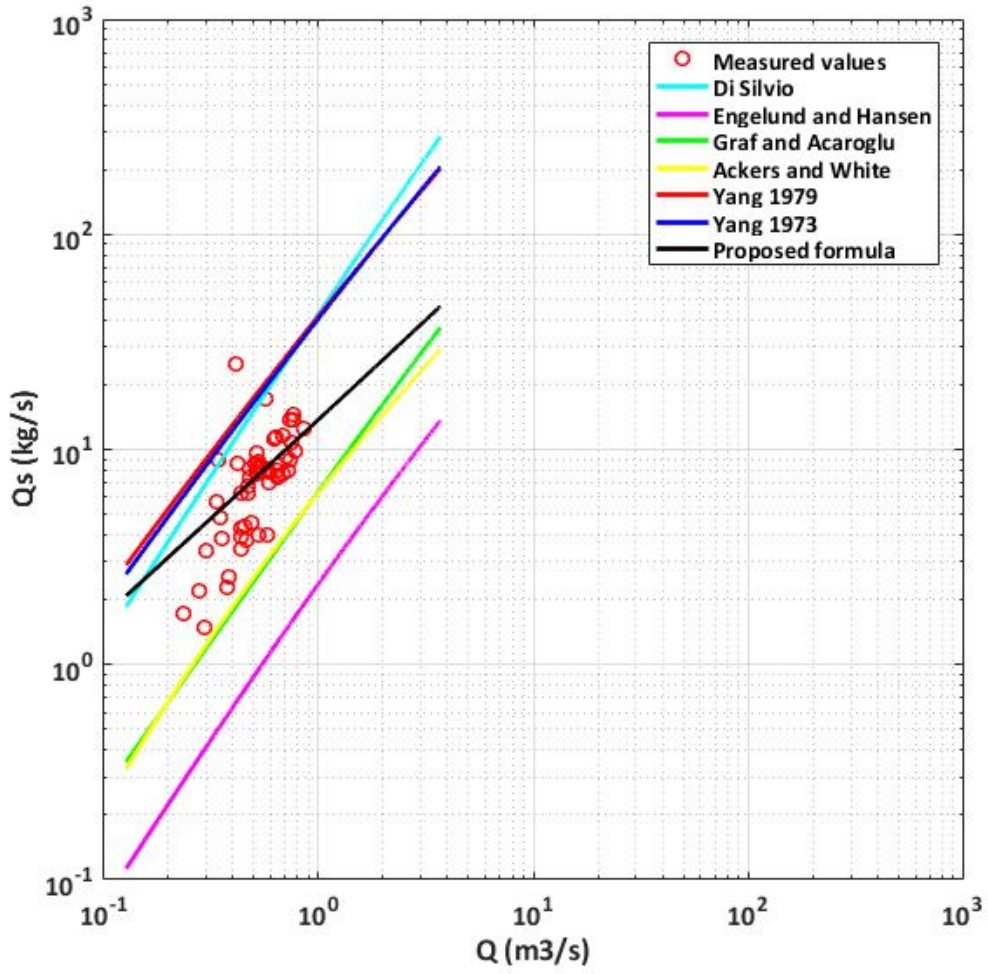


Figure 6.9: Field data versus predicted curves for total load in MOG2.

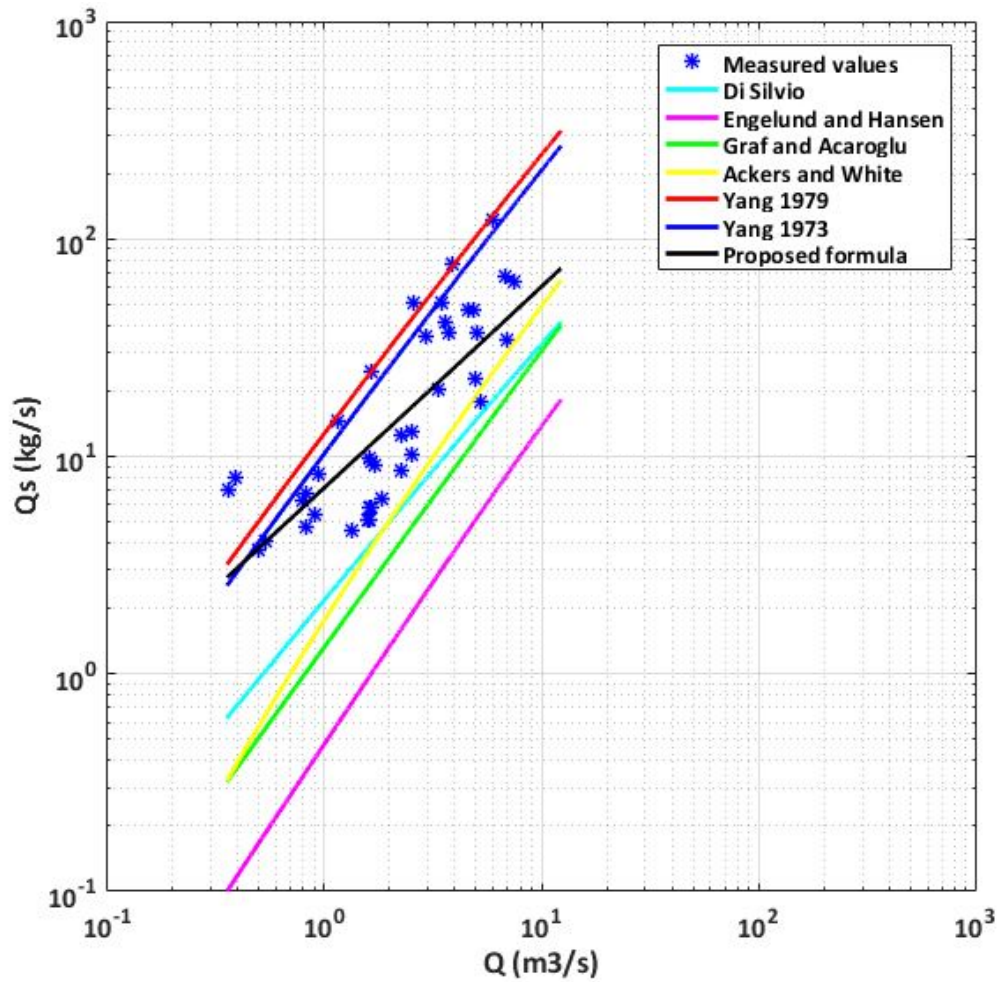


Figure 6.10: Field data versus predicted curves for total load in MOG3.

To relate the two sub-catchments and obtain some recapitulatory graphics, however, data can't be simply joined, because of the different size of Mog2 and Mog3; for that reason, to link data of the two sub-catchments we have to consider the specific discharge of each one, obtained by dividing discharge per the area of the sub-catchment. Discharge values are therefore expressed by

$$\frac{l}{s \cdot km^2}$$

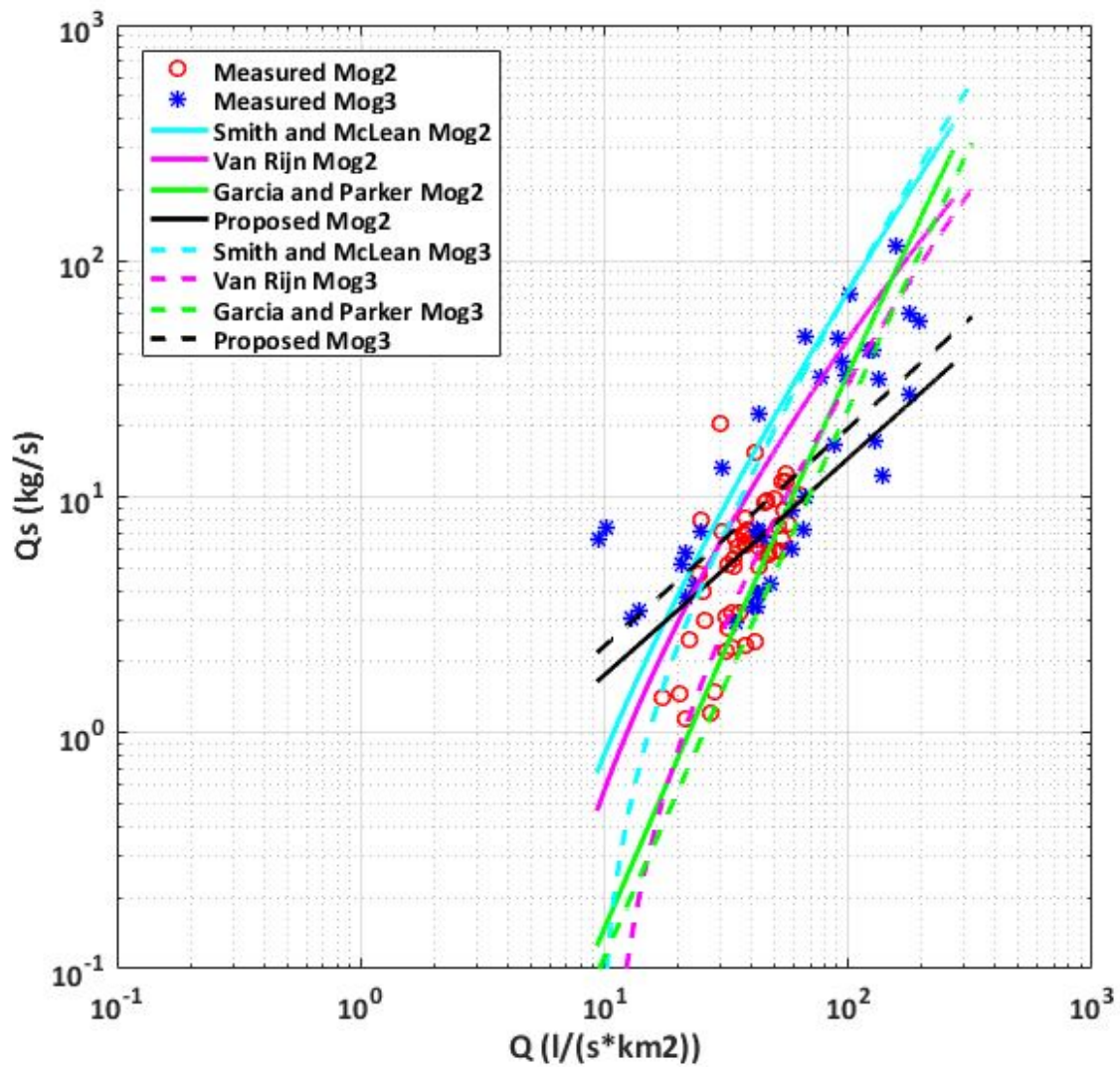


Figure 6.11: Comparison graphic for suspended load with literature formulas and proposed formula (6.5), obtained joining graphics 6.7 and 6.8. Coordinates of the measured data represent the mean specific discharge and the mean sediment discharge of every flood. Calculated curves are obtained evaluating sediment load as a function of specific discharge. Every formula is distinguished by a different colour, and there are two lines for every color: the solid line represents the implementation of that formula in MOG2, whereas the dashed one is referred to MOG3.

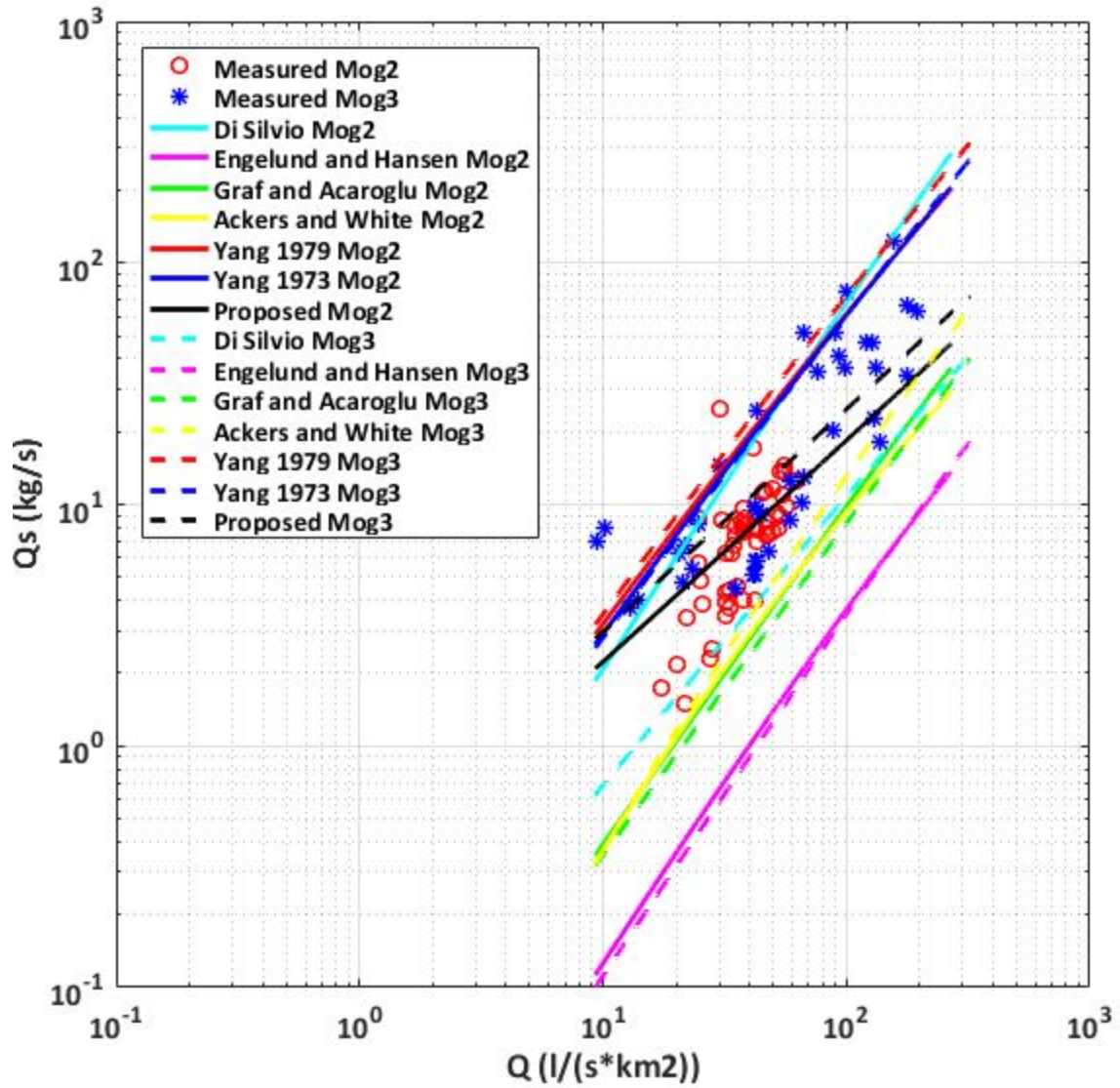


Figure 6.12: Comparison graphic for total load with literature formulas and proposed formula (6.11), obtained joining graphics 6.9 and 6.10. Measured data and tested formulas have to be intended as in the previous graphic. Again, every formula is distinguished by a different colour, solid lines are referred to MOG2 and dashed lines to MOG3.

6.1 Partitioning of total sediment load into suspended load and bedload

The partitioning of total sediment load into suspended load and bedload is often difficult to estimate. In this thesis, as explained, the only field data were about suspended load and the evaluation of total load was performed by adding up a mean bedload value, calculated through literature formulas, with the measured suspended load data.

In literature there are only a few indications about the partitioning of total load, and often it is only provided a "rule of thumb" which is not field-tested. However, Turowski et al. [36] analyzed both data for short-term and long-term partitioning providing an empirical equation to estimate bedload rates from suspended load. The equation for the 50% percentile (median) is:

$$G = \begin{cases} 0.833L^{1.34} & \text{if } L \leq 0.393 \\ 0.437L^{0.647} & \text{otherwise} \end{cases} \quad (6.12)$$

where L is the suspended load and G is bedload, expressed in $\frac{kg}{s}$.

For the present study Turowski's equation was tested against Mog2 and Mog3 calculated values, as shown in the following figure.

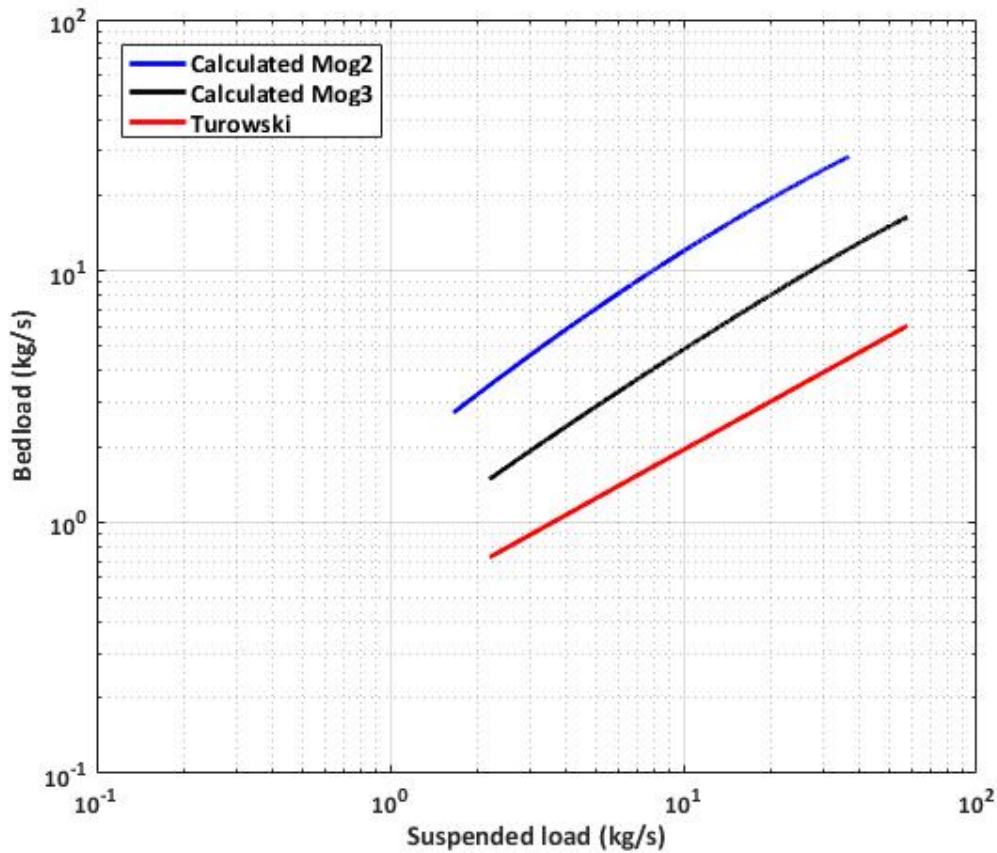


Figure 6.13: Bedload transport rate plotted as a function of suspended load transport rate.

As it is possible to understand from figure 6.13, calculated bedload values are higher than those provided from equation 6.12; however Turowski suggests to use the present relation with care when attempting to predict the partitioning for a particular stream, because its behaviour may differ considerably from the trend. Data from which the relation was obtained have a large scatter, in some cases also four order of magnitude, but show a clear trend.

To better understand if Turowski's equation fits field data we should have bedload measures; since this is not possible, we are not able to determine Turowski's accuracy for Mogtedo watershed. However, it is clear that bedload formulas provide higher values than Turowski's one, but also that bedload formulas cannot be compared to field data.

Another interesting research about the partitioning of total load into suspended load and bedload has been carried out by Alexandrov et al. [2]. Authors analyzed a 15-year record for the semiarid upland of Eshtemoa, Israel. Particularly, the annual sediment yield was divided by the surface of the basin, providing an estimation of specific annual erosion. Here data from Mogtedo are compared to the ones provided by Alexandrov et al., since both of them belong to semi-arid basins. In general we can notice that calculated bedload for Mogtedo is higher than expected from Alexandrov's research, where the mean value is $15.3 \frac{tons}{km^2}$. Also the percentage of total load represented by bedload is lower in Alexandrov's work, since the mean percentage is 5.3% (see next table).

	MOG2 2013	MOG2 2014	MOG3 2013	MOG3 2014
Bedload	67.046	85.527	88.066	174.665
Suspended load	317.872	345.982	680.589	562.242
% of total load represented by bedload	17.418	19.820	11.457	23.702

Table 9: Sediment load values for Mogtedo basin, expressed in $\frac{tons}{km^2}$. Suspended values are the measured ones; bedload values are obtained through a mean of the tested formulas, as in the previous chapter.

In conclusion we can affirm that bedload obtained through literature formulas in Mogtedo basin seems to be overestimated, since both the works of Turowski and Alexandrov suggest a lower bedload value. However, no bedload measures are available in Mogtedo to be compared to predicted values. More analysis could be carried out in the future with bedload measures from Mogtedo to test the partitioning of total load.

6.2 Calculation of Root Mean Square Errors

To better understand which formula better fits field data it is necessary to consider a parameter which describes the differences between calculated and predicted values; the parameter herein considered is the *root mean square error*, defined as

$$RMSE = \sqrt{\frac{\sum_{i=1}^N (\hat{y}_i - y_i)^2}{N}} \quad (6.13)$$

where \hat{y}_i is the i -th predicted value, y_i is the i -th calculated value and N is the number of points. Obviously, the lower the RMSE the better the formula fits well field data.

RMSEs were calculated for Mog2 and Mog3 sub-catchments and also joining the square differences and calculating them on the total values. The obtained values of RMSEs are shown in the following tables.

	Mog2	Mog3	Total
Garcia and Parker	3.892	21.216	14.292
Smith and McLean	10.275	60.947	40.923
Van Rijn	6.120	19.244	13.497
Proposed suspended load	3.209	19.794	13.273

Table 10: Calculated RMSE for suspended load formulas.

	Mog2	Mog3	Total
Di Silvio	10.803	26.884	19.499
Engelund and Hansen	7.888	32.084	21.971
Graf and Acaroglu	6.318	28.333	19.276
Ackers and White	6.247	24.874	17.061
Yang 1979	12.482	40.837	28.516
Yang 1973	11.606	31.010	22.231
Proposed total load	3.555	19.343	13.031

Table 11: Calculated RMSE for total load formulas.

6.3 Student's test

The difference between the calculated RMSEs for the different formulas are in some cases quite low, whereas in other cases are higher. However, we can't say if the difference is due to a statistical variation or if the formulas provide considerably different results. Particularly, we are interested in the confrontation between the proposed formulas and literature ones: literature suspended load formulas are compared with the proposed suspended load equation (6.5) and literature total load ones with the proposed total load one (6.11).

To compare formulas the Student's test (t-test) has been done. Student's test, indeed, compares two mean values and, using the standard deviations and the number of points of the two samples, provides an evaluation of the probability that the two mean values are significantly different.

The null hypothesis H_0 of a Student's test is that the two mean values of the distributions, from which samples have been selected, are equals.

To perform a Student's test the t-parameter is calculated as

$$t = \frac{\bar{X}_1 - \bar{X}_2}{\sqrt{\frac{S_1^2(n_1-1) + S_2^2(n_2-1)}{n_1+n_2-2} \left(\frac{1}{n_1} + \frac{1}{n_2} \right)}} \quad (6.14)$$

with \bar{X}_1 and \bar{X}_2 the two mean values, S_1^2 and S_2^2 the two variances and n_1 and n_2 the number of points.

The number of degrees of freedom is

$$d = n_1 + n_2 - 2 \quad (6.15)$$

Then the calculated t value is compared with to threshold value obtained through the Student's probability density function (pdf), depending on the chosen significance level α and the number of degrees of freedom. If the calculated t is higher than the threshold it means that the null hypothesis can be rejected with a probability of error lower than α .

However, a preliminar analysis should be done on the samples we want to undergo the test. Indeed, in order to correctly apply the t-test, the two samples should have a similar variance (homoscedasticity condition). This condition can be verified with some tests, such as a F-test, which is the most common.

According to the F-test a parameter F is calculated as

$$F = \frac{S_{max}^2}{S_{min}^2} \quad (6.16)$$

where S_{max}^2 is the higher variance and S_{min}^2 is the lower one. This value is compared to a critical value obtained through the F distribution, calculated with a significance level α and two parameters which are equals to the degrees of freedom of the numerator and the denominator. In this case the number of degrees of freedom is equal to the number of point minus 1.

If the calculated F value is lower than the threshold, the homoscedasticity condition can be verified

with a probability of error lower than α . As it is possible to understand from the following table, the previous condition is never respected with a significance level $\alpha = 5\%$.

	Mog2	Mog3	Total
Di Silvio	4.396	2.384	2.410
Engelund and Hansen	3.158	3.738	3.907
Graf and Acaroglu	2.415	2.683	2.771
Ackers and White	2.379	1.873	1.909
Yang 1979	5.132	7.438	7.936
Yang 1973	4.140	2.666	2.797
Garcia and Parker	1.962	1.971	1.819
Smith and McLean	10.850	50.101	52.093
Van Rijn	1.630	2.918	2.736
Critical value of F	1.592	1.704	1.414

Table 12: Calculated values of F compared to critical values.

Since the homoscedasticity condition is not respected, we have to modify little the implementation of the t-test. In this case, indeed, we can use the Satterthwaite method [30].

This method calculates the parameter t as:

$$t = \frac{\bar{X}_1 - \bar{X}_2}{\sqrt{\frac{S_1^2}{n_1} + \frac{S_2^2}{n_2}}} \quad (6.17)$$

The number of degrees of freedom is

$$d' = \frac{\left(\frac{S_1^2}{n_1} + \frac{S_2^2}{n_2}\right)^2}{\frac{\left(\frac{S_1^2}{n_1}\right)^2}{n_1-1} + \frac{\left(\frac{S_2^2}{n_2}\right)^2}{n_2-1}} \quad (6.18)$$

which must be approximated to the lower integer d'' .

With this method the parameters t were calculated for every pair of mean values both for Mog2 and Mog3 and for the joined data. Results of the test are showed in the next tables, were those cases in which calculated t value is higher than critical one are highlighted, meaning the two formulas have a significantly different mean. As explained, the values of t are calculated between the indicated literature formulas and the proposed ones, for suspended load or total load according to the type of the literature formula.

	Mog2		Mog3		Total	
	t calculated	t (p=0.05)	t calculated	t (p=0.05)	t calculated	t (p=0.05)
Garcia and Parker	0.580	1.986	0.241	1.994	0.259	1.974
Smith and McLean	5.693	2.000	2.361	2.021	2.355	1.986
Van Rijn	3.444	1.985	0.094	1.999	0.059	1.976

Table 13: Results of the t-test for suspended load formulas.

	Mog2		Mog3		Total	
	t calculated	t (p=0.05)	t calculated	t (p=0.05)	t calculated	t (p=0.05)
Di Silvio	6.390	1.993	1.000	1.997	1.357	1.975
Engelund and Hansen	3.468	1.990	1.589	2.002	1.682	1.978
Graf and Acaroglu	2.106	1.988	1.179	1.998	1.237	1.976
Ackers and White	2.047	1.988	0.762	1.994	0.846	1.974
Yang 1979	8.245	1.994	2.351	2.010	2.562	1.981
Yang 1973	7.678	1.993	1.620	1.998	1.982	1.976

Table 14: Results of the t-test for total load formulas.

The calculated t values for Mog3 are in general lower than for MOG2; this means that for MOG3 the H_0 condition can be rejected more rarely. This is probably due to the fact that Mog3 data are more scattered than MOG2's, and therefore the variance is higher. As shown in equation 6.17, the variance is in the denominator, and a higher variance leads to a lower t value. This is easy to understand, because if data are more scattered the same difference in the measured means is obviously related to a lower probability that data belong to distributions with different means. Garcia and Parker's formula is the only one which never has a t higher than the critical one. This formula, indeed, seems to be the one which better fits field data between literature ones. Van Rijn's has a t higher than critical one for MOG2, but for MOG3 and for the total value it can be considered a good approximation of the proposed formula. Smith and McLean's, instead, provides always a t higher than the critical value, and it doesn't fit well data, since its difference from the proposed formula is statistically too high to be considered negligible. As regards total load, all the formulas reject the H_0 hypothesis for Mog2: the proposed formula can't be replaced by any of the others. For MOG3, instead, only Yang 1979 formula has a t higher than the critical, and concerning total values this happens only with the two Yang's formulas. In conclusion, we can say that only Smith and McLean's and the two Yang's formulas have a RMSE whose difference from the RMSE of the proposed formulas is statistically significant, if we consider both MOG2 and MOG3. However, this consideration is highly affected from MOG3 higher variance, which makes the test globally less restrictive. Considering only MOG2 data, indeed, the only formula whose variation from the proposed one is not statistically significant is Garcia and Parker's.

7 Conclusions

In the Sahelian region rains are only concentrated in a short period of the year, named wet season. The storage of water in small reservoirs to be used in the rest of the year is therefore of paramount importance. However, sediment transport from rivers which provide water to the reservoirs is continuously decreasing the available storage capacity (reservoirs siltation).

Different sediment transport formulas were tested in the present work on Mogtedo watershed, in Burkina Faso: six concerning total sediment load, three suspended load and three bedload. Calculated values were compared to field data obtained through concentration measures at the two catchment outlets.

The purpose of this thesis is to assess which formula better fits field data and proposing a new sediment transport formula for small Sahelian rivers. The new relation was searched through a comparison between dimensionless sediment discharge ϕ and dimensionless shear stress τ^* .

The dimensionless sediment discharge is defined as

$$\phi = \frac{\frac{q_s}{q} U R}{\sqrt{(s-1)g d_{50}^3}}$$

where q_s and q are the sediment discharge per unit width and the discharge per unit width, U the mean flow velocity, R the hydraulic radius, s the specific gravity of the sediment, g the acceleration due to gravity and d_{50} the grain diameter for which 50% by weight is finer.

The dimensionless shear stress is defined as

$$\tau^* = \frac{R i_f}{(s-1)d_{50}}$$

where i_f is the bed slope and R , s , and d_{50} are the same as in ϕ .

The two previous parameters were calculated for every flood analysed in this work and plotted on a graphic. Different trend lines were tested to find the function which better interpolates graphic points. A power law, relating dimensionless sediment discharge and dimensionless shear stress, was proposed to estimate suspended load. The proposed power law is the following.

$$\phi = 24 \cdot \tau^{* 1.493}$$

The same procedure was followed considering also a mean calculated value of bedload and thus obtaining a formula for total load evaluation. The proposed trend line was again a power law, whose expression is herein shown.

$$\phi = 30.35 \cdot \tau^{* 1.489}$$

The partitioning of total load into suspended load and bedload was performed using the relation proposed by Turowski et al. for the calculation of bedload G from suspended load L (both

expressed in $\frac{kg}{s}$).

$$G = \begin{cases} 0.833L^{1.34} & \text{if } L \leq 0.393 \\ 0.437L^{0.647} & \text{otherwise} \end{cases}$$

Also the work of Alexandrov, about a 15-year study in a semiarid basin in Israel, was compared to Mogtedo data. Results were quite different from what Turowski and Alexandrov suggest, since it seems that evaluation of bedload for Mogtedo with literature formulas leads to an overestimation. However, no field data about bedload were available.

The differences between field data and calculated values were evaluated through the *root mean square error* (RMSE). The Student's test was used to verify if differences among formulas were statistically significant. As regards suspended load, the literature formulas which provided the lowest differences from the proposed one were Garcia and Parker's and Van Rijn's. Concerning total load, the only formulas whose RMSE is statistically different from the proposed formula's are the two Yang's formulas. Ackers and White's formula provides the closest values to the ones obtained through the proposed formula.

In the near future, more research could be carried out with more detailed data. Information on local grain size distribution should be needed to improve the parameter estimation used in the literature formulas.

8 Bibliography

- [1] Peter Ackers and William R White. Sediment transport: new approach and analysis. *Journal of the Hydraulics Division*, 99(hy11), 1973.
- [2] Yulia Alexandrov, Hai Cohen, Jonathan B Laronne, and Ian Reid. Suspended sediment load, bed load, and dissolved load yields from a semiarid drainage basin: A 15-year study. *Water resources research*, 45(8), 2009.
- [3] A Armanini. Non-uniform sediment transport: dynamics of the active layer. *Journal of Hydraulic Research*, 33(5):611–622, 1995.
- [4] Aronne Armanini. On the dynamic impact of debris flows. In *Recent developments on debris flows*, pages 208–226. Springer, 1997.
- [5] Kazuo Ashida and Masanori Michiue. Study on hydraulic resistance and bed-load transport rate in alluvial streams. In *Proceedings of the Japan Society of Civil Engineers*, volume 1972, pages 59–69. Japan Society of Civil Engineers, 1972.
- [6] Djanteng Wandji Caleb. Etude hydromorphologique du cours d'eau principal en amont de la retenue de mogtedo.
- [7] Edward Robert Corino and Robert S Brodkey. A visual investigation of the wall region in turbulent flow. *Journal of Fluid Mechanics*, 37(1):1–30, 1969.
- [8] Suzanne E Cotillon and G Gray Tappan. Landscapes of west africa: A window on a changing world. 2016.
- [9] IV Egiazaroff. Calculation of nonuniform sediment concentrations. *Journal of the Hydraulics Division*, 91(4):225–247, 1965.
- [10] Hans Albert Einstein et al. *The bed-load function for sediment transportation in open channel flows*, volume 1026. Citeseer, 1950.
- [11] Frank Engelund and Eggert Hansen. A monograph on sediment transport in alluvial streams. *Technical University of Denmark Ostervoldgade 10, Copenhagen K.*, 1967.
- [12] R Fernandez Luque and R Van Beek. Erosion and transport of bed-load sediment. *Journal of hydraulic research*, 14(2):127–144, 1976.
- [13] Marcelo Garcia and Gary Parker. Entrainment of bed sediment into suspension. *Journal of Hydraulic Engineering*, 117(4):414–435, 1991.
- [14] WALTER H GRAF and ERTAN R ACAROGLU. Sediment transport in conveyance systems (part 1)/a physical model for sediment transport in conveyance systems. *Hydrological Sciences Journal*, 13(2):20–39, 1968.

- [15] WH Graf and MS Altinakar. Hydraulique fluviale-tome 2-écoulement non permanent et phénomènes de transport. *Traité de Génie Civile de l'Ecole polytechnique fédérale de Lausanne, presses polytechniques et universitaires romandes*, 1996.
- [16] Stefania Grimaldi, Irene Angeluccetti, Velio Coviello, and Paolo Vezza. Cost-effectiveness of soil and water conservation measures on the catchment sediment budget—the laaba watershed case study, burkina faso. *Land Degradation & Development*, 26(7):737–747, 2015.
- [17] Francis Guyon and Eric Hallot. Origines des apports sédimentaires des retenues d'eau d'irrigation echelle des sous bassins versants. Technical report.
- [18] Francis Guyon and Eric Hallot. Plan de gestion de la retenue d'eau de mogtedo et de son bassin versant.
- [19] Eric Hallot, Francis Guyon, Didier de Thysebaert, and François Petit. Establishment of a sedimentation monitoring system of irrigation dams in burkina faso: The padi project. 2013.
- [20] RD Hey, JC Bathurst, and CR Thorne. Gravel-bed rivers.-j, 1979.
- [21] Pamoussa Guilga Ouesséni Kafando. Elaboration d'une méthode d'évaluation physique de cours d'eau a l'échelle du bassin versant: cas du bomborè.
- [22] Stephen J Kline, WC Reynolds, FA Schraub, and PW Runstadler. The structure of turbulent boundary layers. *Journal of Fluid Mechanics*, 30(4):741–773, 1967.
- [23] A Lamberti, L Montefusco, and E Paris. Considerazioni sulla portata dominante nei torrenti montani. *Proc. of Seminario di Idraulica del Territorio Montano, Bressanone, Italy*, 1984.
- [24] Eugen Meyer-Peter and R Müller. Formulas for bed-load transport. In *IAHSR 2nd meeting, Stockholm, appendix 2*. IAHR, 1948.
- [25] Gary Parker. Hydraulic geometry of active gravel rivers. *Journal of the Hydraulics Division*, 105(9):1185–1201, 1979.
- [26] M Pica and F Preti. Bed load transport and stable thalweg slopes. 1: Theoretic and experimental fundamentals. *Rivista di Ingegneria Agraria (Italy)*, 1999.
- [27] Leo C van Rijn. Sediment transport, part ii: suspended load transport. *Journal of hydraulic engineering*, 110(11):1613–1641, 1984.
- [28] Yamgouba Jules Stanislas ROMBA. Caracterization de l'érodibilité des sols a l'échelle du bassin versant du barrage dee mogtedo au burkina faso.
- [29] Hunter Rouse. Modern conceptions of the mechanics of turbulence. *Trans. ASCE*, 102:463–543, 1937.
- [30] Franklin E Satterthwaite. An approximate distribution of estimates of variance components. *Biometrics bulletin*, 2(6):110–114, 1946.

- [31] G Seminara. Equilibrio morfodinamico, stabilità ed evoluzione di correnti a fondo mobile. *Proc. Nuovi sviluppi applicative dell'idraulica dei corsi d'acqua, Bressanone, Italy*, pages 93–121, 1997.
- [32] Albert Shields. Application of similarity principles and turbulence research to bed-load movement. 1936.
- [33] J Dungan Smith and SR McLean. Boundary layer adjustments to bottom topography and suspended sediment. In *Elsevier Oceanography Series*, volume 19, pages 123–151. Elsevier, 1977.
- [34] L Solari, G Zolezzi, and G Seminara. Curvature driven distorsion of free bars in river bends. In *Symposium on River, Coastal, Estuarine Morphodynamics*, pages 563–572. [Arti Grafiche Lux], 1999.
- [35] T Takahashi. Debris flow, iahr monograph series, aa balkema: Rotterdam. *Doi.org/10.1201/9780203946282*, 1991.
- [36] Jens M Turowski, Dieter Rickenmann, and Simon J Dadson. The partitioning of the total sediment load of a river into suspended load and bedload: a review of empirical data. *Sedimentology*, 57(4):1126–1146, 2010.
- [37] LC Van Rijn. Simple general formulae for sand transport in rivers, estuaries and coastal waters. Retrieved from www.leovanrijn-sediment.com, pages 1–16, 2013.
- [38] Kenneth C Wilson. Bed-load transport at high shear stress. *Journal of the hydraulics division*, 92(6):49–59, 1966.
- [39] PN Windmeijer and W Andriess. *Inland valleys in West Africa: an agro-ecological characterization of rice-growing environments*. Number 52. ILRI, 1993.
- [40] Chih Ted Yang. Incipient motion and sediment transport. *Journal of the hydraulics division*, 99(10):1679–1704, 1973.
- [41] Chih Ted Yang. Unit stream power equations for total load. *Journal of Hydrology*, 40(1-2):123–138, 1979.
- [42] Jürg Zeller. *Einführung in den Sedimenttransport offener Gerinne*. Versuchsanstalt f. Wasserbau u. Erdbau an d. Eidgenöss. Techn. Hochschule, 1963.